AD E 300 621

DNA 4873F-1

BOUNDARY LAYER MEASUREMENT PROGRAM

Volume I — Boundary Layer Acoustic Monitor Development Characterization and Installation (PVM 12 and 13, STM-12)

Kaman Sciences Corporation
P.O. Box 7463
Colorado Springs, Colorado 80933

30 June 1978

Final Report for Period 1 August 1975—30 June 1978

CONTRACT No. DNA 001-76-C-0080

Prepared for

Director

DEFENSE NUCLEAR AGENCY

Washington, D. C. 20305

DDC
RECEIVED
DEC 4 1979
A

79 11 01 004

Destroy this report when it is no longer
needed. Do not return to sender.

REPORT DOCUMENTATION PAGE		READ INSTRUCTIONS BEFORE COMPLETING FORM
1. REPORT NUMBER DNA 4873F-1	2. GOVT ACCESSION NO.	3. RECIPIENT'S CATALOG NUMBER
4. TITLE *(and Subtitle)* BOUNDARY LAYER MEASUREMENT PROGRAM. Volume I, Boundary Layer Acoustic Monitor Development Characterization and Installation (PVM 12 and 13, STM-12).		5. TYPE OF REPORT & PERIOD COVERED Final Report for Period 1 Aug 75—30 Jun 78
		6. PERFORMING ORG. REPORT NUMBER K-79-54(R)-VOL-1
7. AUTHOR(s) Vernon D. Peckham		8. CONTRACT OR GRANT NUMBER(s) DNA 001-76-C-0080
9. PERFORMING ORGANIZATION NAME AND ADDRESS Kaman Sciences Corporation P.O. Box 7463 Colorado Springs, Colorado 80933		10. PROGRAM ELEMENT, PROJECT, TASK AREA & WORK UNIT NUMBERS Subtask N99QAXAA112-06
11. CONTROLLING OFFICE NAME AND ADDRESS Director Defense Nuclear Agency Washington, D.C. 20305		12. REPORT DATE 30 June 1978
		13. NUMBER OF PAGES 106
14. MONITORING AGENCY NAME & ADDRESS(*if different from Controlling Office*) DNA, ...		15. SECURITY CLASS (*of this report*) UNCLASSIFIED
		15a. DECLASSIFICATION/DOWNGRADING SCHEDULE

16. DISTRIBUTION STATEMENT *(of this Report)*

Approved for public release; distribution unlimited.

17. DISTRIBUTION STATEMENT *(of the abstract entered in Block 20, if different from Report)*

18. SUPPLEMENTARY NOTES

This work sponsored by the Defense Nuclear Agency under RDT&E RMSS Code
B342077464 N99QAXAA11206 H2590D.

19. KEY WORDS *(Continue on reverse side if necessary and identify by block number)*
Boundary Layer Noise
Acoustic Monitor
Wind Tunnel Test
Reentry Vehicle Measurements

20. ABSTRACT *(Continue on reverse side if necessary and identify by block number)*

A Boundary Layer Acoustic Monitor (BLAM) was developed for determining boundary layer characteristics by sensing the external surface pressure fluctuation transmitted through to the inside surface of the heatshield by acoustical stress waves. Laboratory and wind tunnel tests were conducted to characterize and evaluate the BLAM. Flight hardware was developed and flight qualification tests were conducted for the PVM 12, PVM 13 and STM 12 flights.

DD FORM 1473 EDITION OF 1 NOV 65 IS OBSOLETE
1 JAN 73

PREFACE

The work accomplished on the Defense Nuclear Agency
"Boundary Layer Measurement Program," DNA001-76-C-0080 is
described in a two volume set of final reports as follows:

1. Volume I - Boundary Layer Measurement Program -
    Boundary Layer Acoustic Monitor Development,
    Characterization and Installation (PVM 12 and
    13, STM-12), K-79-54(R), DNA 4873-1.

2. Volume II - Boundary Layer Measurement Program -
    Aerodynamic Phenomena Transducer Development,
    K-79-54(R), DNA 4873-2.

Volume I describes the development of the Boundary Layer
Acoustic Monitor (BLAM) in addition to the laboratory and wind
tunnel tests which characterized and evaluated the BLAM. Also
described in Volume I are the flight qualification tests and
flight hardware characteristics used on the PVM 12, PVM 13 and
STM-12 flights.

Volume II describes the laboratory development and evaluation
of the Aerodynamic Phenomena Transducer (APT) which is designed
to simultaneously monitor the presence of acoustic fluctuations
(turbulent flow) and measure the static pressure exerted on a
heatshield during flight. Arc heater test results are included.

The authors wish to acknowledge the efforts of Lt. Cmdr.
R. Nibe and Major T. Swartz of the Defense Nuclear Agency,
Lt. Col. J. McCormack and Capt. M. Elliot of SAMSO (ABRES)/RSSE
and Lt. Col. R. Jackson of SAMSO/MNNR, in addition to Mr. Wally
Grabowski of the Aerospace Corporation. Each of these individuals
contributed significantly to the success of this overall program.
The KSC program manager for these efforts was Mr. T. Meagher.

CONVERSION FACTORS FOR U. S. CUSTOMARY TO METRIC (SI)
UNITS OF MEASUREMENT

To Convert From	To	Multiply By
angstrom	meters (m)	$1.000\ 000 \times E -10$
atmosphere (normal)	kilo pascal (kPa)	$1.013\ 25 \times E +2$
bar	kilo pascal (kPa)	$1.000\ 000 \times E +2$
barn	$meter^2\ (m^2)$	$1.000\ 000 \times E -28$
British thermal unit (thermochemical)	joule (J)	$1.054\ 350 \times E +3$
calorie (thermochemical)	joule (J)	$4.184\ 000$
cal (thermochemical)/cm^2	mega joule/m^2 (MJ/m^2)	$4.184\ 000 \times E -2$
curie	giga becquerel (GBq)*	$3.700\ 000 \times E +1$
degree (angle)	radian (rad)	$1.745\ 329 \times E -2$
degree Fahrenheit	degree kelvin (K)	$t_K = (t^\circ f + 459.67)/1.8$
electron volt	joule (J)	$1.602\ 19 \times E -19$
erg	joule (J)	$1.000\ 000 \times E -7$
erg/second	watt (W)	$1.000\ 000 \times E -7$
foot	meter (m)	$3.048\ 000 \times E -1$
foot-pound-force	joule (J)	$1.355\ 818$
gallon (U.S. liquid)	$meter^3\ (m^3)$	$3.785\ 412 \times E -3$
inch	meter (m)	$2.540\ 000 \times E -2$
jerk	joule (J)	$1.000\ 000 \times E +9$
joule/kilogram (J/kg) (radiation dose absorbed)	Gray (Gy)**	$1.000\ 000$
kilotons	terajoules	4.183
kip (1000 lbf)	newton (N)	$4.448\ 222 \times E +3$
kip/$inch^2$ (ksi)	kilo pascal (kPa)	$6.894\ 757 \times E +3$
ktap	newton-second/m^2 $(N-s/m^2)$	$1.000\ 000 \times E +2$
micron	meter (m)	$1.000\ 000 \times E -6$
mil	meter (m)	$2.540\ 000 \times E -5$
mile (international)	meter (m)	$1.609\ 344 \times E +3$
ounce	kilogram (kg)	$2.834\ 952 \times E -2$
pound-force (lbf avoirdupois)	newton (N)	$4.448\ 222$
pound-force inch	newton-meter (N·m)	$1.129\ 848 \times E -1$
pound-force/inch	newton/meter (N/m)	$1.751\ 268 \times E +2$
pound-force/$foot^2$	kilo pascal (kPa)	$4.788\ 026 \times E -2$
pound-force/$inch^2$ (psi)	kilo pascal (kPa)	$6.894\ 757$
pound-mass (lbm avoirdupois)	kilogram (kg)	$4.535\ 924 \times E -1$
pound-mass-$foot^2$ (moment of inertia)	kilogram-$meter^2$ $(kg·m^2)$	$4.214\ 011 \times E -2$
pound-mass/$foot^3$	kilogram/$meter^3$ (kg/m^3)	$1.601\ 846 \times E +1$
rad (radiation dose absorbed)	Gray (Gy)**	$1.000\ 000 \times E -2$
roentgen	coulomb/kilogram (C/kg)	$2.579\ 760 \times E -4$
shake	second (s)	$1.000\ 000 \times E -8$
slug	kilogram (kg)	$1.459\ 390 \times E +1$
torr (mm Hg, 0° C)	kilo pascal (kPa)	$1.333\ 22 \times E -1$

*The becquerel (Bq) is the SI unit of radioactivity; 1 Bq = 1 event/s.
**The Gray (Gy) is the SI unit of absorbed radiation.

A more complete listing of conversions may be found in "Metric Practice Guide E 380-74,"
American Society for Testing and Materials.

TABLE OF CONTENTS

3

LIST OF ILLUSTRATIONS

LIST OF ILLUSTRATIONS

LIST OF ILLUSTRATIONS

LIST OF TABLES

SECTION 1

INTRODUCTION

PVM PROGRAM

The PVM Boundary Layer Acoustic Monitor (BLAM) had the major objective of placing acoustic instruments on flight test RV's which would acquire data on boundary layer transition during reentry.

The BLAM is a new concept for determining boundary layer characteristics by sensing the external surface pressure fluctuation transmitted through to the inside surface of the heatshield by acoustical stress waves. This concept had first been tested on a Flame* flight sponsored by DNA; the results of that test indicated that significant acoustic amplitudes were present and that transition phenomena were detected.

The positive results obtained on the flame experiment stimulated additional flight and reported herein. The flight data was generated on MK-12 type reentry bodies of the Space and Missle Systems Organization (SAMSO). Two BLAM channels were on each of two reentry bodies on two Production Vehicle Monitor (PVM) 12 and 13 flights (total of 8 channels). Subsequently, four BLAMs were installed on the System Test Monitor (STM) 12W flight. These data were all generated on ICBM trajectories on the Western Test Range.

---

*Flight-Launched Advanced Material Experiment.

9
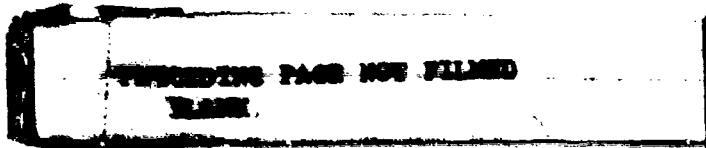
Before the BLAM could be applied to a full-scale RV, several equipment modifications and tests were necessary which were included as tasks in the PVM BLAM effort. The contract called for work to be accomplished in the following areas:

1) Sensor design and fabrication;

2) Electronics modification;

3) Flight qualification testing;

4) Liaison with RV contractor and DoD organizations involved with the flight test;

5) Participation in an on-going wind tunnel test program.

The primary objective of the STM-12 effort was that of instrumenting the RV's with small BLAM sensors which occupied smaller volume than the PVM sensors. The sensor was designed with half the diameter and approximately the same height as the PVM gage. In addition to flight test installation and qualification tests, more extensive data were taken of the installed BLAM frequency and directionality responses.

Sections 2 through 5 of this report relate the work accomplished on the PVM/STM BLAM efforts. In Section 2 the sensor optimization, characterization and electronics design modifications are described. Section 3 describes the flight qualification tests and Section 4 is a summary of flight test activities. Section 5 reports the results of ground tests, principally in two wind tunnels, and conclusions are reported in Section 6.

SECTION 2

GAGE OPTIMIZATION AND CHARACTERIZATION

2.1 SENSOR DESIGN

The Flame and PVM-12 BLAM utilizes a 2.54-cm diameter quartz crystal which converts acoustical stress waves into electric charge. This charge is converted to a voltage in a high impedance load at the input to a transistor preamplifier, which in turn, drives a coaxial cable connected at its other end to a signal conditioner. The output voltage of the signal conditioner (or electronics) provides a 5-volt full-scale signal to the RV telemetry which is related to the acoustic pressure fluctuation amplitude on the RV surface.

This gage, a photo of which is shown in Figure 1, is identical to that used on Flame with the exception of material added on the outside surfaces to provide electrical isolation from the heatshield. Fibreglass sheet (.025-cm thick) was placed on the front face of the crystal and .0076-cm mylar on the exposed crystal cylindrical surface.

Mechanical mounting is provided by bonding the front surface to the heatshield with a thin uniform layer of epoxy glue. Additional strength is given by three screws through a flange to the substructure of the RV. The screws can be insulated from the aluminum case by fiber shoulder washers as required.

The electrical voltage output of the sensor is in direct proportion to the stress in the crystal. Stress is appled to the crystal by external acoustic pressures being transmitted through the heatshield to the sensor located on the inside

11

Figure 1   BLAM SENSOR

surface. The mounting face (as seen in Figure 1) is coated with thin metal and is also connected to the cable shield. The back face of the crystal is connected to the internal preamplifier. This construction ensures good shielding from stray electric fields.

Two simulation techniques were applied during the PVM effort to provide characterization data on the frequency response of the BLAM. The first was that of applying a known sine wave voltage to a crystal which was acoustically coupled to the heatshield at the BLAM position. The second method imposed a sinusoidal force on a small area surface of the heatshield by an electrostatic technique. Because the crystal exciter used in the first method was itself resonant, it was used only for qualitative checks of the BLAM installation. A drawing of the exciter and application technique is shown in Figure 2. The output of the BLAM during these tests appeared at frequencies associated principally with the exciter crystal resonances. However, the technique proved very useful to check the entire as-installed BLAM system.

The electrostatic or capacitive simulator was used to determine frequency response functions of the BLAM installation. A typical response curve is shown in Figure 3; peaks are seen to occur at frequencies of 50, 113, and 168 kHz. Lower amplitude responses below 30 kHz and above 300 kHz are also exhibited by the gage but are not shown on the plot. The response can be electrically filtered by the signal conditioner as appropriate to remove the low or high frequency content. The data in Figure 3 were taken with the sensor mounted on 1.27-cm thick carbon phenolic material and a surface acoustic pressure of approximately 35 N/m^2.
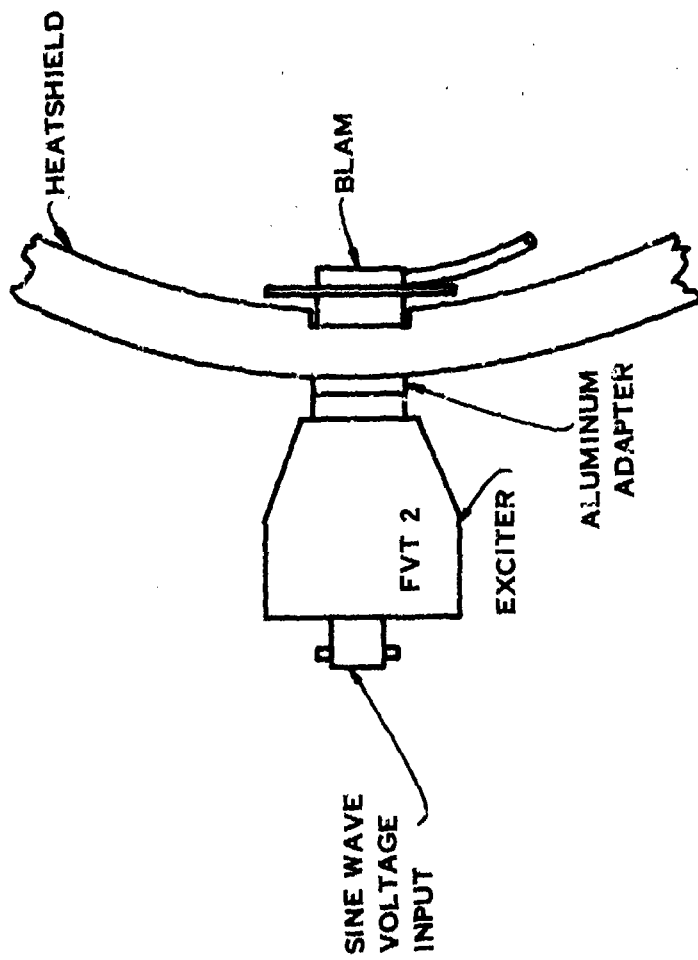
FIGURE 2 FVT-2 CRYSTAL EXCITER APPLICATION

14
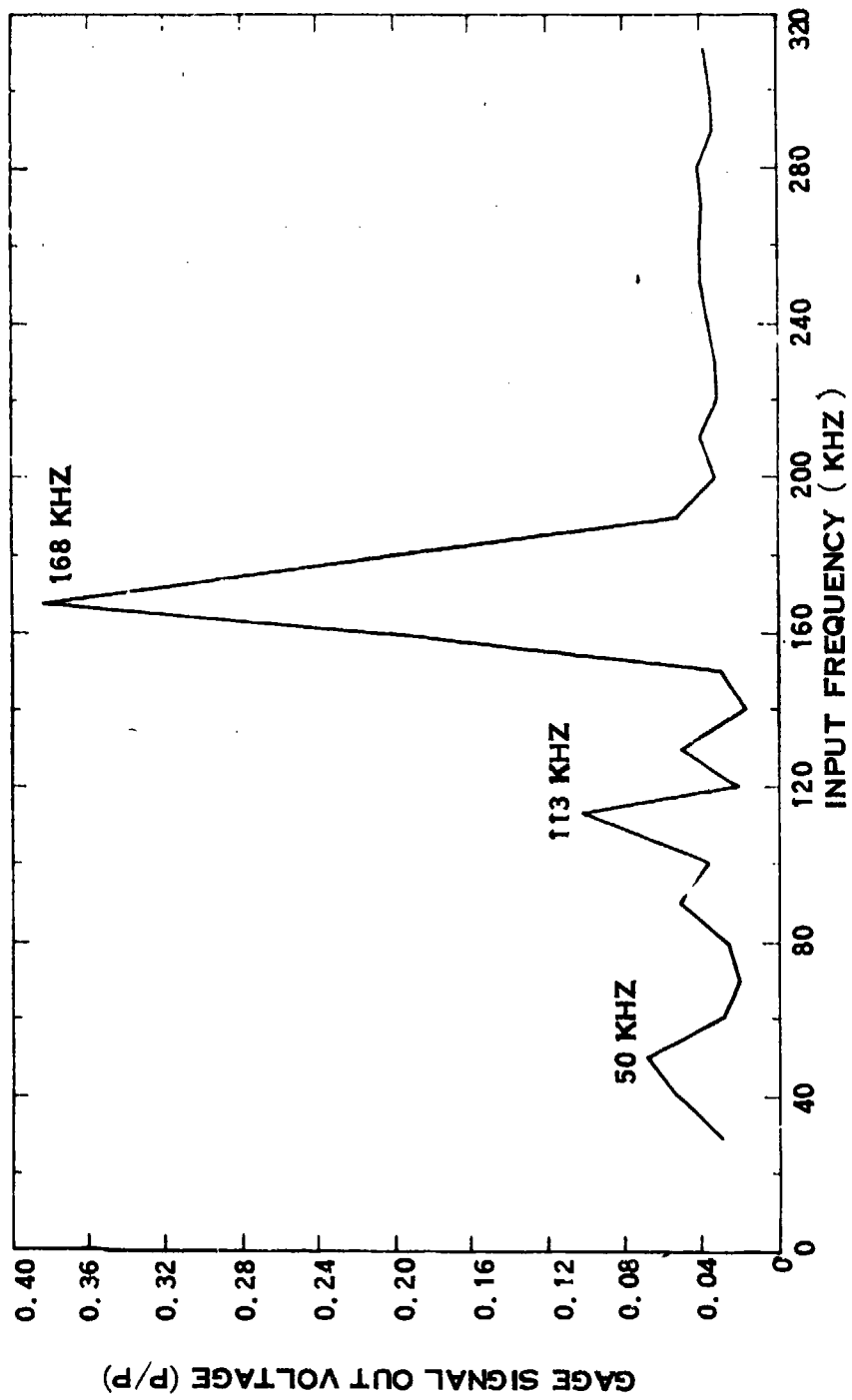
FIGURE 3 PVM ACOUSTIC MONITOR RESPONSE

15

STM-12

The BLAM developed for the STM-12 application is similar
to the PVM gage excepting for a smaller diameter. The STM-12
sensor includes a 1.27-cm diameter quartz crystal and the case
size is proportioned accordingly. A photograph of this BLAM
is shown in Figure 4.

The BLAM's installed on the STM-12 vehicles were tested
using a portable electrostatic stimulator built for that
purpose. This apparatus included a high output voltage
amplifier and a variable frequency oscillator. Approximately
500 volts peak-to-peak sine wave from 10 to 150 kHz was
obtained for exciting the acoustic waves on the surface of the
RV. The surface of the RV was protected from the high voltage
by placing an intermediate aluminum electrode between the
exciter and heatshield. A thin RTV membrane coupled the
acoustic wave from this auxiliary electrode to the heatshield.

Results of the as-installed BLAM tests are shown in
Figures 5, 6, 7 and 8. Each gage was measured at two
frequencies at which resonance peaks had been observed.
These curves show the directionality of the gages vary with
location but consistently drop off in response within one to
four cage diameters. Transducers 1 and 2 were installed at
an aft station which has lower curvature and exhibit greater
rate of amplitude decrease with distance when compared with
number 3 which is behind a highly-curved surface farther
forward on the RV.

A frequency response curve for one of these gages is
shown in Figure 9; this curve exhibits a typical BLAM
response showing resonance peaks at 34, 80, 140 and 280 kHz.
All four gages had similar frequency responses.

16
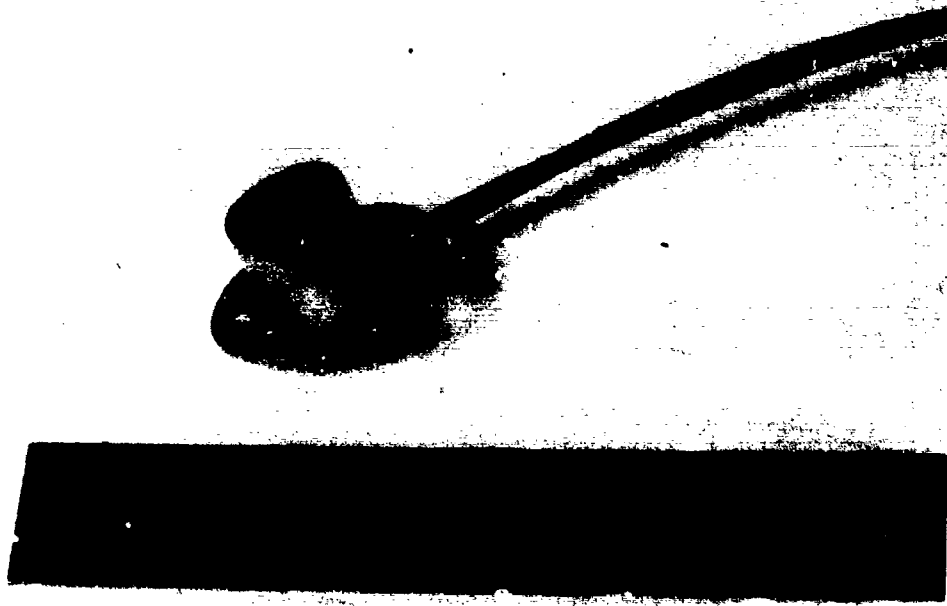
FIGURE 4   STM 12 BLAM
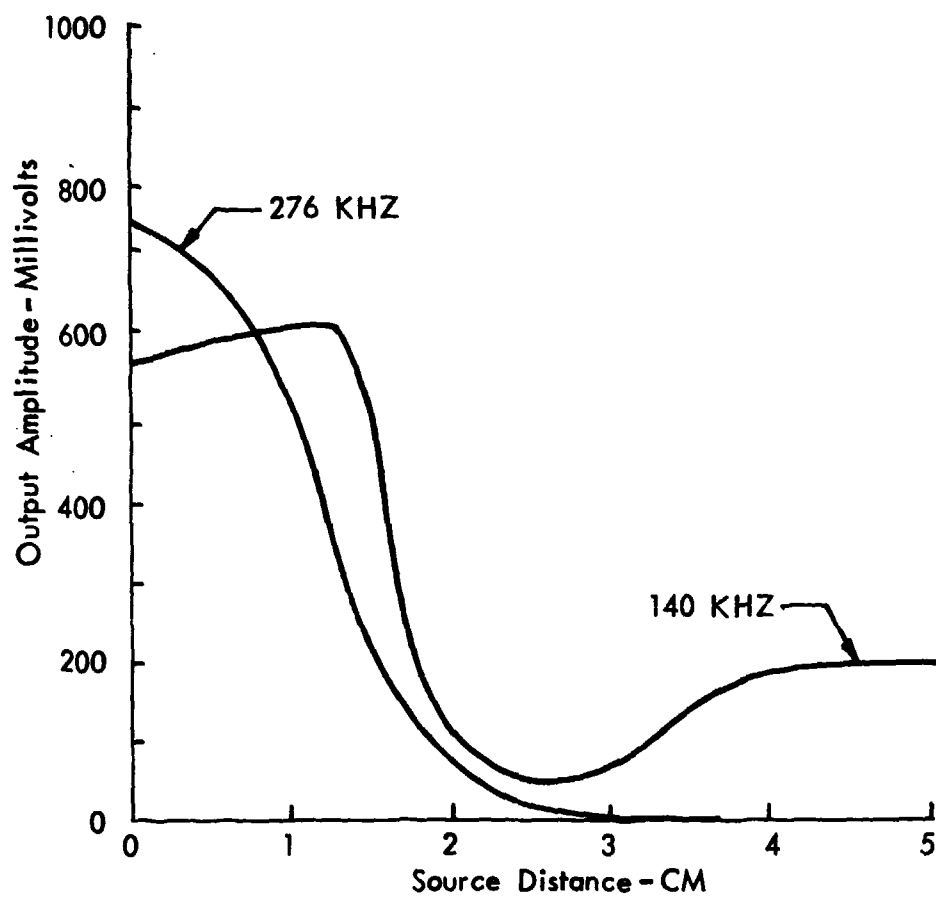
FIGURE 5   DIRECTIONALITY DATA; STM 12 BLAM 1
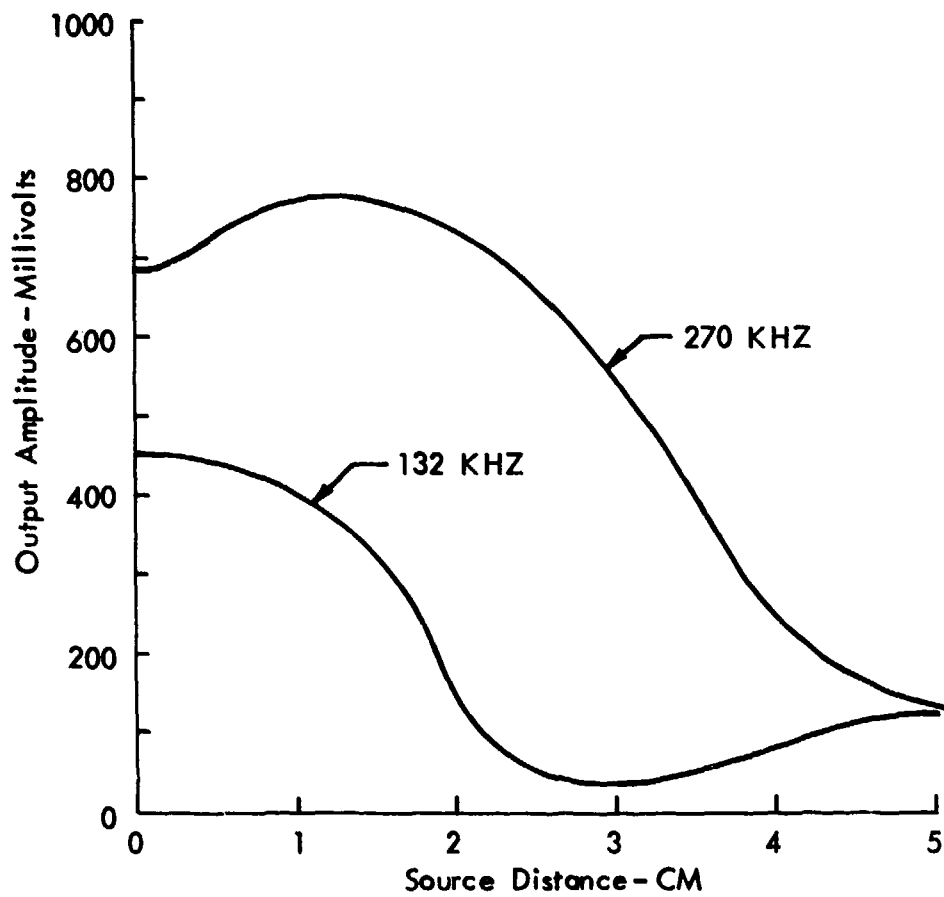
FIGURE 6   Directionality Data; STM 12 BLAM 2
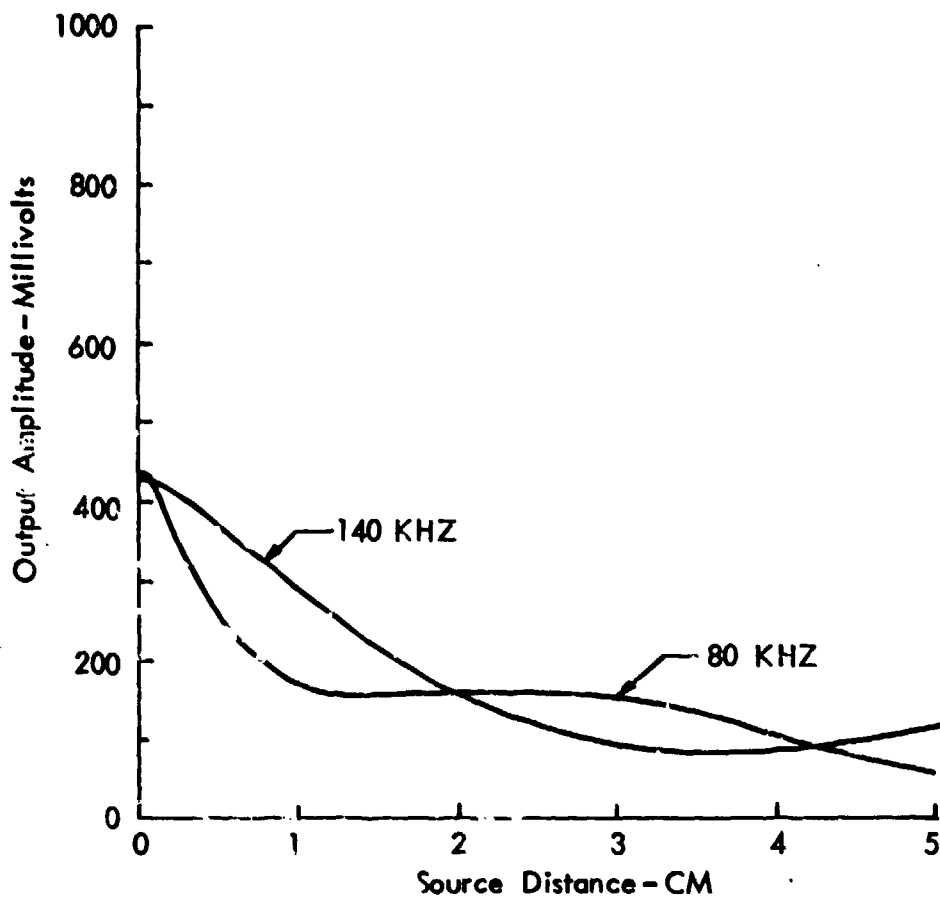
FIGURE 7   DIRECTIONALITY DATA; STM 12 BLAM 3
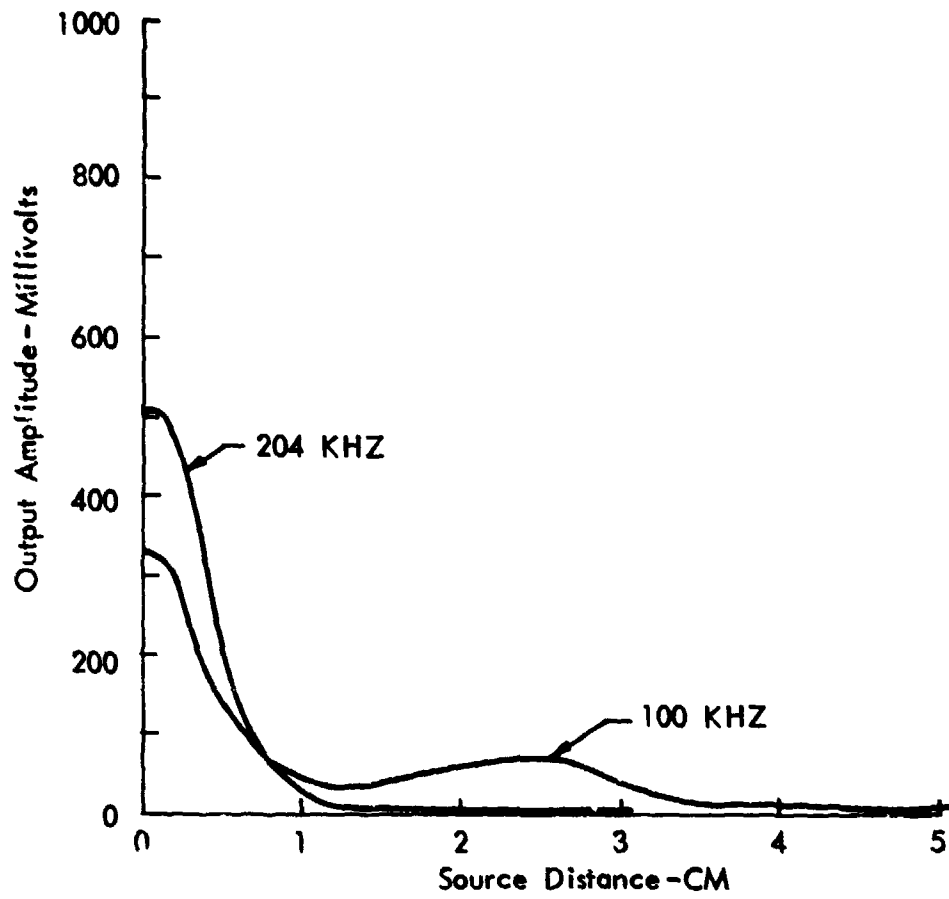
FIGURE 8   DIRECTIONALITY DATA; STM 12 BLAM 4

21
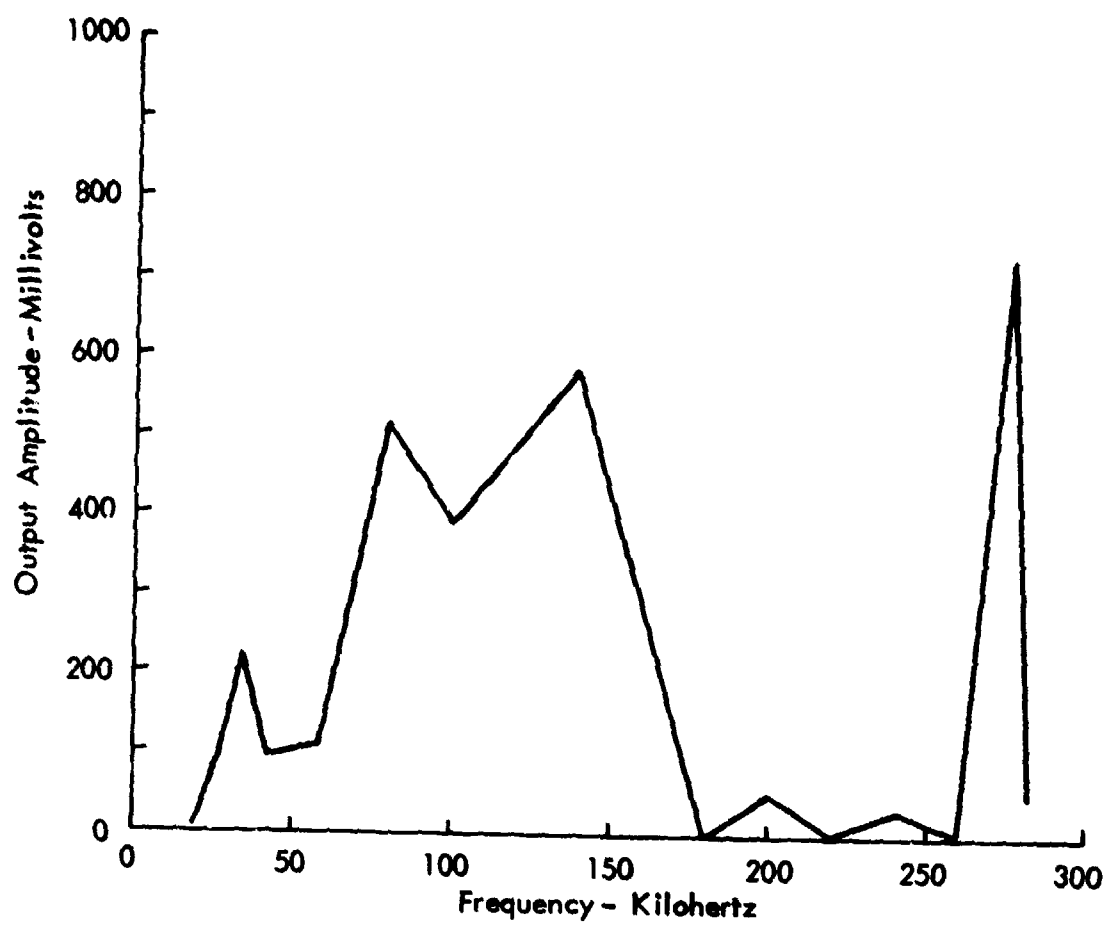
FIGURE 9   STM 12 BLAM INSTALLATION FREQUENCY RESPONSE

2.2 ELECTRONICS DESIGN

An extensive optimization of the electronics was under-
taken to improve performance over that obtained from the
Flame gage. In Flame, an automatic gain control (AGC)
amplifier was used producing the input-output voltage
characteristic curve shown in Figure 10. It can be seen that
resolution above 2 volts output is poor, thus necessitating a
modification of the circuit. Because the magnitude of the
noise to be detected was unknown, it was decided to continue
with the non-linear amplifier principle used on Flame, but
design it to have a linear characteristic when plotted
logarithmically.

The block diagram of the resulting circuit is shown in
Figure 11 and its amplitude input-output characteristic is
plotted in Figure 12. While the curve is not fully linear,
the resolution was improved greatly over the previous circuit;
approximately 4.5 orders of magnitude are spanned by the
amplifier. The circuit includes a simple input voltage
regulator and a temperature-compensated differential detector
in the output. The circuit performs well up to 1 MHz and has
a low frequency roll-off starting at about 100 kHz. The curves
of Figure 13 show the amplifier frequency response at two
output levels.

Components of the amplifier are mounted on a small printed
circuit board which is placed in an aluminum box and hard-
potted with epoxy. Mechanical design of the amplifier box is
shown in Figure 14. Weight of this amplifier is 80 grams.

23
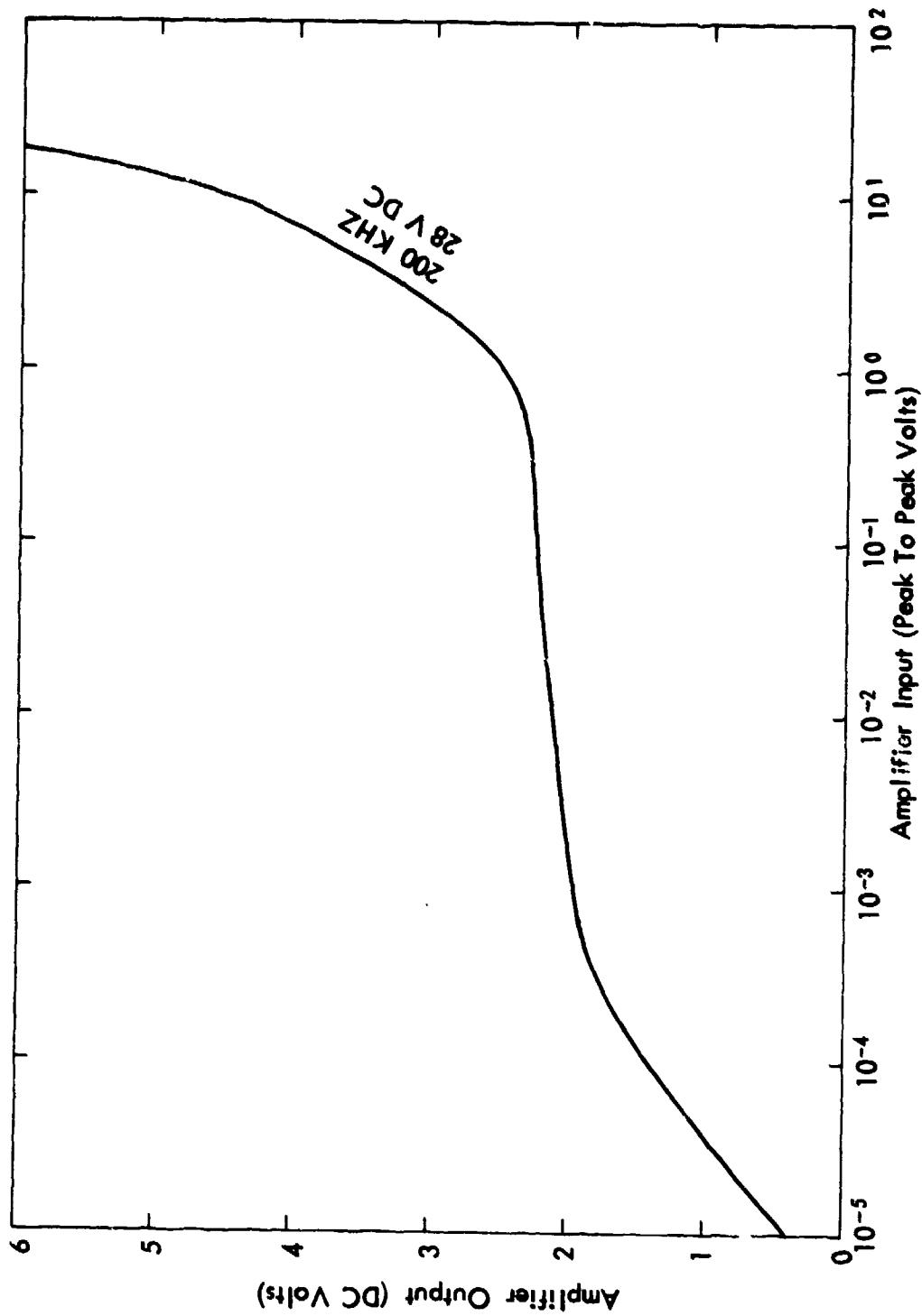
FIGURE 10   BOUNDARY LAYER ACOUSTIC MONITOR AMPLIFIER GAIN
CHARACTERISTICS FLAME VERSION
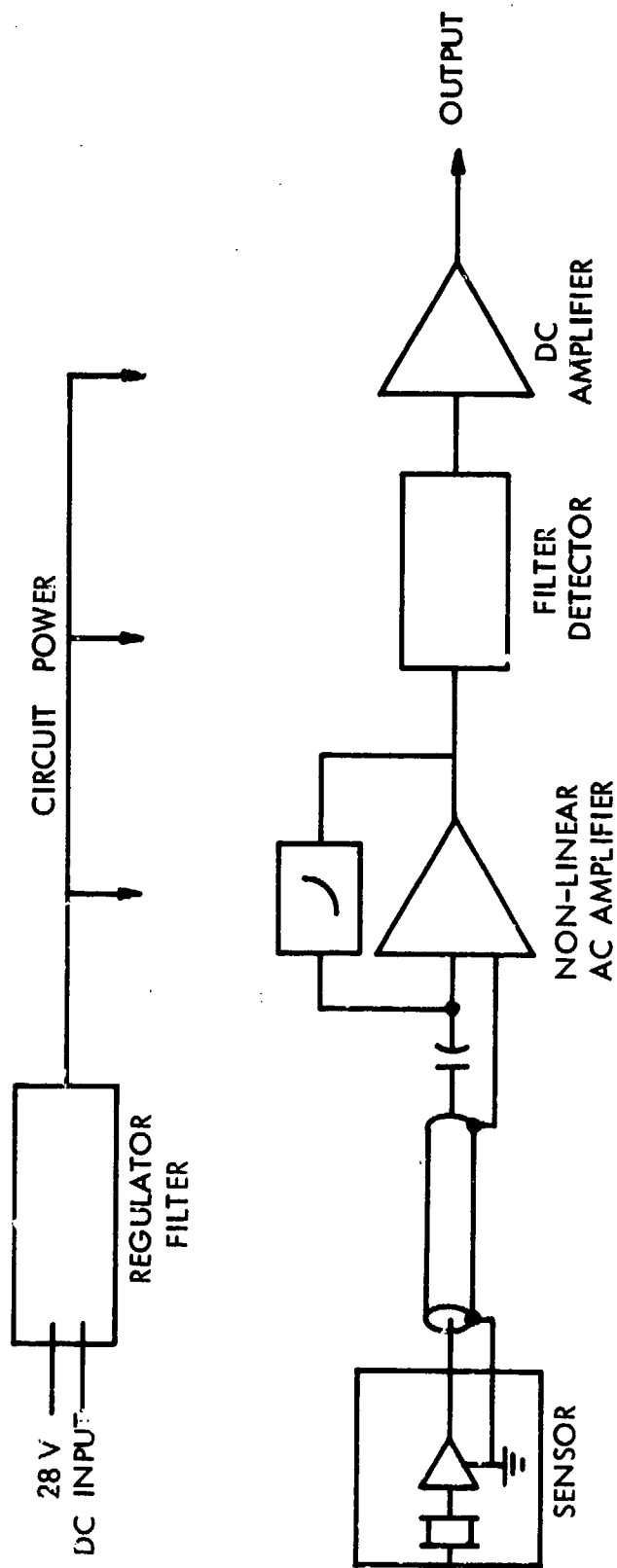
FIGURE 11   BLAM AMPLIFIER BLOCK DIAGRAM

25
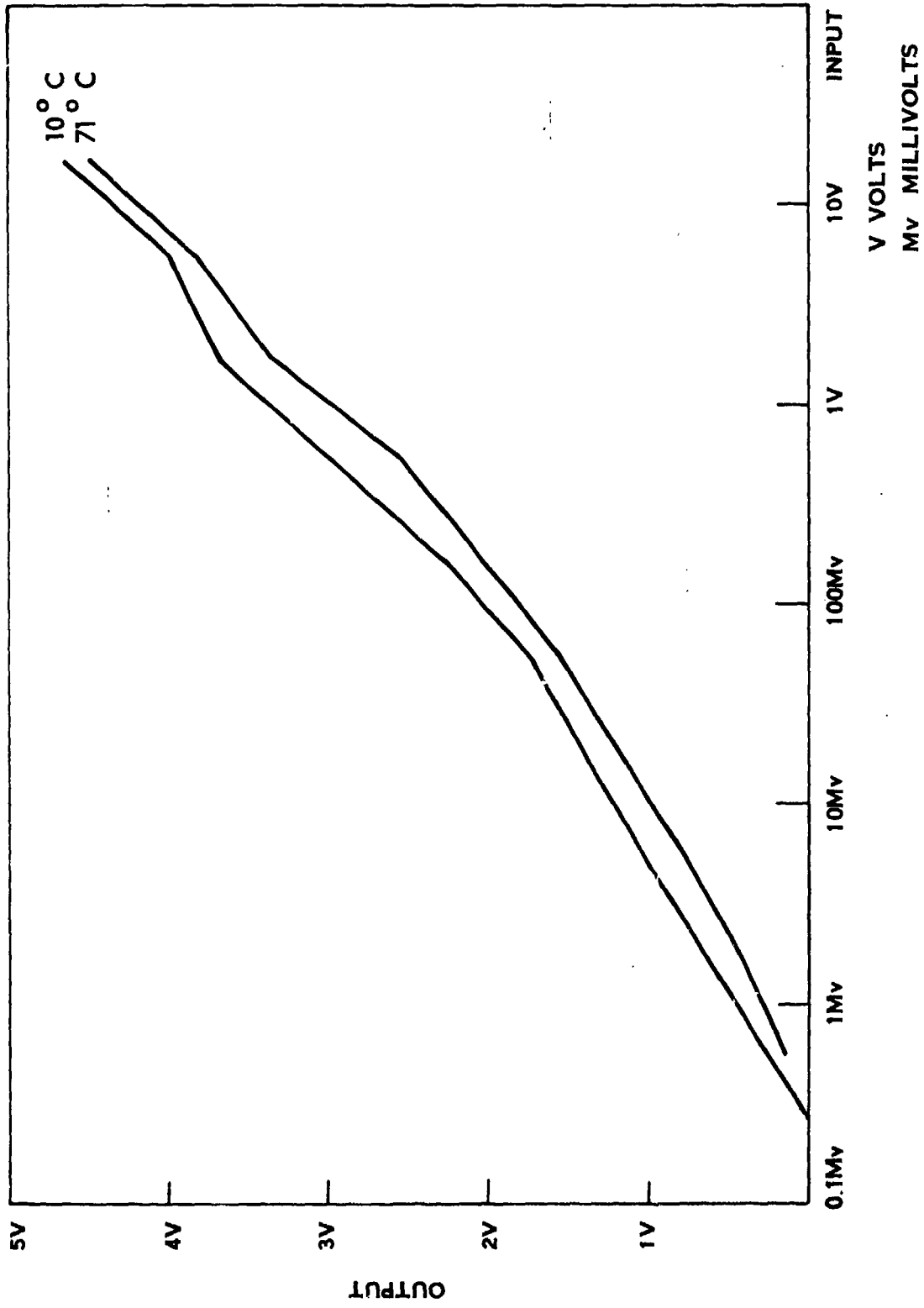
FIGURE 12 ACOUSTIC MONITOR AMPLIFIER CHARACTERISTICS

26
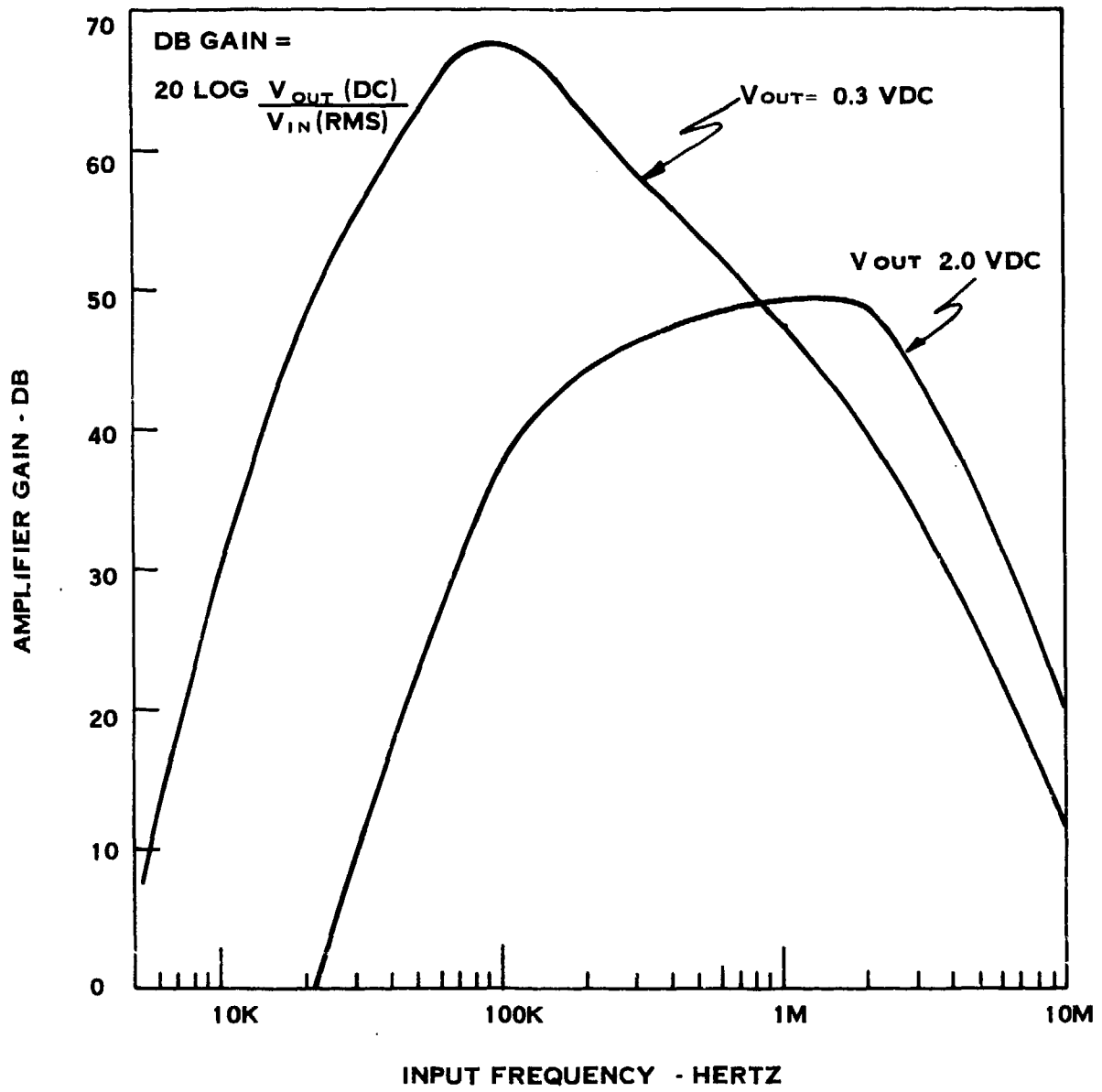
FIGURE 13   BLAM AMPLIFIER FREQ. RESPONSE

27

ELECTRICAL SPECIFICATIONS

1. INPUT REQUIREMENTS
   28 ± 4V DC
   15 m AMP

2. OUTPUT
   0-5VDC
   50 μSEC RISE TIME
   Zo ≤ 10K

TO +28 VDC

SIGNAL OUTPUT

TO TRANSDUCER

1.52 CM

6.35 CM

5.72 CM
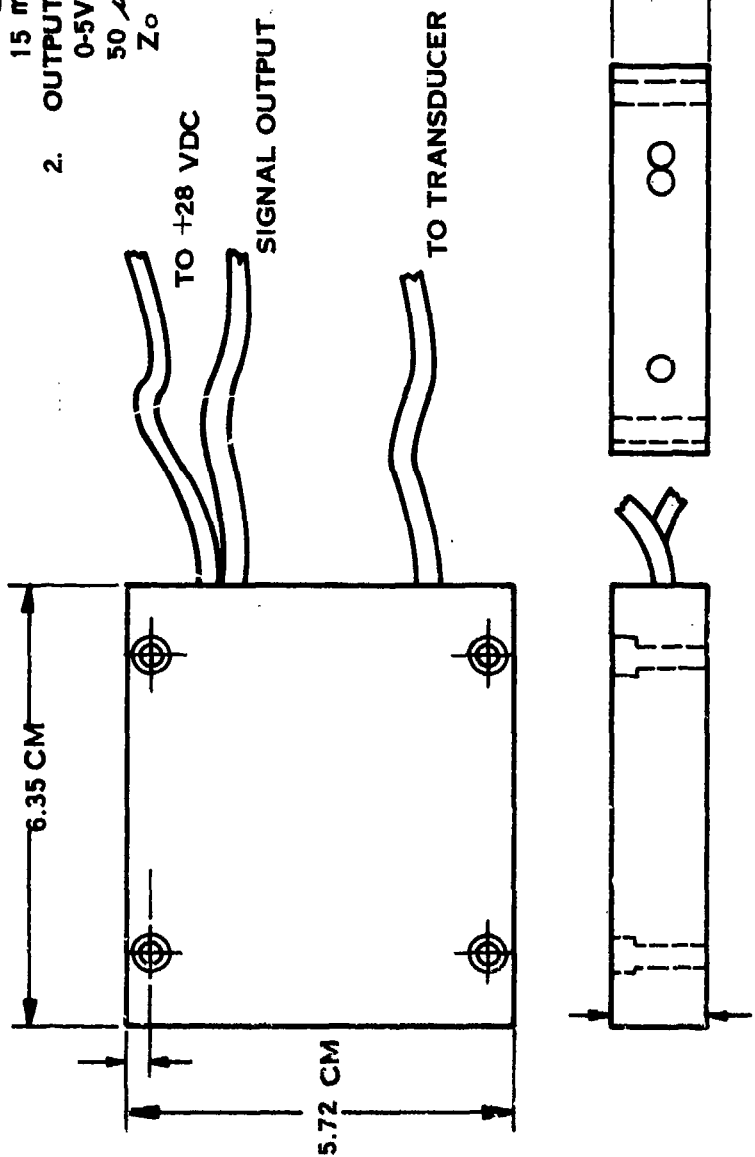
NOTES: 1. CABLE LENGTHS TO BE SPECIFIED FOR EACH APPLICATION.

2. CONNECTOR TYPES OR PIGTAILS TO BE SPECIFIED FOR EACH APPLICATION

3. CABLE MASS — 3.6 g PER FOOT

FIGURE 14   AMPLIFIER FOR BOUNDARY LAYER ACOUSTIC MONITOR

SECTION 3

FLIGHT QUALIFICATION TESTS

To establish reliability of the BLAM, a comprehensive set of environmental tests were conducted. The criteria for these tests were established during discussions with Aerospace, General Electric Company, TRW, and SAMSO personnel directly concerned with the PVM 12 and 13 flights.

The types and levels of environments resulting from these communications are given in Table 1. Tests were conducted on two complete PVM BLAM channels as per Table 1 and were 100% successful. A report of this work was completed and forwarded to concerned organizations[8]. Additional tests of the same type and level were completed on the sensor developed for the STM-12 RV's. As with the PVM sensor, the results were successful (no failures). A report was completed and forwarded[10].

TABLE 1   FLIGHT QUALIFICATION ENVIRONMENTS

Vibration-Powered Flight   Random. Level 25g rms dis-
                                    tributed as per required
                                    spectrum.

Shock-Powered Flight   Up to 825g as per required
                                    shock spectrum.

Acceleration-Linear   140 g's 2 minutes

Temperature $71.1^{\circ}C$ one hour

Spin/Spin Acceleration $2000^{\circ}/sec^2$ to $2000^{\circ}/sec$
                                    operating

                                    $2000^{\circ}/sec^2$ to $8000^{\circ}/sec$ non-
                                    operating

Endurance   150 hours

Electromagnetic Interference
    Conducted Emission   Less than 50 MV p-p

    Conducted Susceptibility   Less than 25 MV p-p for specified
                                    input conditions.

Humidity (Non-operating)   MIL-STD-310 Method
                                    507.1 Temperature
                                    $57.2^{\circ}C$ max.

SECTION 4

FLIGHT TEST ACTIVITIES

4.1 GAGE CHARACTERIZATION TESTS

Each of the PVM and STM-12 BLAM channels fabricated for delivery to G.E. for later installation or for spares were subjected to a series of tests for operational assurability purposes. Statements governing the Operational Assurability tests were included in a specification for the BLAM[9]. The OA tests included temperature soak at 71.1°C and sinusoid-swept vibration from 60 to 2000 Hz at 3.5 g rms level.

All flight test amplifiers were tested for their input-output voltage transfer characteristic in accordance with the specification[9]. The data for the amplifiers delivered to G.E. are included in this report in Appendix A. These curves are obtained by exciting a preamplifier at its input and recording the d.c. voltage output; the input frequency used was 200 kHz for both PVM and STM amplifiers.

4.2 LIAISON/ICD ACTIVITIES

Early meetings were held at G.E. in order to agree on Interface Control Drawing details necessary for the installation of the BLAM's on the PVM and STM RV's. Documentation provided by KSC included circuit diagram, sensor and electronics mechanical drawings, cabling and connection data. The drawing was produced by G.E. and signed off by all organizations.

Installation of the sensors on the RV's was to be physically effected by G.E. with KSC present and monitoring. To facilitate this operation KSC prepared an instruction memorandum detailing the steps to be followed. After installation and with electronics connected, a checkout procedure was written which would permit a qualitative excitation of the BLAM to ensure that the channels are operative.

All gages were installed successfully and produced good results as reported elsewhere.

SECTION 5

GROUND TESTS

5.1 INTRODUCTION

Wind tunnel tests were planned and carried out to test the BLAM in a controlled flow environment with the purpose of characterizing its mode of operation. It was hoped that the results of the ground tests would then be used to provide better understanding of BLAM flight test data.

The first test was completed in the small laboratory, room temperature, continuous running Mach 3 tunnel at Aeronutronic Ford* in Newport Beach, California. Dr. A. Demetriades is in charge of this facility and assisted in planning and carrying out the test.

The second test utilized Tunnel 8 at the Naval Surface Weapons Center in White Oak, Maryland. Dr. Fred Morrison and Mr. Frank Baltakis provided planning and test assistance.

In both tests, the approach was similar; the free-stream Reynolds number of the flow was varied to cause transition in the boundary layer to move across the positions where the BLAM's were installed. Output from the BLAM's were compared with temperature and pressure sensors. The following sections describe the individual tests in greater detail.

---

*Now Ford Aerospace and Communications Corporation.

5.2 AERONUTRONIC FORD SUPERSONIC WIND TUNNEL TEST

The test arrangement is shown in Figure 15. The BLAM was placed at various locations on the exterior surface of the tunnel side wall. A ported pressure transducer was installed 28 cm downstream from the nozzle. The tunnel side wall is 1.9-cm thick lucite. Flow parameters for the test were as follows:

Mach No.:	$3.0 \pm .03$
Total Temperature:	$38^{\circ}C$
Supply Pressure P_o:	210 to 730 mm Hg abs
Reynolds Number:	1,970,000 to 6,693,000 $meter^{-1}$

By varying the supply pressure from low to high, the transition region was caused to traverse the side walls from downstream at low pressure thence upstream past the BLAM location towards the nozzle.

Results from a pressure sweep are shown in Figure 16 for both transducers: BLAM and ported pressure. It can be seen that the pressure gage responded very well to transition on the side wall. The BLAM output, however, appears to be linearly related to the total pressure, not indicating a significant change in output in the transition zone.

An explanation for the apparent lack of BLAM response to transition is that the frequency response of the blam extends from 75 kHz upward to 500 kHz while the ported pressure gage responds to frequencies below 20 kHz. In wind tunnel experiments of this type, transition pressure fluctuations in the boundary layer may be significantly higher at low frequencies.

34
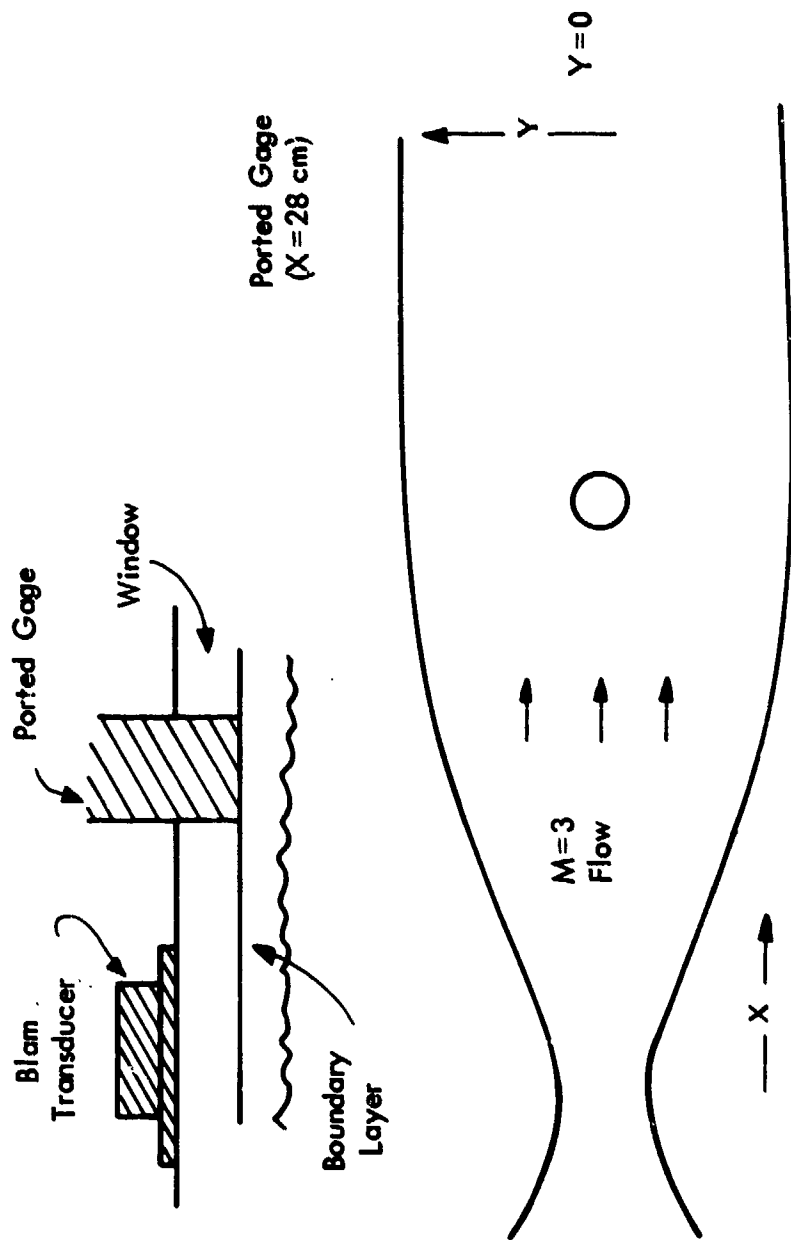
FIGURE 15   TEST INSTALLATION

Window

Ported Gage

Blam
Transducer

Boundary
Layer

Ported Gage
(X = 28 cm)

Y = 0

Y

M = 3
Flow

X

35
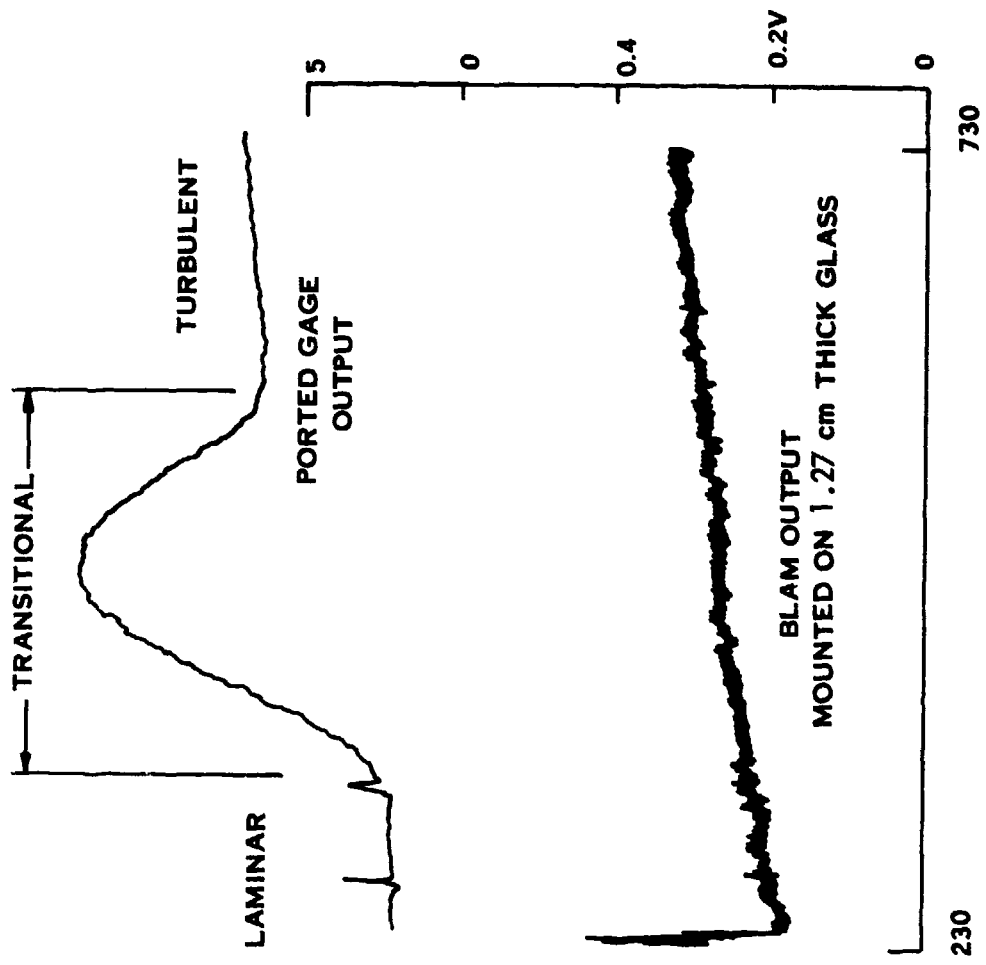
FIGURE 16   TRANSDUCER OUTPUT COMPARISON

High frequency components in the boundary layer are not lacking but must compete with the relatively high noise background from the nozzle and other upstream disturbances.

In addition to radiated tunnel noise, the tunnel wall vibrating in a diaphram mode added to the sensor output. During the test, both d.c. voltage from the electronics signal conditioner and the a.c. output from the sensor were monitored. It was noticed that the sensor output had a dominant frequency of 16 kHz or 25 kHz depending on the thickness of the tunnel side wall window. For 1.27-cm optical glass, the frequency was 25 kHz and for 2.54-cm lucite it was 16 kHz. While higher than the lowest plate resonance, such frequencies could well be excited on walls of these thicknesses.

Table 2 is a listing of BLAM data from the test. Listed are the d.c. output levels, corresponding sensor a.c. levels and the amplifier midband gain compared to the ratio of sensor and d.c. outputs. These data show that the dominant frequencies in the sensor output, even though amplified much less, could have obscured the presence of high frequencies generated by trans-itional/turbulent boundary layers.

TABLE 2   BLAM DATA - AF/SWT

P_O = 730 mm Hg

RUN	PREDOMINANT FREQUENCY kHz	SENSOR OUTPUT mv r.m.s.	ELECTRONICS D.C. OUTPUT mv	RATIO DC/AC	MEASURED MIDLAND AMPL. GAIN
2	25	3.6			
				88.9	3900
4	25		320		
5	16	4.4			
				43.2	4090
6	16		190		

Overall conclusions from this test were that low frequency
attenuation or mechanical mounting to eliminate acceleration
response must be added prior to future wind tunnel tests.
Some indication of transition was present in the data of
Figure 16 in that the slope at lower pressures was steeper
than that after transition. The signal-to-noise in the data
is too low to permit a positive conclusion in this feature.

5.3   NSWC TUNNEL 8 TEST

5.3.1   Summary

This test was planned with the following objectives

a)   BLAM characterization

b)   Correlation of the acoustic level and thermal
     transition monitors

c)   Measurement of transition movement over the model
     surface

d)   Provide backup data for the PVM flight tests.

38

The facility NSWC Tunnel 8, was chosen because it provided parameters suitable for measurement of boundary layer transition phenomena on conical models. This tunnel is well calibrated and has the performance characteristics seen in Figure 17 for the Mach 8 nozzle. Additionally, another DNA program with contractor Prototype Development Associates (PDA) was being planned in the same facility and it was requested by DNA that KSC implement this test in a cooperative effort, using PDA hardware and entry to Tunnel 8. Since PDA had designed the sting interface and data acquisition system,

KSC then designed the mating heatshield and nosetip. After some liaison, this approach was worked out and the remainder of the test was designed.

The test matrix is shown in Table 3. Test variables included angle of attack, spin rate, and Reynolds number (or total pressure - see Figure 17). Runs were patterned to provide increasing complexity of conditions and to permit comparisons of parameters before proceeding with the next run. The four runs shown in the matrix were completed over a two day period.

The test model was a 9° half-angle sharp cone with 20.3 cm base diameter; the nosetip was stainless steel fabricated by KSC and the frustum was carbon-phenolic heatshield procured from Hitco. The frustum thickness was 0.953 cm. The frustum was instrumented with six BLAM's and six thermal sensors installed as shown in Figure 18.

The BLAM's installed on the heatshield for this test were identical to those described in Section 2.0 which were installed on the PVM-12 and PVM-13 reentry vehicles. The thermal sensors were similar to calorimeters and are illustrated in the cross-section drawing of Figure 19. The thermal sensors were fabricated from a short piece of ceramic

39

TABLE 3   NSWC TEST MATRIX

RUN NO.	CONDITIONS		ACTIVITY
1	$\alpha = 0$ Non-Spinning R_E Sweep	●	Tunnel and Instrumentation Set Up
2	$\alpha = 0$ Non-Spinning R_E Sweep	● ●	Acoustic-Thermal Comparison Shadowgraph Correlation
3	$\alpha = 0$ Non-Spinning Tunnel Pre-Heat R_E Sweep	● ●	Acoustic-Thermal Comparison Shadowgraph Correlation
4	$\alpha = 2.5^O$ Spinning Tunnel Pre-Heat R_E Plateau	● ●	Acoustic Directionality Shadowgraph Correlation
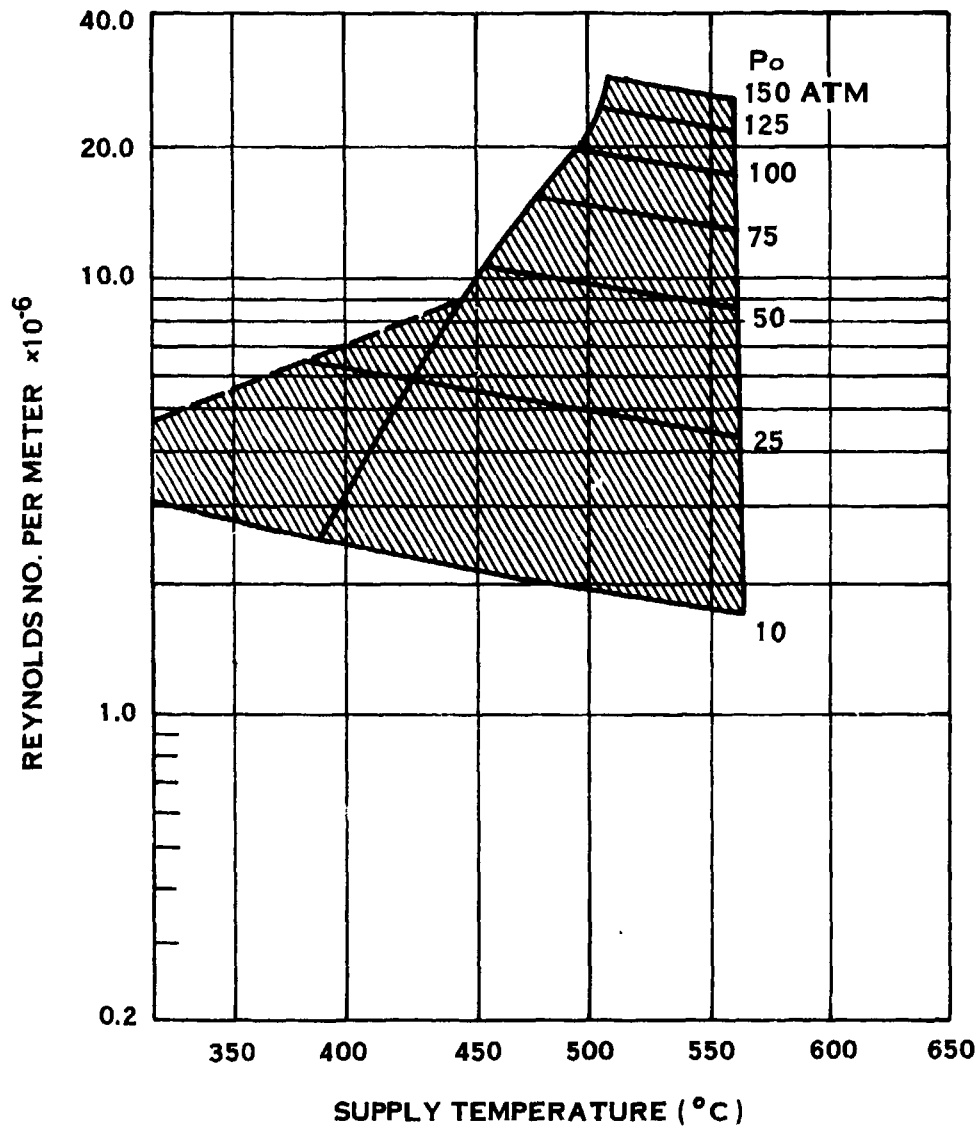
FIGURE 17   MACH 8 NOZZLE CAPABILITY

41

20.32 CM

63.98 CM

TEMP. SENSORS

TRANSDUCERS

NOSE TIP

9°
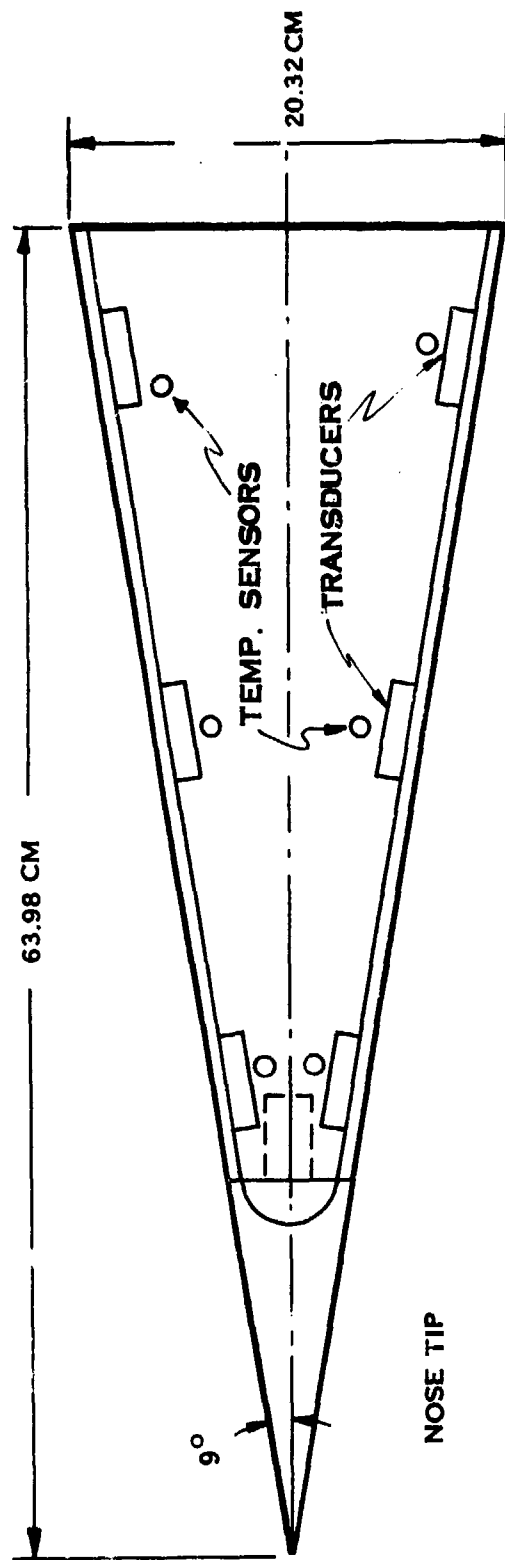
FIGURE 18 WIND TUNNEL TEST MODEL, THERMAL AND
BLAM SENSORS MOUNTED
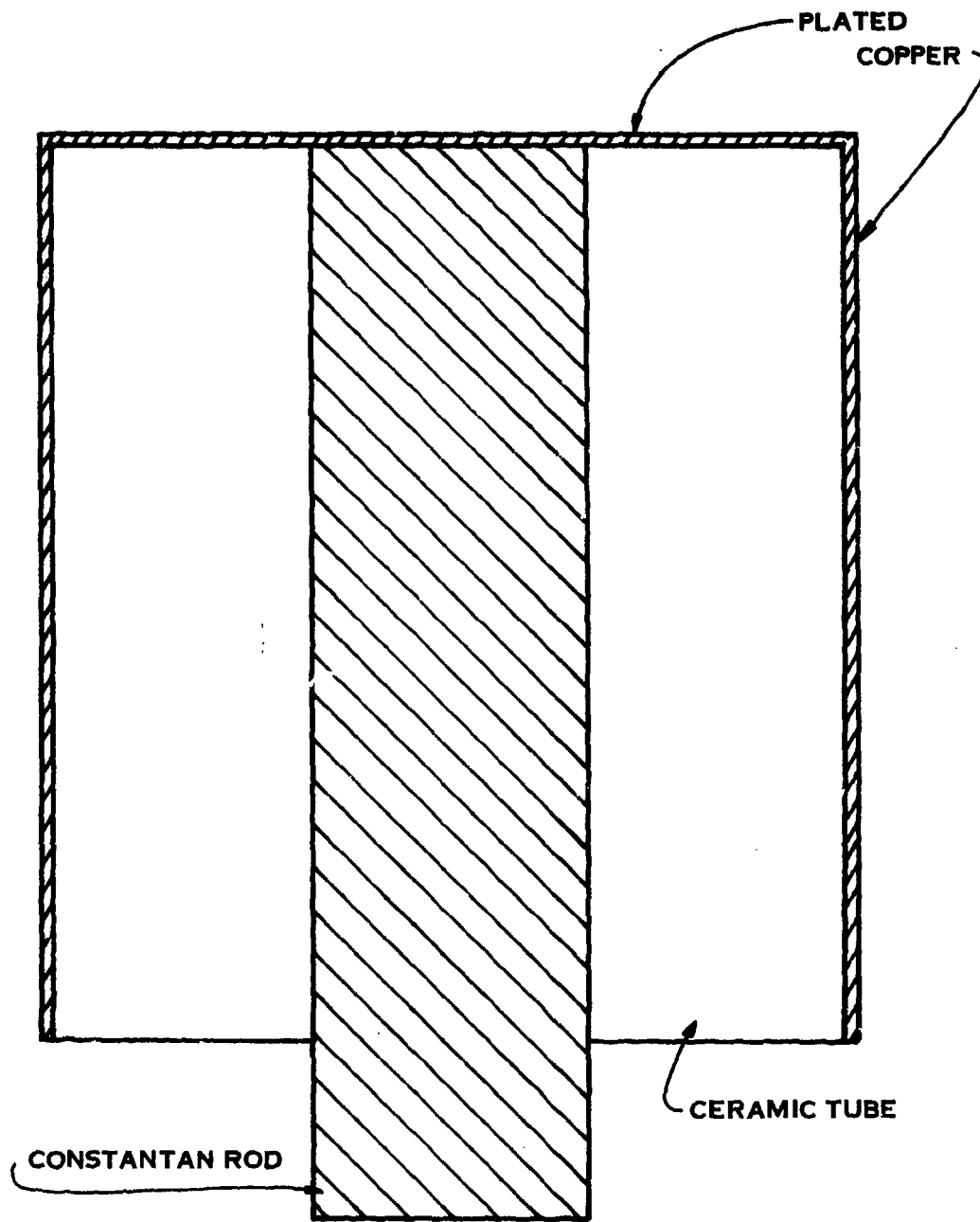
FIGURE 19   WIND TUNNEL MODEL THERMOCOUPLE SENSOR

tube, one end of which a copper film was vapor deposited. A constantan wire was then inserted in the tube and peened over to hold it in place. The final step was to plate the end of this assembly with copper to form a .005 cm end covering. The sensing thermocouple junction was formed by the copper plating in contact with the constantan rod. This sensor exhibited a time constant near 15 msec.

After the Aeronutronic-Ford test, it was recognized that additional filtering and acoustic isolation would be needed to obtain good signal-to-noise ratio. Two specific measures were undertaken: 1) Provide acoustic isolation for the heatshield to decouple it from the sting vibration and 2) electronically filter out the low frequency components picked up by the BLAM sensor. Figure 20 illustrates the method used to isolate the heatshield from the substructure. "O" rings were used between support rings and a silicone rubber damping wafer was placed between the nosetip and heatshield.

To filter out the low frequency components in the sensor output, an amplifier was designed to have sharp rolloff below 200 kHz. The frequency response function of this amplifier is shown in Figure 21. This amplifier was also designed to have a linear amplitude function as contrasted with the BLAM amplifier. A linear gain was used because the boundary layer noise was expected to be very low in amplitude due to low static pressures on the model.

5.3.2 Tunnel 8 Test Results

Data from the test model were recorded by NSWC either digitally with a computerized sampling system or on analog tape with a Honeywell 5500 c.c. recorder. Model thermal sensors

44
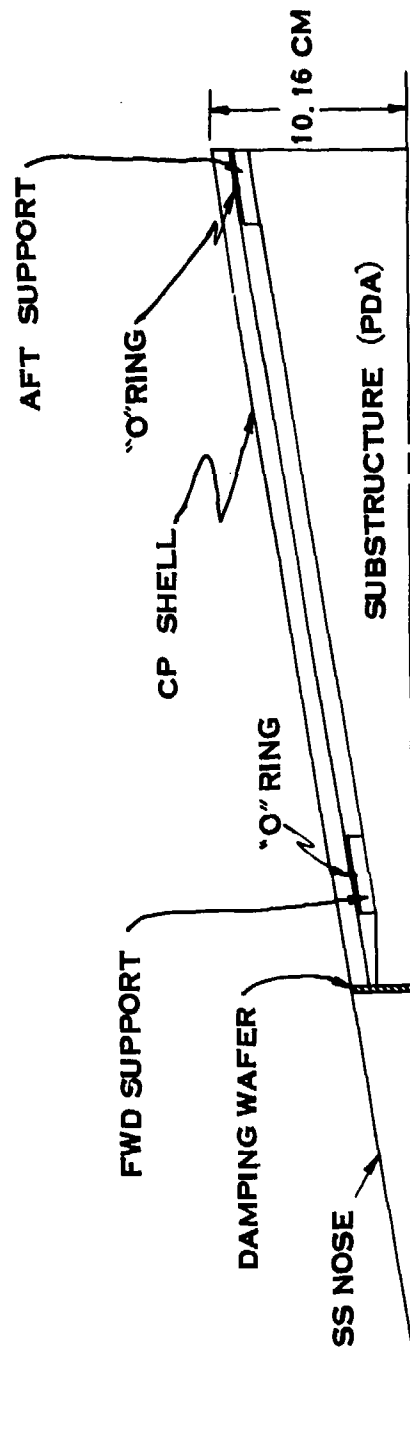
FIGURE 20   VIBRATION ISOLATION NSWC 9° TEST MODEL

45

OUTPUT LEVEL =2.0 VDC

DB GAIN =20 LOG

$$\frac{2}{V_{IN} (RMS)}$$
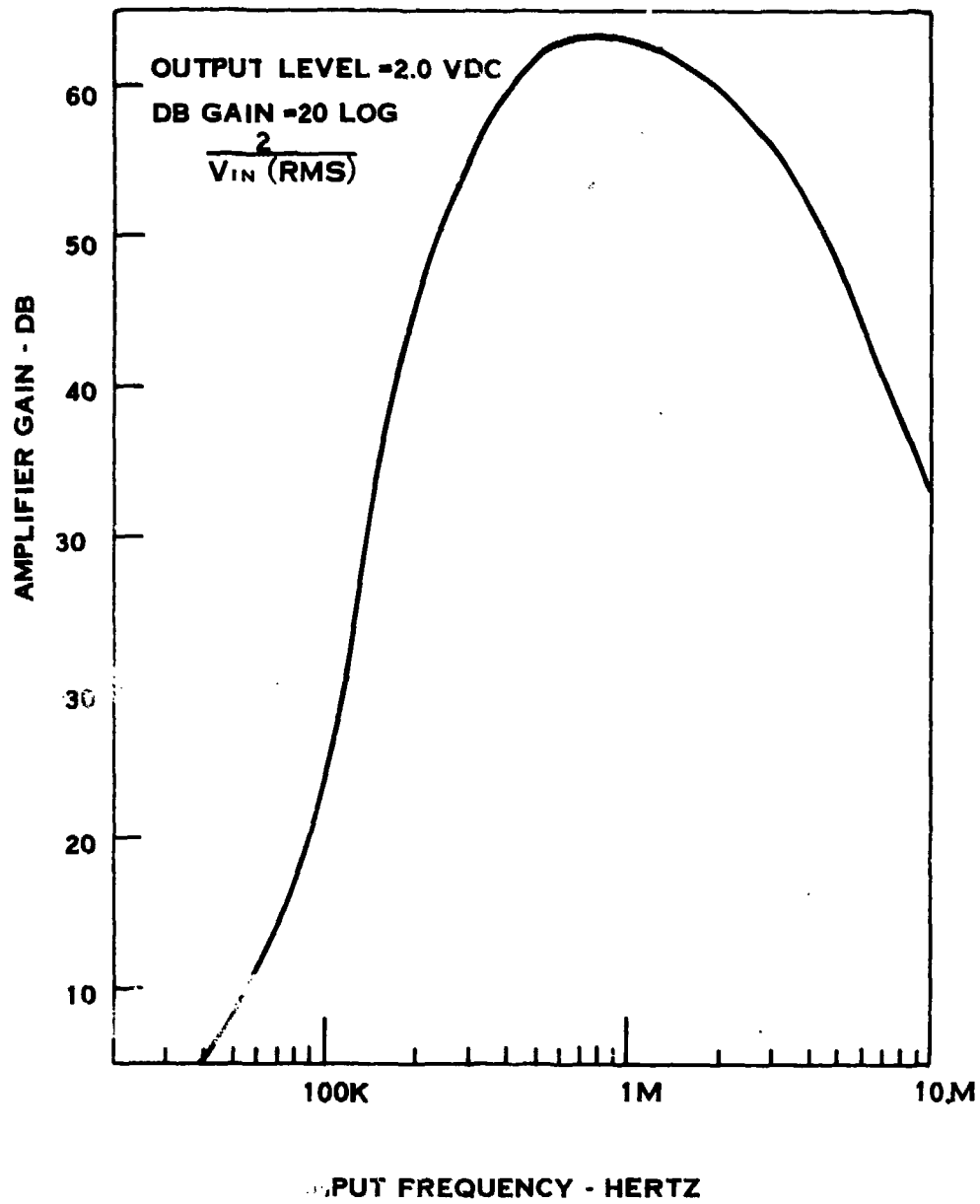
FIGURE 21   WIND TUNNEL TEST AMPLIFIER FREQ. RESPONSE

46

and tunnel conditions plus a timing signal were recorded on
the digital system at a rate of approximately 50 samples per
second. Data channel allocations are shown in Table 4.

<div align="center">TABLE 4   TUNNEL 8 TEST DATA CHANNELS</div>

Digital

0 through 7	PDA Force balance outputs
8	Time shared: P_O scan 1
	T_O scan 2
9	α - angle of attack
10 through 15	KSC thermal sensors T1 through T6
16	Time

Analog Recorder

1 through 6	KSC BLAM outputs
7	IRIG Time

5.3.2.1 Run 1. This test was a 20 sec. run intended
to establish data quality and levels prior to a data run.
It was found that a large low-frequency noise content obscured
BLAM data and that the thermocouple output was very low.
Filters were added to the BLAM circuitry and gain was
increased in the thermocouple channels prior to Run 2.

5.3.2.2 Run 2. During this 25 second test, P_O was
increased gradually over the test period to provide a R_∞
sweep. A plot of the tunnel conditions is given in Figure 22
showing P_O and R_∞ versus time. The R_∞ data were obtained
using P_O and T_O plus the conditions of Figure 17. The tunnel
was not pre-heated prior to taking data.
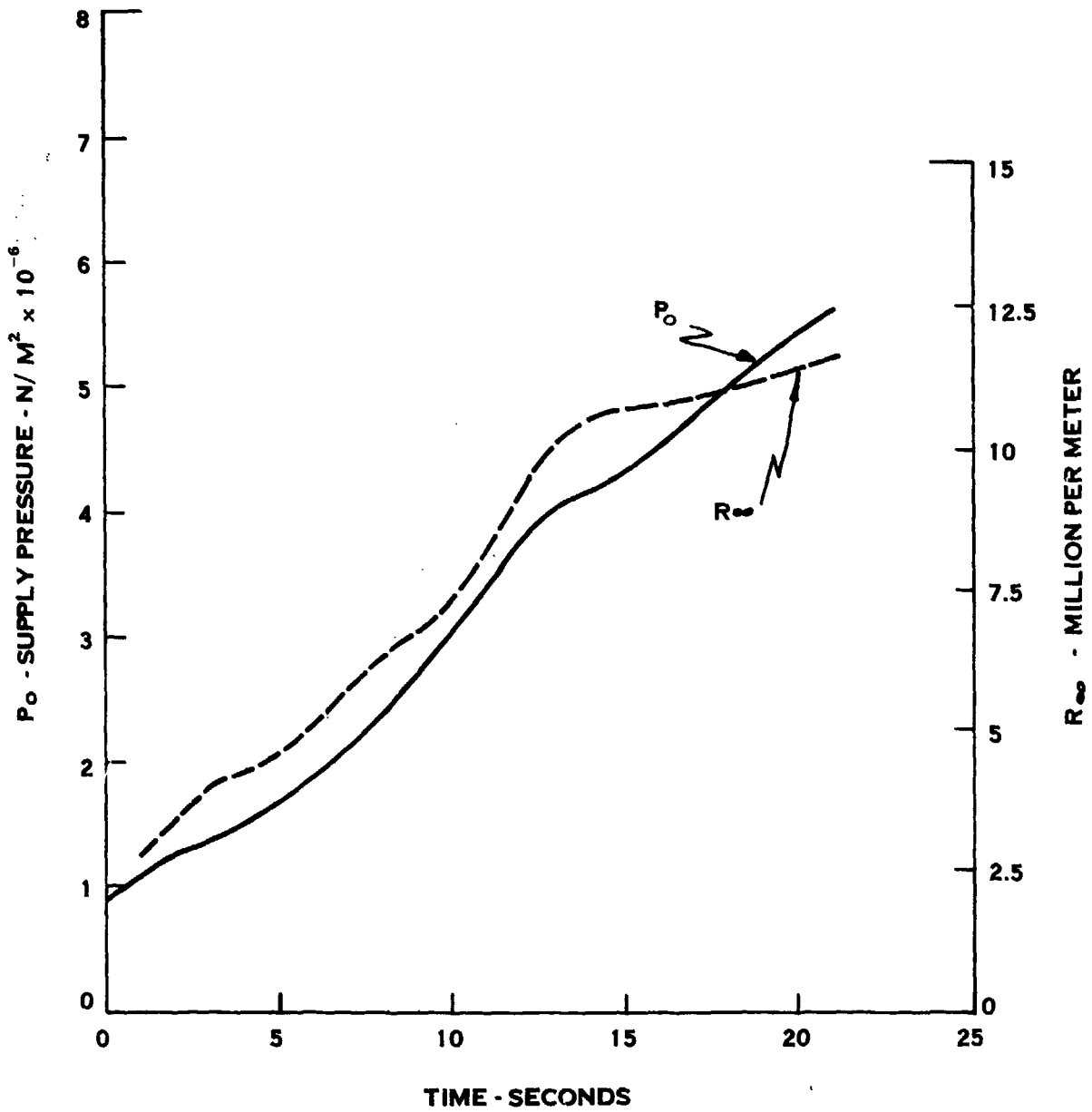
FIGURE 22   RUN 2 FLOW PARAMETERS M8

48

Data from the BLAM and temperature sensors are plotted in Figures 23 through 28. The adjacent thermocouples and BLAM's have been assigned the same numbers and plotted in the same figures. There is some uncertainty as to the relative placement of the BLAM data on the time scale because time code was not recorded during Run 2. By using discontinuities in the data, an attempt was made to line up the traces, but a one or two second error could exist. Sensors numbered 1 and 4 are at the forward-most station on the model, diametrically opposed. Numbers 2 and 5 are located in the center and 3 and 6 are near the aft end. Sensors 1, 2, and 3 are on one azimuth as are 4, 5, and 6 (see Figure 18 for reference locations).

Several features are of particular importance in these figures relating measured noise level to flow characteristics. First, it can be noted that the BLAM channels exhibit a change of level between 10 and 12 seconds into the run and that all except the forward thermocouple traces show a change of slope at about the same time. The tunnel flow conditions at this time are pressure of 3 to 4×10^6 N/m^2 and Reynolds number of 6.9 to 7.5 million per meter.

Other investigators[1,2,3,4,5,6] who made measurements of boundary layer noise in wind tunnels have reported similar noise amplitude characteristics, showing that the root-mean-square noise level in the transitional boundary layer increased orders of magnitude over that of laminar flow. The transition nois level was also larger than that from the boundary layer at Reynolds numbers (R_∞) where full turbulence had been just achieved. These same researchers also noted that the boundary layer condition can be related to R_∞; i.e. the flow progressed from laminar to transitional to full turbulence as R_∞ was increased.
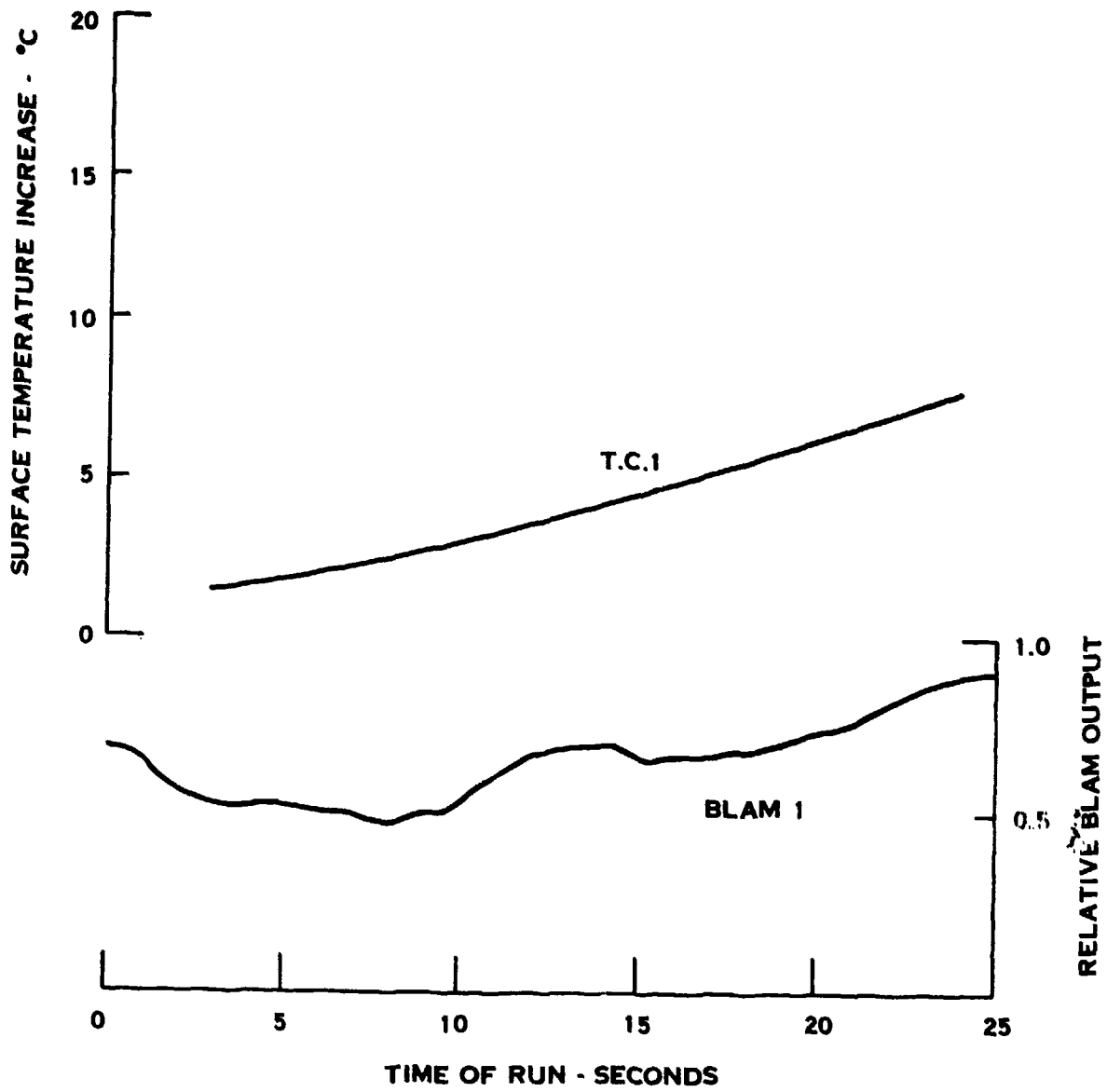
FIGURE 23   RUN 2, BLAM CHANNEL 1, TEMP. SENSOR 1

50
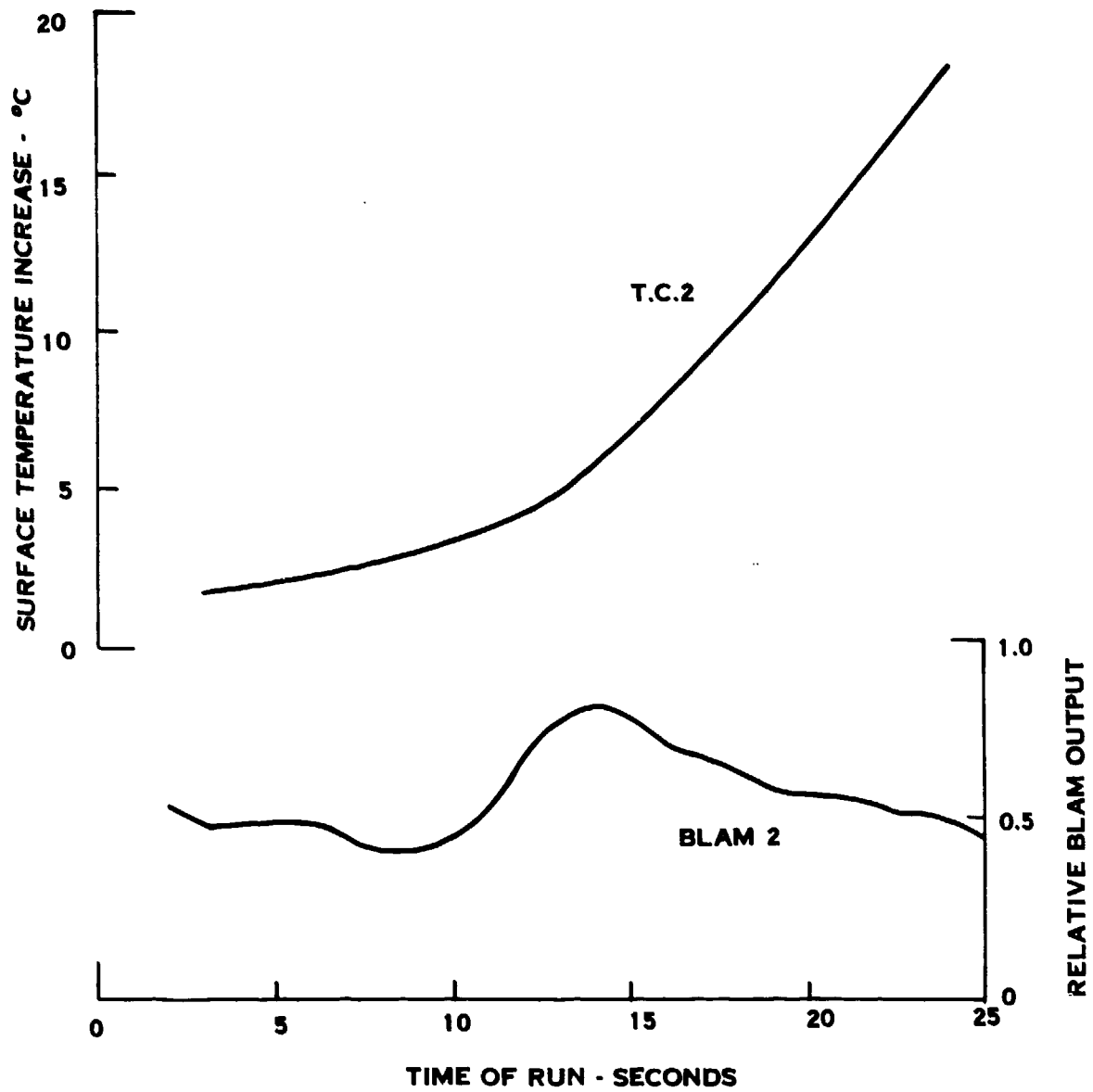
FIGURE 24   RUN 2, BLAM CHANNEL 2, TEMP. SENSOR 2

51
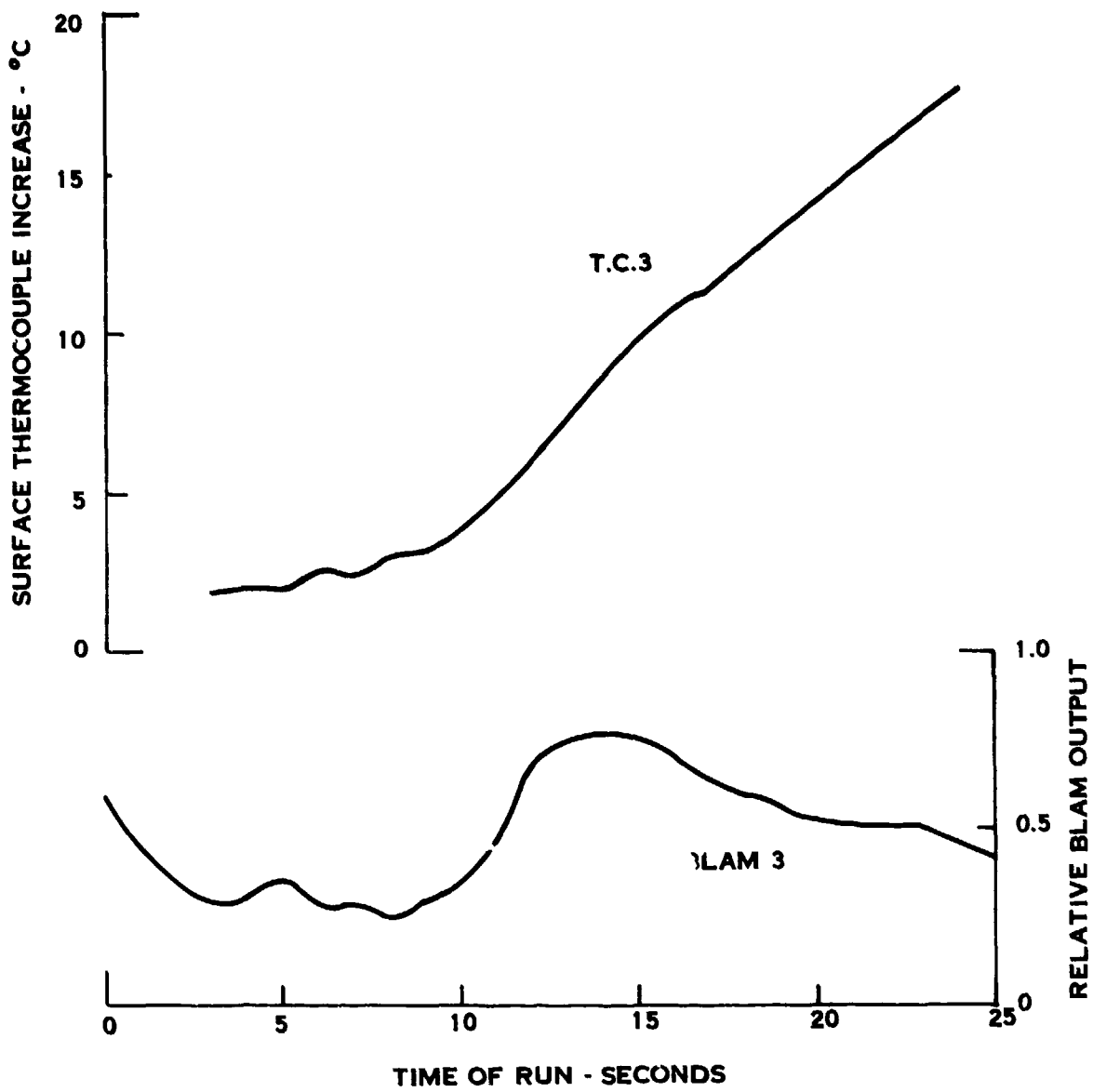
FIGURE 25   RUN 2, BLAM CHANNEL 3, TEMP. SENSOR 3

52
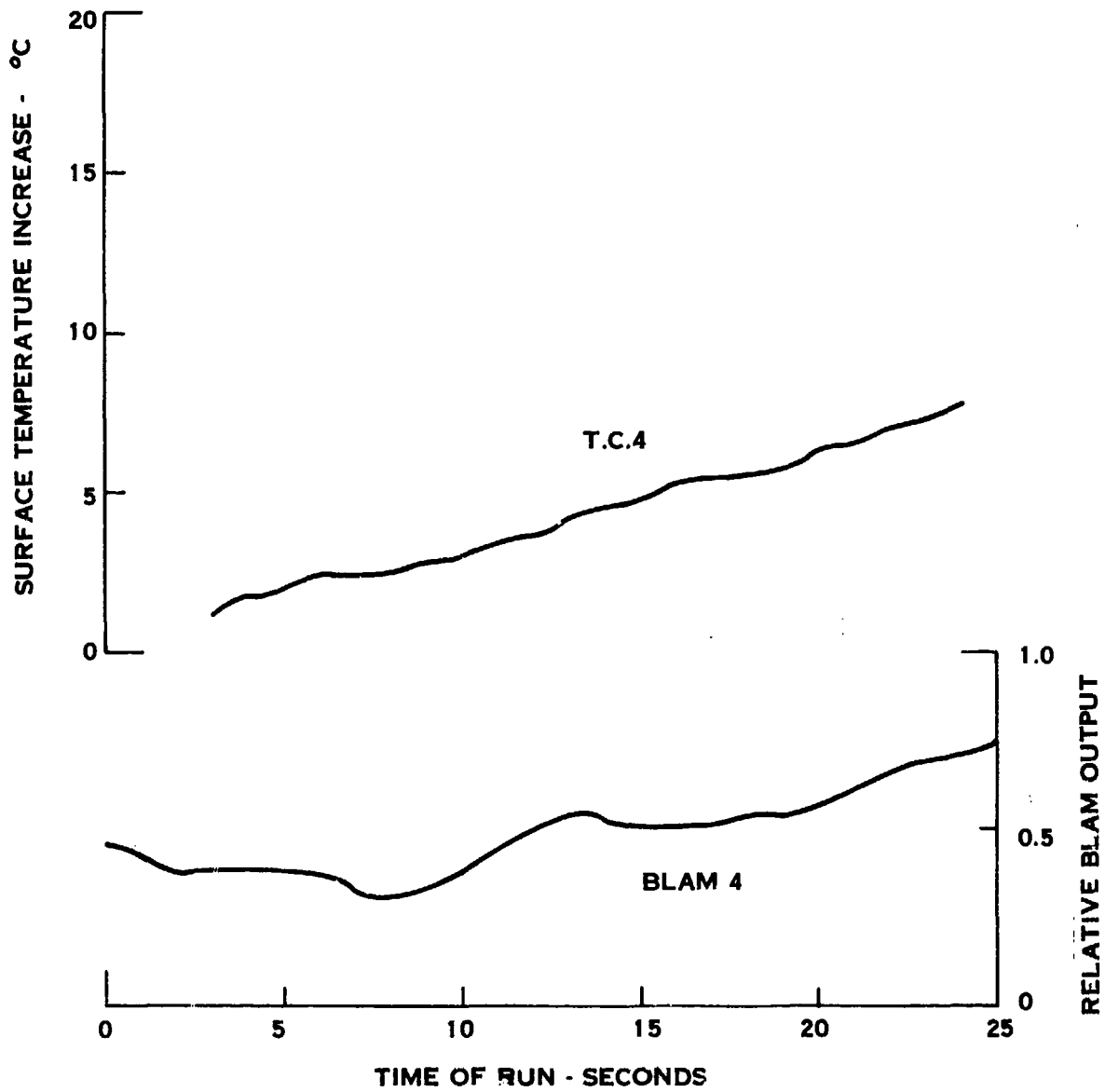
FIGURE 26   RUN 2, BLAM CHANNEL 4, TEMP. SENSOR 4

53
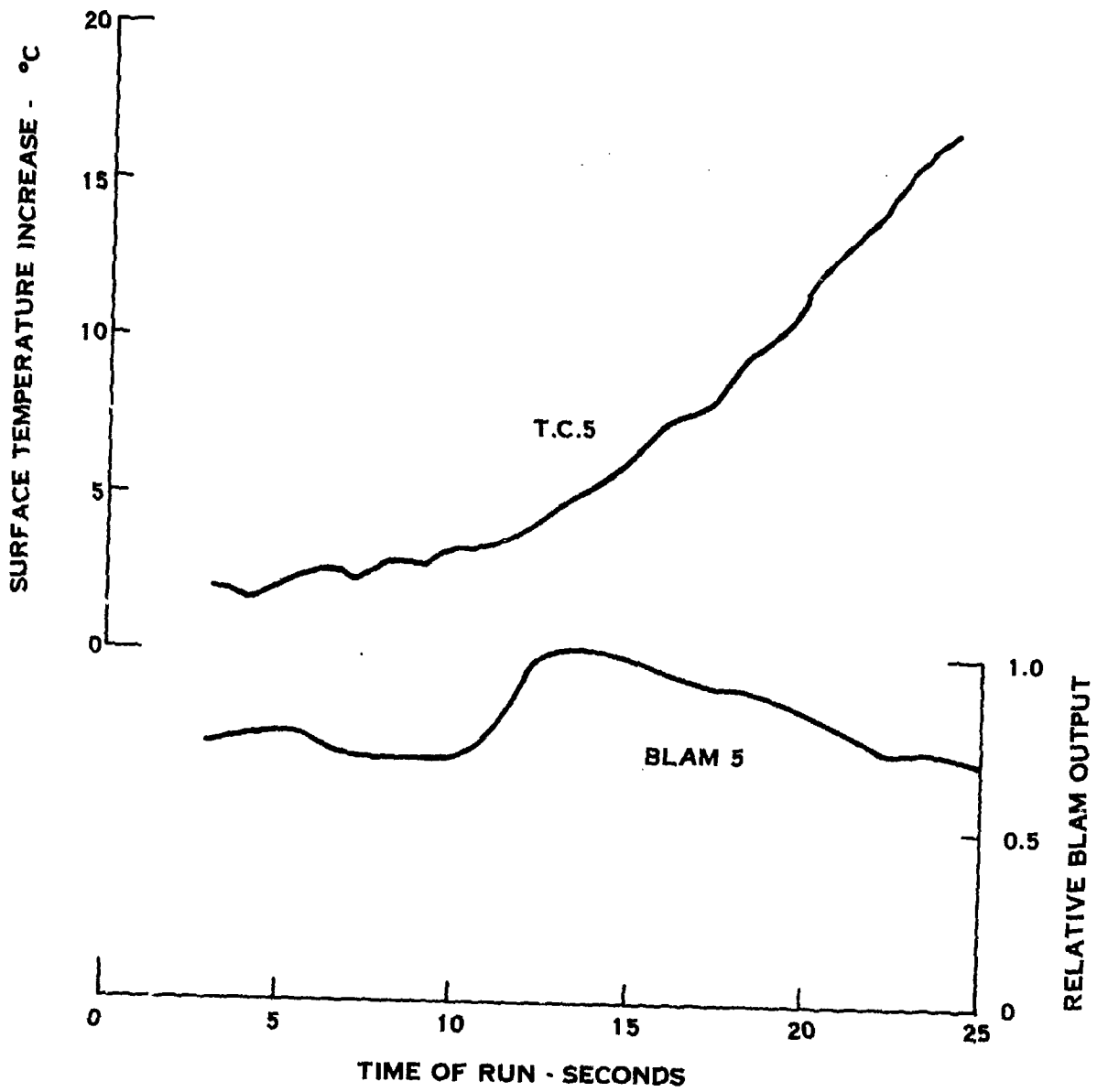
FIGURE 27   RUN 2, BLAM CHANNEL 5, TEMP. SENSOR 5

54
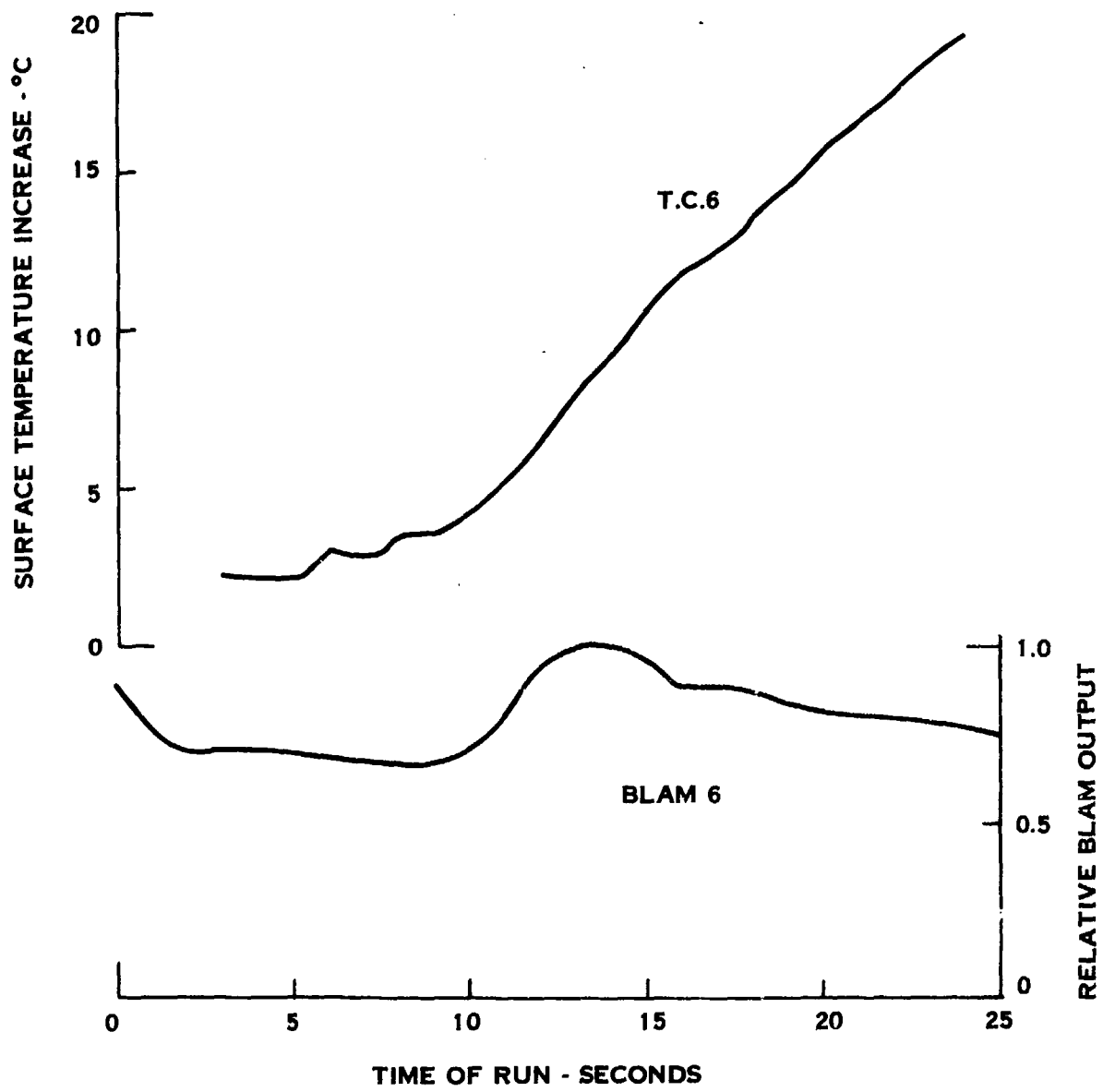
FIGURE 28   RUN 2, BLAM SENSOR 6, TEMP. SENSOR 6

The acoustic level traces in Figures 23-28 early in the run were high then decreased immediately, a feature which can be attributed to tunnel or tape recorder transient. As R_∞ increased and the boundary layer entered transition, peak noise was measured near 14 seconds on all channels corresponding to R_∞ of about 10^7 m^{-1}.

The thermal sensors which were placed along side the BLAM's indicated a significant change in heating rate occurring at about 9 or 10 seconds. This heating rate change is seen in the slope of the temperature curves which are plotted in Figures 23-28. The forward stations (Transducers 1 and 4, Figures 23 and 26) did not show this characteristic in the thermal data, whereas the BLAM's at these forward stations did show a small transitional bump in the data. The transition bumps in transducers 5 and 6 were much greater in amplitude and closely correlated with the temperature rate increase.

5.3.2.3 Run 3. This test was similar to Run 2 in that a pressure sweep was used to vary the boundary layer conditions in an attempt to record transition on the model. The major difference was that a higher pressure was achieved in Run 3 and the tunnel was pre-heated to obtain more uniform flow. Tunnel flow parameters and sensor data are plotted in Figures 29 through 35.

Data from the BLAM's prior to 8 seconds were not recorded in this test due to the tape recorder not being turned on in time. The aft and center stations, channels 2, 3, 5 and 6 do not show transition except for a slight increase at the beginning of the traces. The thermal data for these stations indicate transition occurring prior to 8 seconds which would be consistent with the Reynolds number at which transition occurred in Run 2.
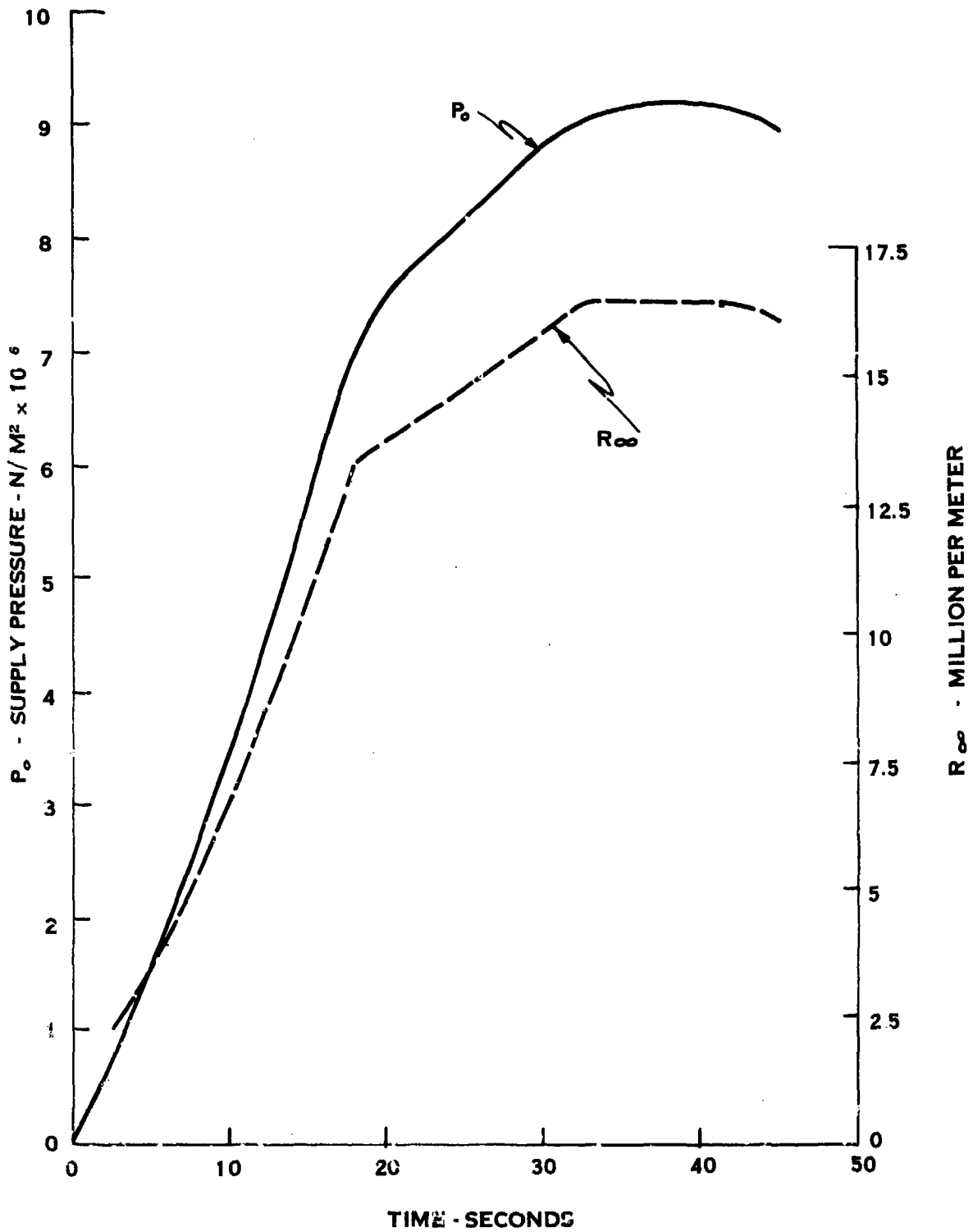
FIGURE 22 RUN 3, FLOW PARAMETERS

57
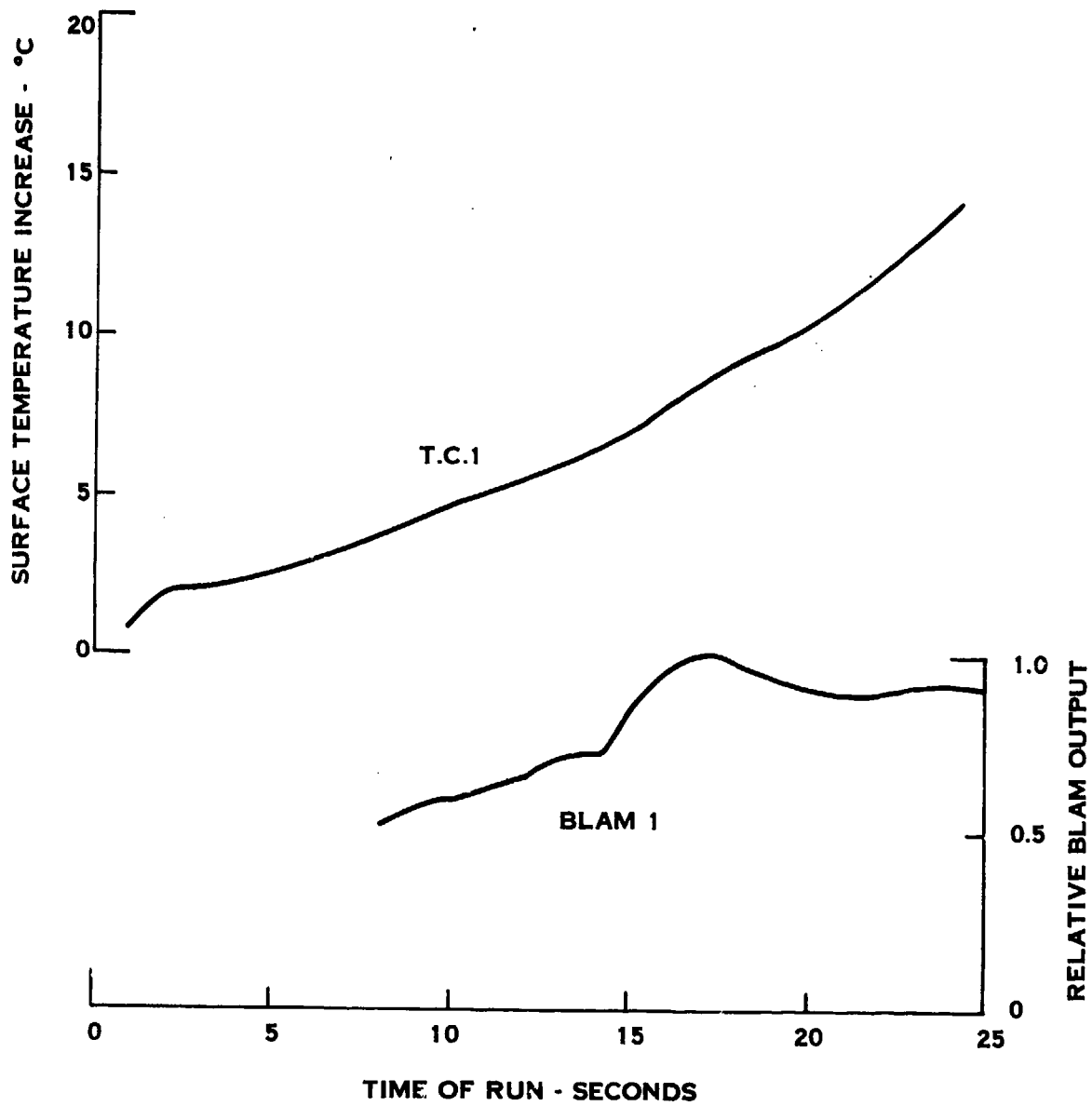
FIGURE 30   RUN 3, BLAM CHANNEL 1, TEMP. SENSOR 1

58
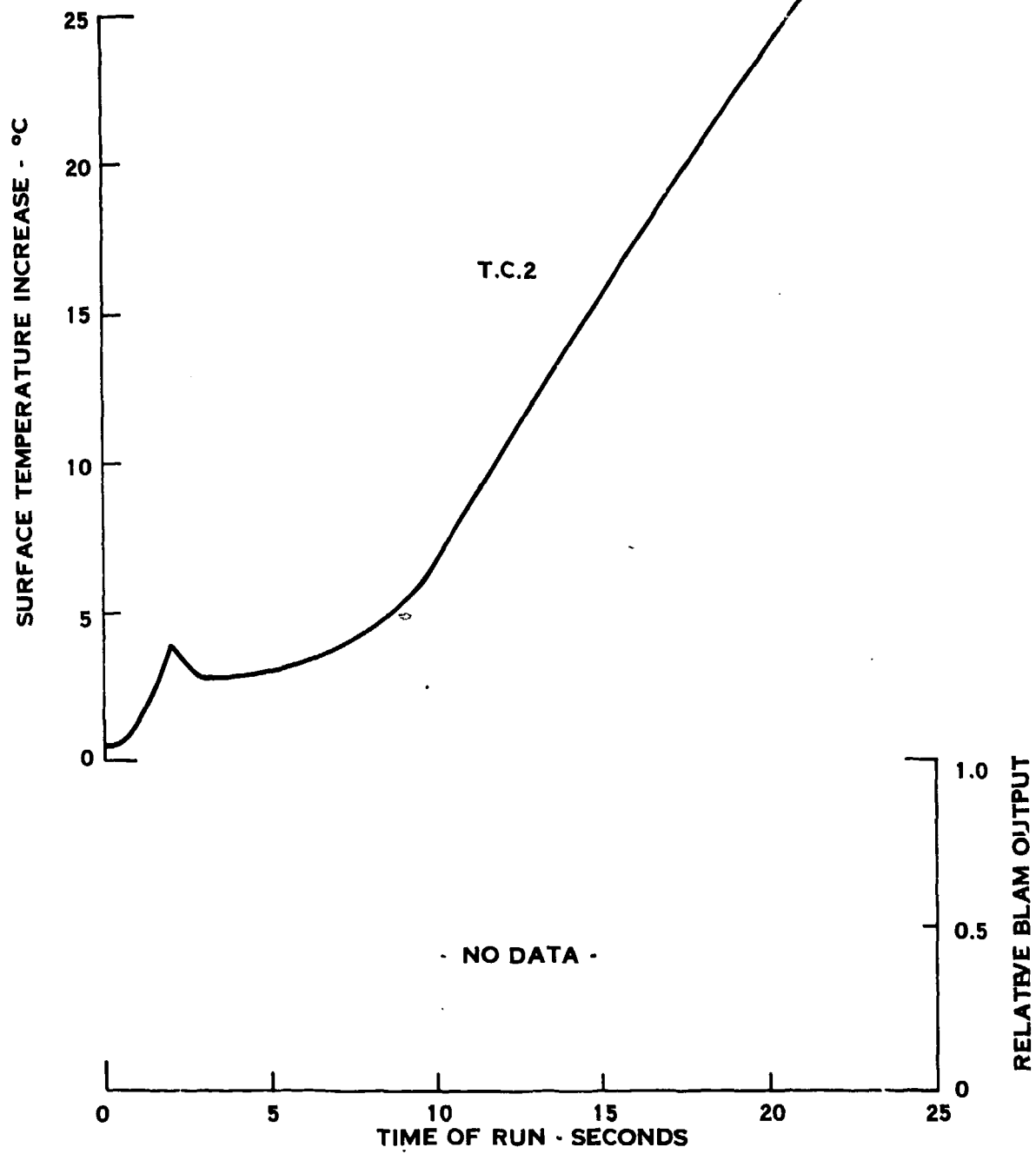
FIGURE 31   RUN 3, BLAM CHANNEL 2, TEMP. SENSOR
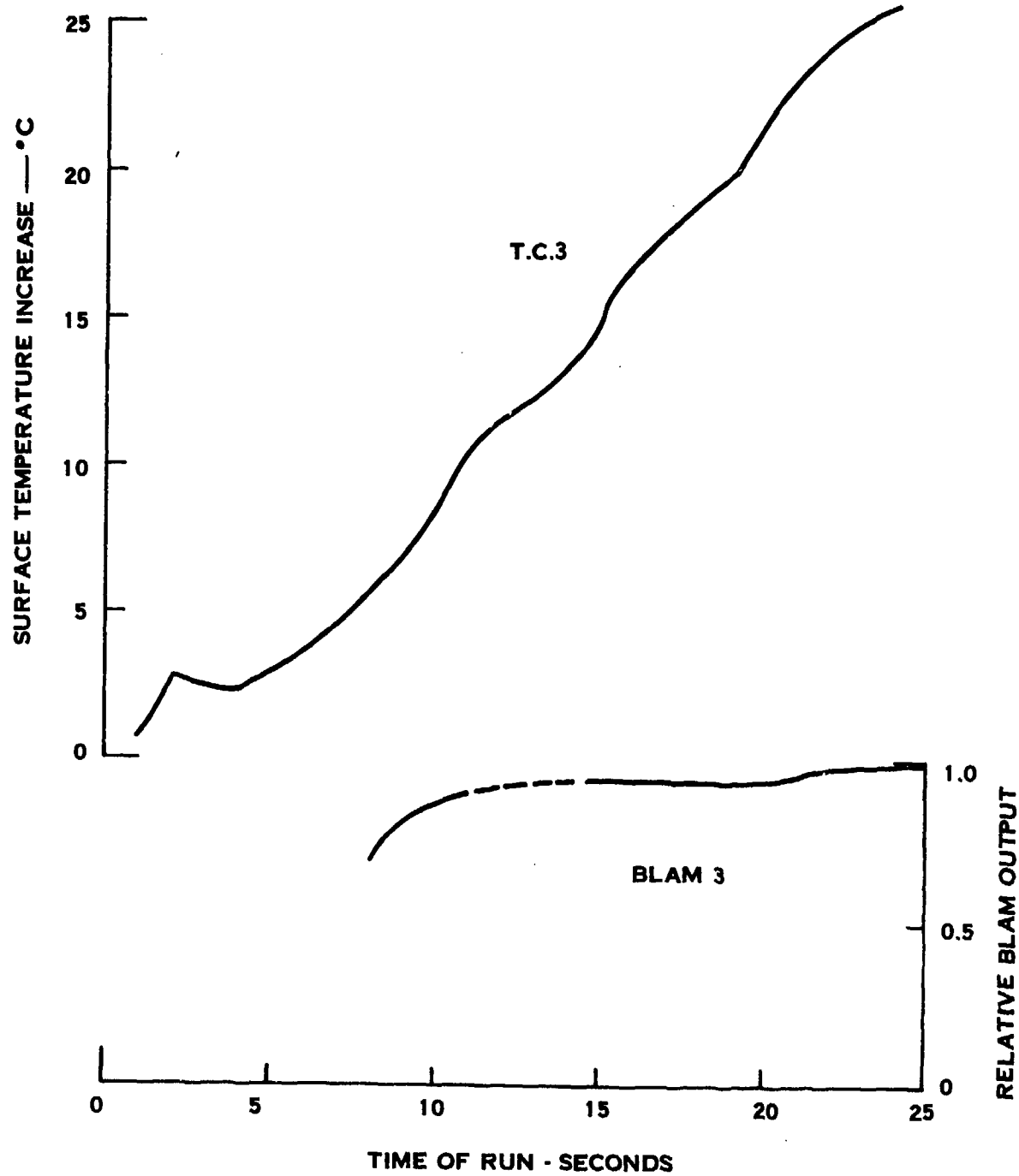
FIGURE 32   RUN 3, BLAM CHANNEL 3, TEMP. SENSOR 3

60
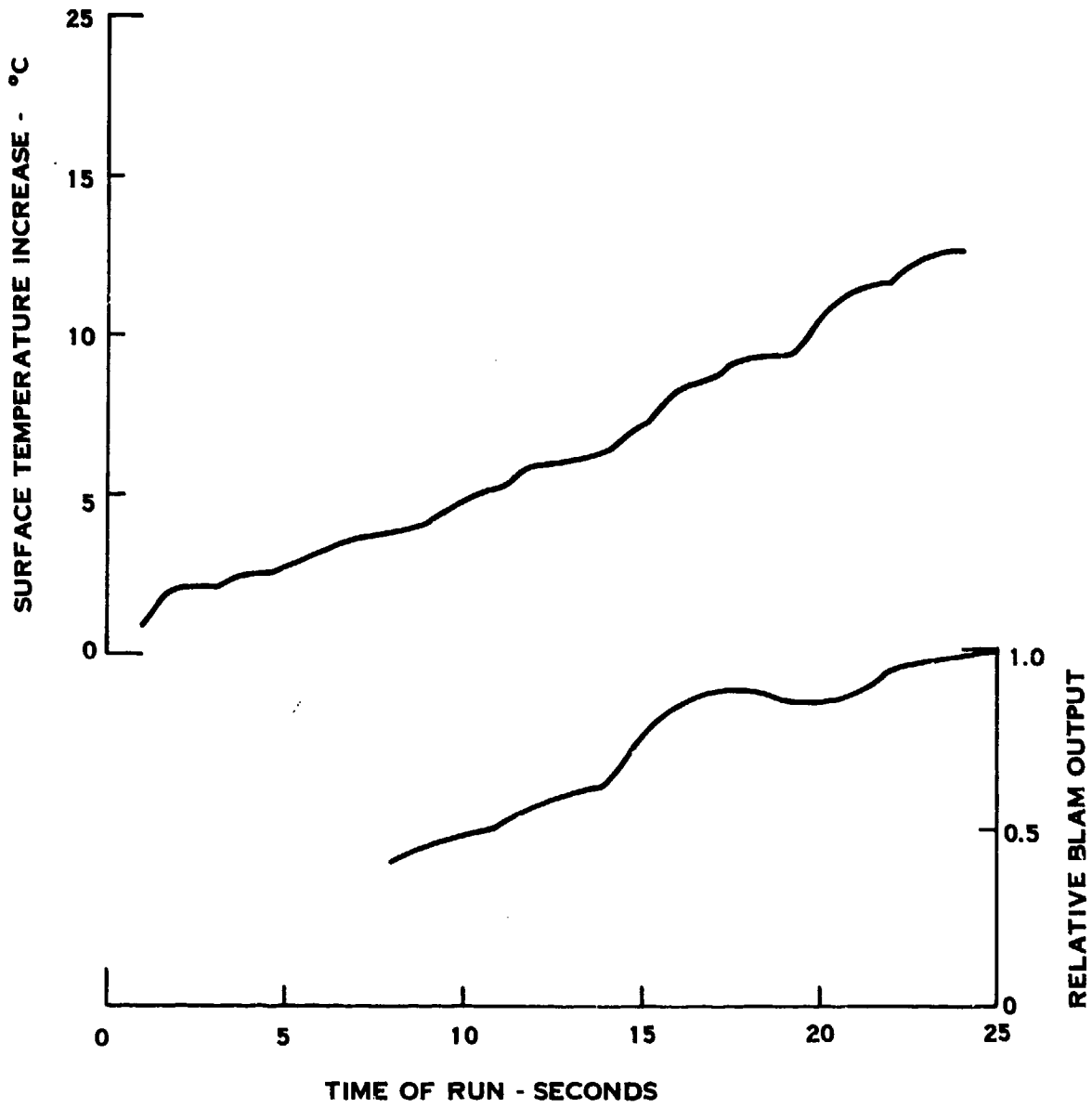
FIGURE 33   RUN 3, BLAM CHANNEL 4, TEMP. SENSOR 4

61
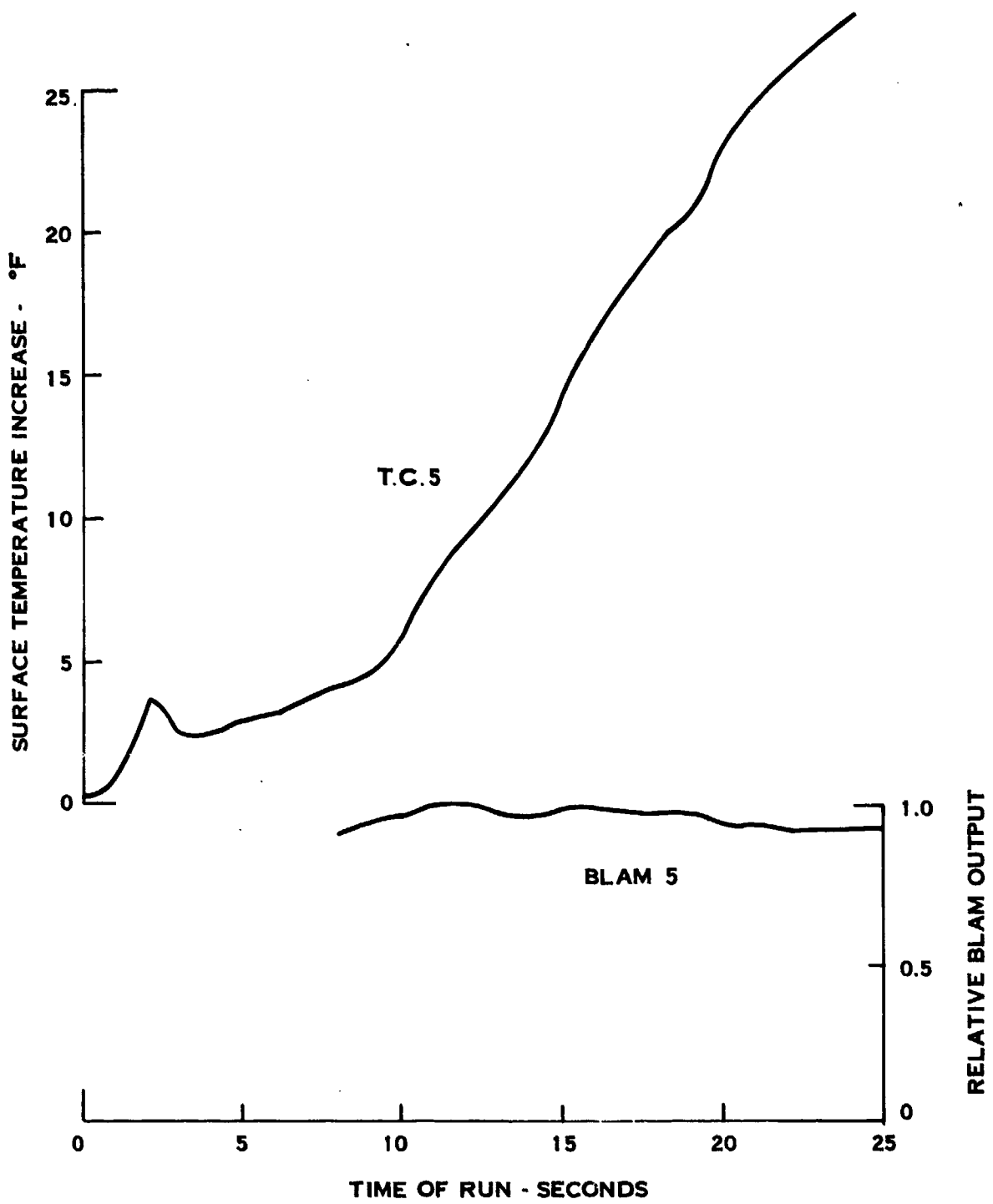
FIGURE 34   RUN 3, BLAM CHANNEL 5, TEMP. SENSOR 5

62
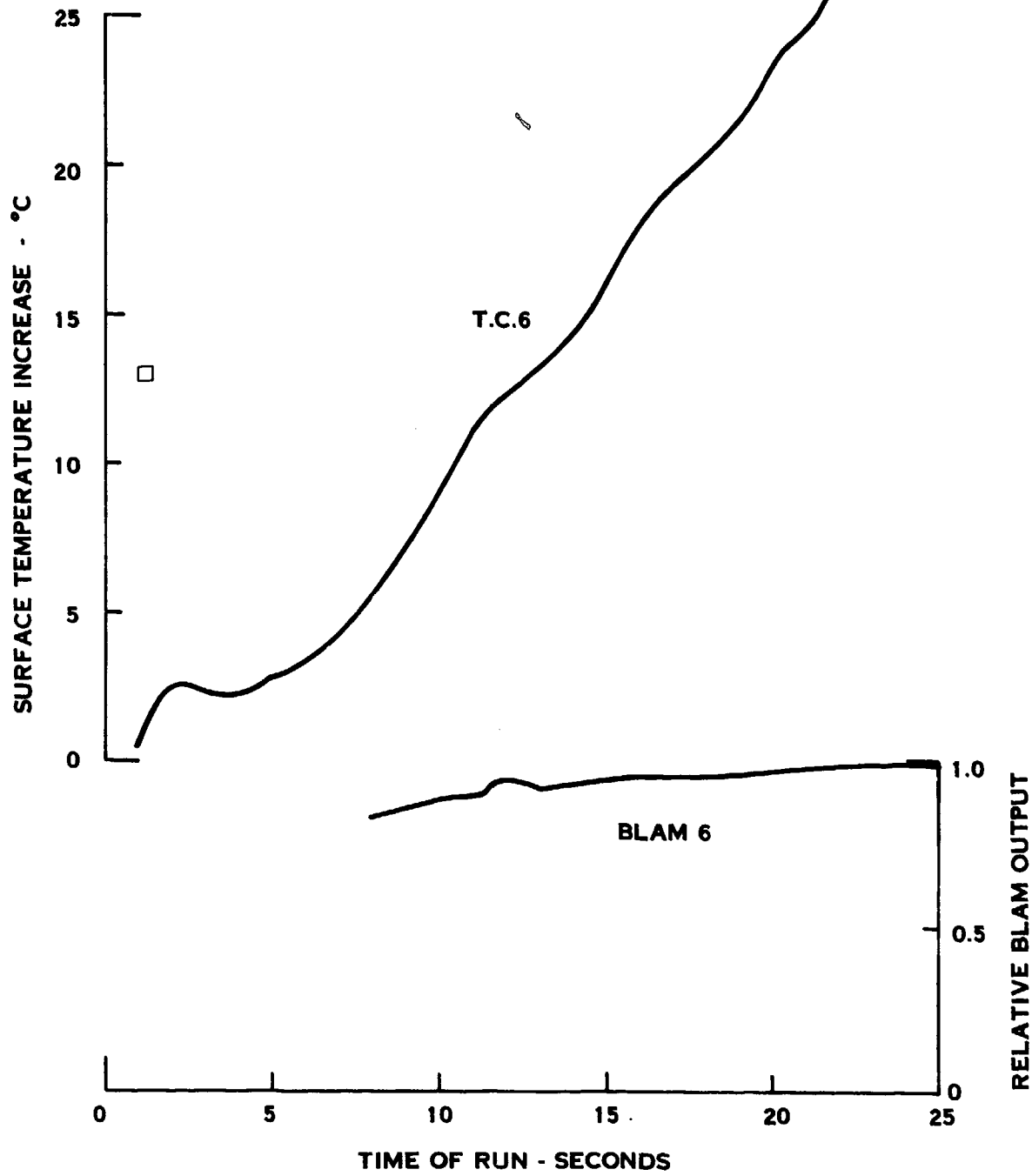
FIGURE 35   RUN 3, BLAM CHANNEL 6, TEMP. SENSOR 6

63

BLAM channels 1 and 4, on the forward part of the model, show the characteristic transition bump but at a higher R_∞ that was experienced in Run 2. This bump is a good indicator of transition since it is known that transition on a cone moves forward as R_∞ increases. Thermal sensors 1 and 4 show slight increases in slope at the acoustic transition time indicated by the BLAM's.

A series of Schleiren photos taken during Run 3 are included in Appendix B, Figures 54 through 59. These photos show progression of boundary layer turbulence from aft toward the model tip as the flow Reynolds number increases. While not having the best contrast, the primary indicator in the photos showing turbulence is the fine white line close to the model wall. This line is not visible where full turbulence exists.

While the correlation of optical indicators and acoustical signals has not been established, the photos show transition near BLAM's 2 and 5 at 10 to 12 seconds in the run. This corresponds reasonably well with acoustic and thermal data shown in Figure 34. It is believed that the acoustic signal is generated in the transition zone in the boundary layer forward of the zone of breakup seen in the Schleiren photographs.

5.3.2.4 <u>Run 4</u>. In this run, data were taken with the model spinning and at a 2.5° angle of attack with respect to the flow. Tunnel operating parameters are given in Figure 36 which shows three R_∞ plateaus of 4.6×10^6 m^{-1}, 6.6×10^6 m^{-1} and 10×10^6 m^{-1}. Data were taken during each of these plateaus from the BLAM channels. Due to the long duration of the test, temperature data were meaningless due to thermal saturation.

BLAM data from channels 1 and 4, the forward-most sensors, indicated a fluctuating level corresponding to the spin rate of the model. The traces obtained are shown in Figure 37.
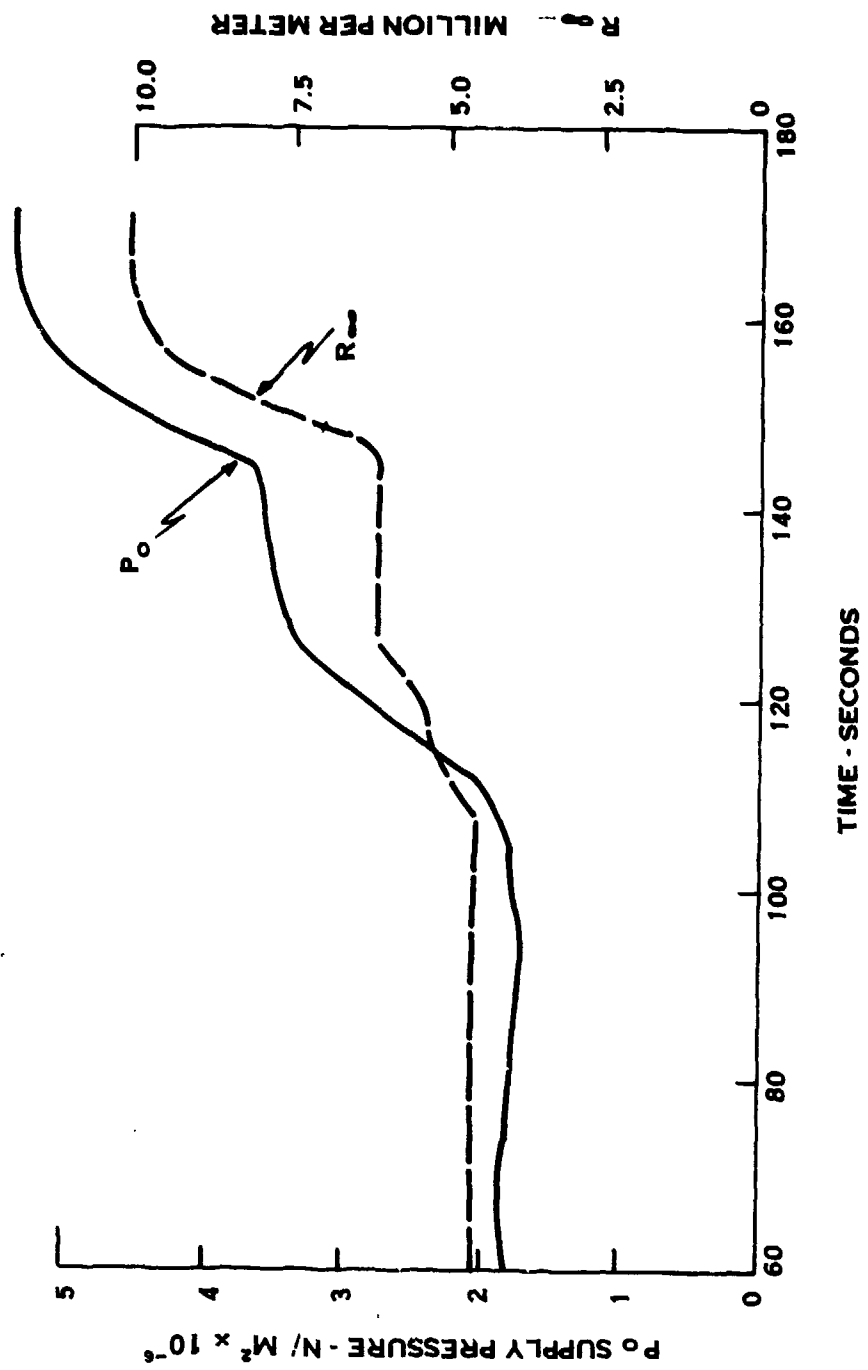
FIGURE 36   RUN4 FLOW PARAMETERS M8

CHANNEL 1 TIME REF.

CHANNEL 2 TIME REF.
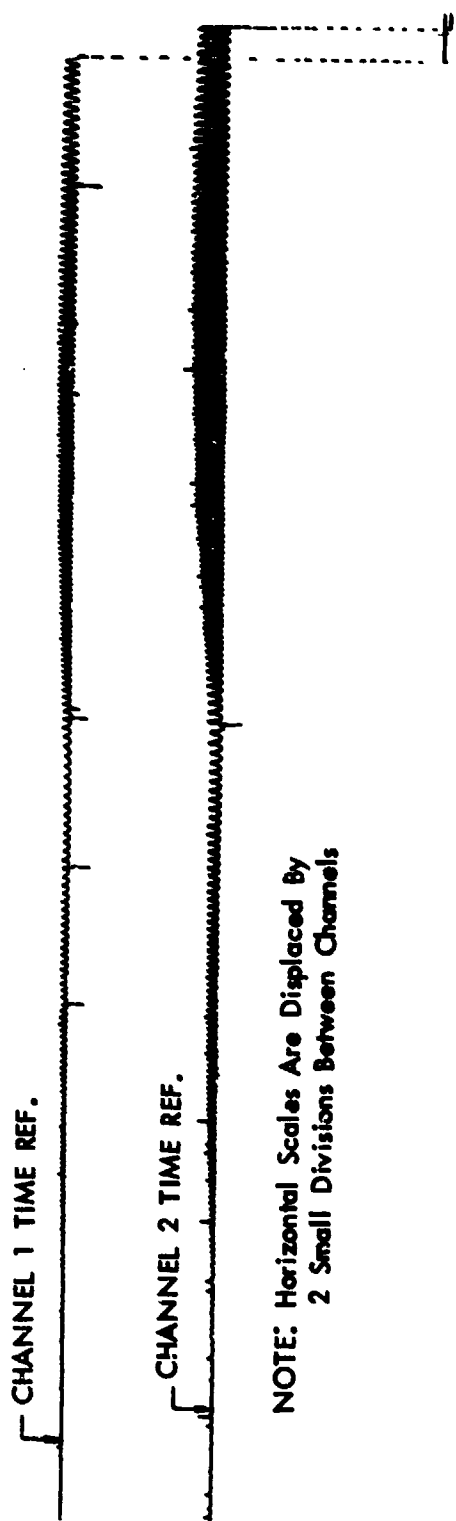
NOTE: Horizontal Scales Are Displaced By
2 Small Divisions Between Channels

FIGURE 37   RUN 4 BLAM DATA CHANNELS 1 AND 4

Data from the remaining BLAM channels were poor in quality and are not included herein.

An analysis of the data showed that the outputs were phased 180° with respect to each other, which would be a proper indication if the noise source were greater in strength on the side of the model which was fixed with respect to the flow. A close comparison of film and BLAM records (which both had good IRIG timing marks) showed that the peak of the oscillation occurred when the BLAM was on the leeside of the model with respect to the upstream direction.

Martelucci[7] showed that in such hypersonic flow conditions at an angle of attack transition will move forward on the lee-side ray. The relative amplitude of the BLAM sensors correspond well to that from Run 3 (e.g. Figure 30) at similar Reynolds numbers.

An expanded view of simultaneous output from channels 1 and 4 is presented in Figure 38. The BLAM output exhibits asymmetry and a central dip in amplitude on the peak, both of which features can be expected as a result of asymmetric trans-ition on cones. The dip in the peak can be attributed to a narrow zone of full turbulence in between transition zones. The photos of Figure 38 also illustrate the directionality of the BLAM in that the zones of transition are well defined. This is particularly visible in channel 4 trace where the dip at the peak on the leeward side is apparent. Details less than 0.1 the circumference of the model can be seen, an excellent indication of directionality.

Additional confirmation of boundary layer condition was given by Schleiren photos, in Figure 39A, B, and C. Figure 39C was taken at time 50 seconds, just prior to the data shown in Figure 38. All photographs show a well-defined boundary layer
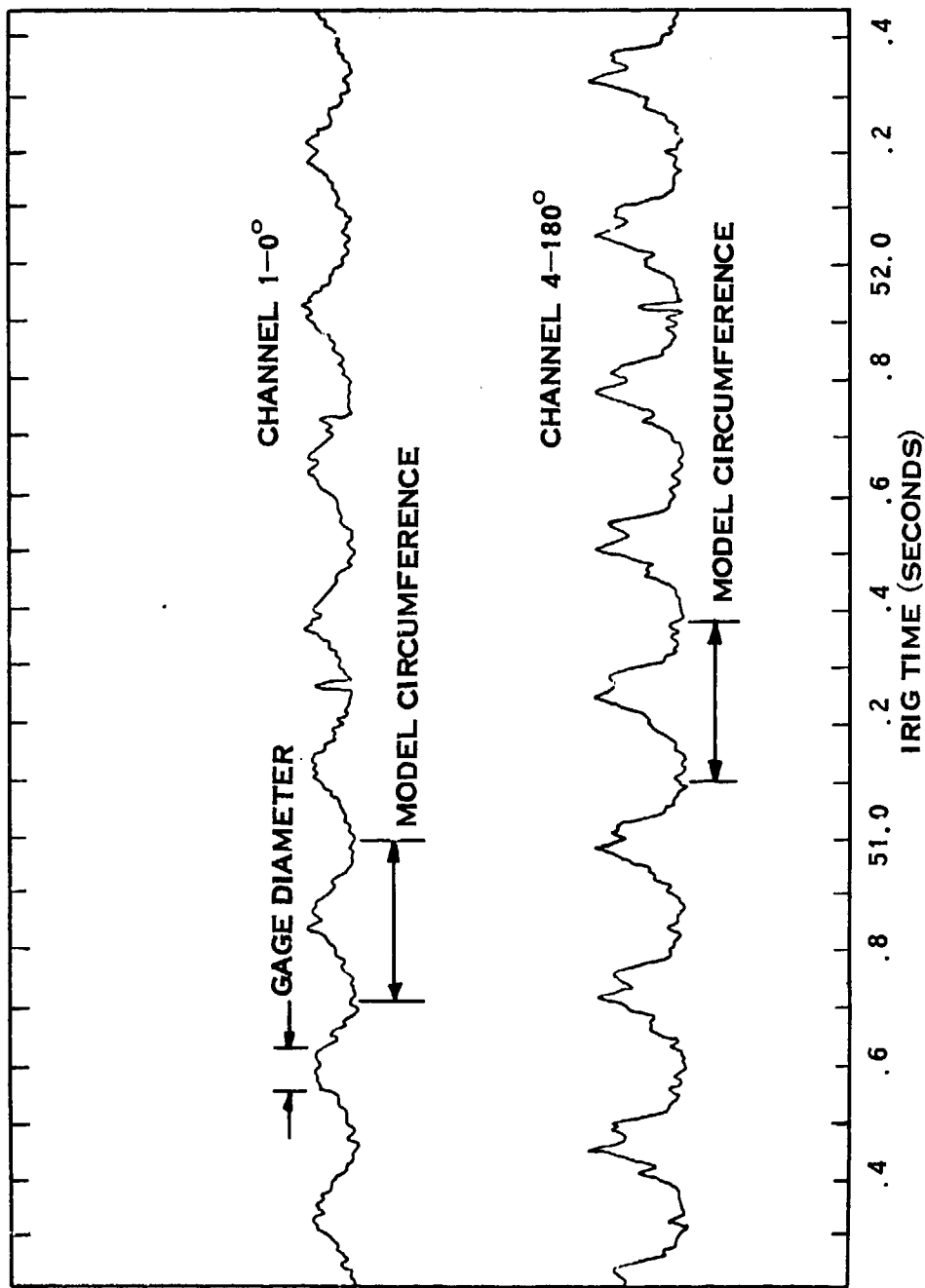
FIGURE 38   BLAM COMPARISONS SPINNING MODEL NSWC TUNNEL
8, MACH 8, 5.4X10^6 N/M^2, $\alpha = 2.5°$, R∞=10^6 M^{-1}

68
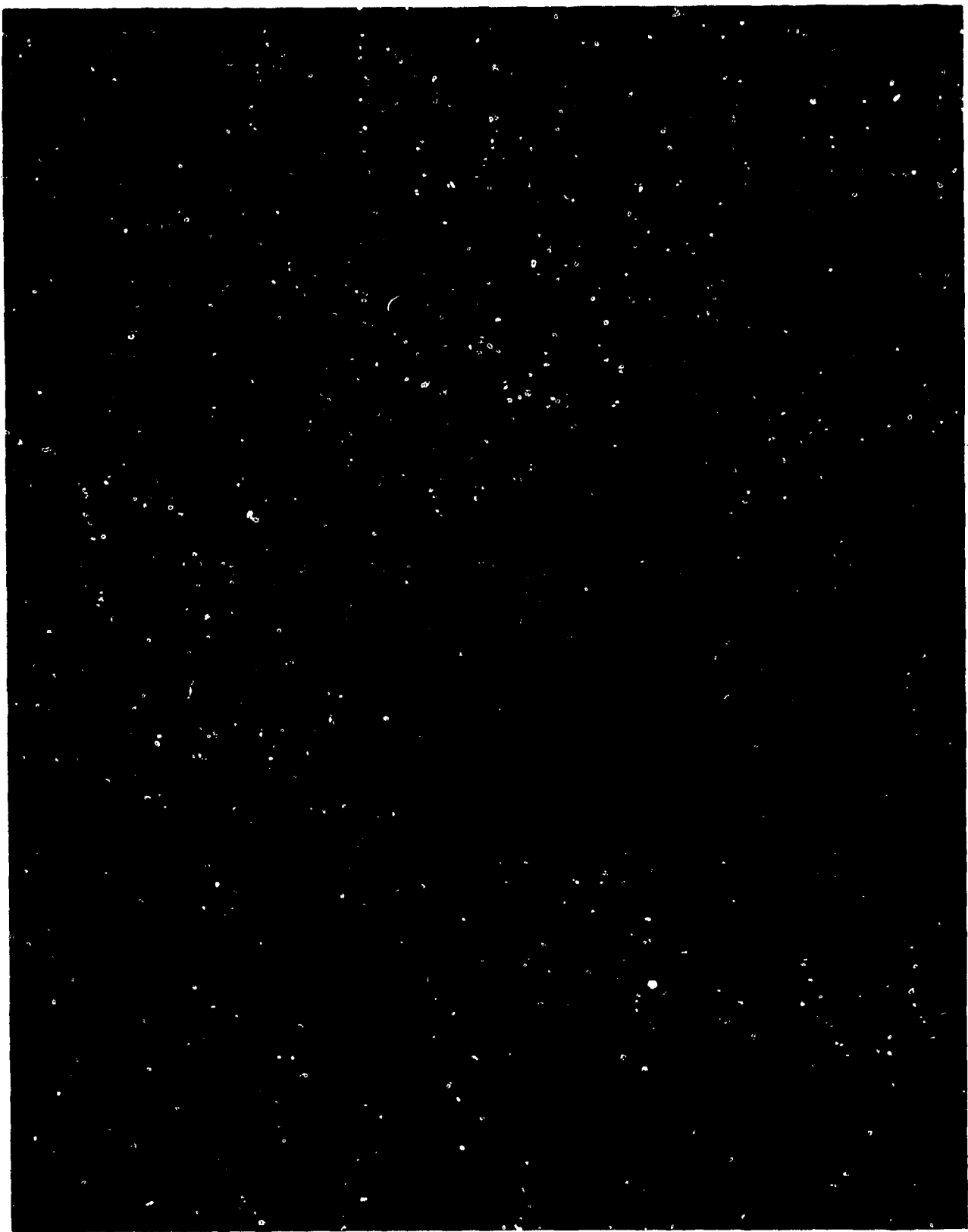
FIGURE 39A   RUN 4 BOUNDARY LAYER PHOTO

$R_\infty = 3.6 \times 10^6 \text{ m}^{-1}$

$\alpha = 2.5^\circ$

69

FIGURE 39B   RUN 4 BOUNDARY LAYER PHOTO

$R_\infty = 6 \times 10^6 \text{ m}^{-1}$

$\alpha = 2.5^\circ$

70
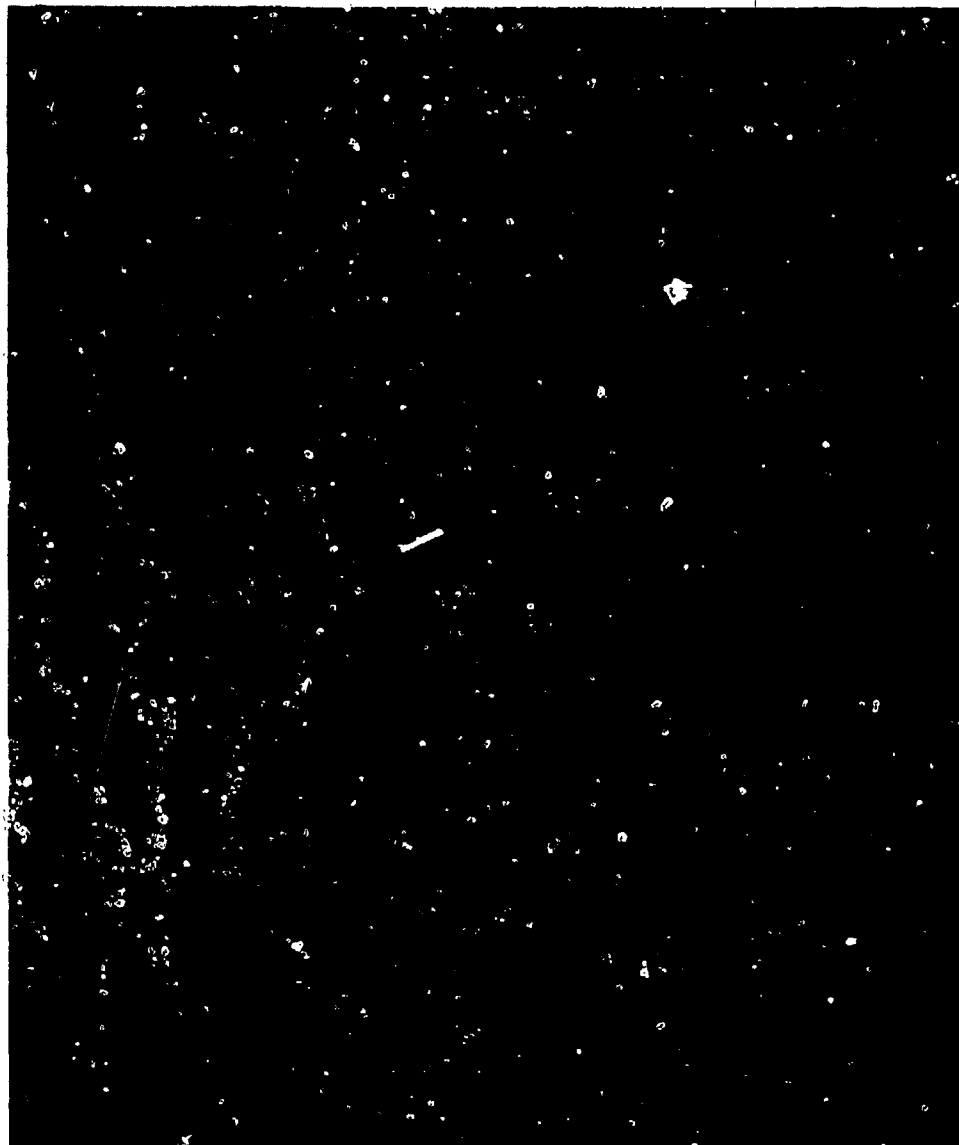
FIGURE 39C RUN 4 BOUNDARY LAYER PHOTO

$$R_\infty = 10^{+7} m^{-1}$$

$$\alpha = 2.5^\circ$$

on the windward side; on the leeside, no defined layer can be
seen so that the flow is probably fully turbulent. The appear-
ance of the boundary layer on the leeward side is such that
turbulence extends forward to the position of transducers 1 and
4 at all these Reynolds numbers. On the windward side a forward
progression can be seen in the turbulent zone as Reynolds number
increases.

SECTION 6

CONCLUSIONS

BLAM sensors were successfully fabricated to meet the environmental requirements of an actual RV and were installed on schedule in both the PVM & STM vehicles. The 2.54 cm diameter sensor was characterized as having resonant peaks at 50, 113, and 168 kHz when installed on a carbon phenolic heatshield with 1.27-cm thickness. The smaller sensor developed for STM-12 application exhibited resonance peaks at 40, 80, 220, and 280 kHz. The BLAM electronics were designed to have nearly a five-order-of-magnitude dynamic range by utilizing a logarithmic technique. This amplifier permits recording of acoustic data not heretofore obtained in flight tests.

All PVM and STM-12 BLAM units successfully passed the flight qualification tests with no failures. The reliability of these units was also established by the flight test results in which 100% data were obtained.

Wind tunnel tests were partially successful and showed that the BLAM and heating rate sensors responded similarly to the boundary layer transition. In addition, the sensors produced an output which fluctuated with the aspect angle on a spinning sharp nose model. Because this output occurred on the leeside of the model, the conclusion was made that transition was being detected.

73

REFERENCES

1. Pate, S. R. and Brown, M. D., <u>Acoustical Measurements in Supersonic Transitional Boundary Layers</u>, AEDC-TR-69-182, Arnold Engineering Development Center, October 1969.

2. Owen, F. K., Horstman, C. C., Stainback, P. C. and Wagner, R. D., <u>Comparison of Wind Tunnel Transition and Freestream Disturbance Measurements, AIAA Journal</u>, Vol. 13, No. 3, March 1975, p. 266.

3. Beckwith, I. E., <u>Development of a High Reynolds Number Quiet Tunnel for Transition Research</u>, AIAA Journal, Vol. 13, No. 3, March 1975, p. 300.

4. Harvey, W. D., Stainback, P. C., Anders, J. B. and Cary, A. M., <u>Nozzle Wall Boundary Layer Transition and Freestream Disturbances at Mach 5</u>, AIAA Journal, Vol. 13, No. 3, March 1975, p. 307.

5. Potter, J. Leith, <u>Boundary Layer Transition on Supersonic Cones in an Aeroballistic Range</u>, AIAA Journal, Vol. 13, No. 3, March 1975, p. 270.

6. Demetriades, A., <u>Hydrodynamic Stability and Transition to Turbulence in the Hypersonic Boundary Layer Over a Sharp Cone</u>, Aeronutronic Publication No. U-6139, Aeronutronic Ford Corp., April 1975.

7. Martelucci, A., <u>Asymmetric Transition Effects on the Static Stability and Motion History of a Slender Vehicle</u>, General Electric Company, SAMSO TR-70-141, January 1970.

8. Jackson, R. <u>Flight Proof Tests of the Boundary Layer
    Acoustic Monitor</u>, K-75-88U(R) Kaman Sciences Corp.,
    2 Oct. 1975.

9. <u>Specification for Boundary Layer Acoustic Monitor Set</u>,
    Kaman Sciences Corp. October 1975.

10. Jackson, R. <u>Flight Proof Tests of the Boundary Layer
    Acoustic Monitor</u>, NM-4 Transducer, K-76-119U CR),
   October 20, 1976.

APPENDIX A

PVM AND STM

BLAM CALIBRATION CURVES
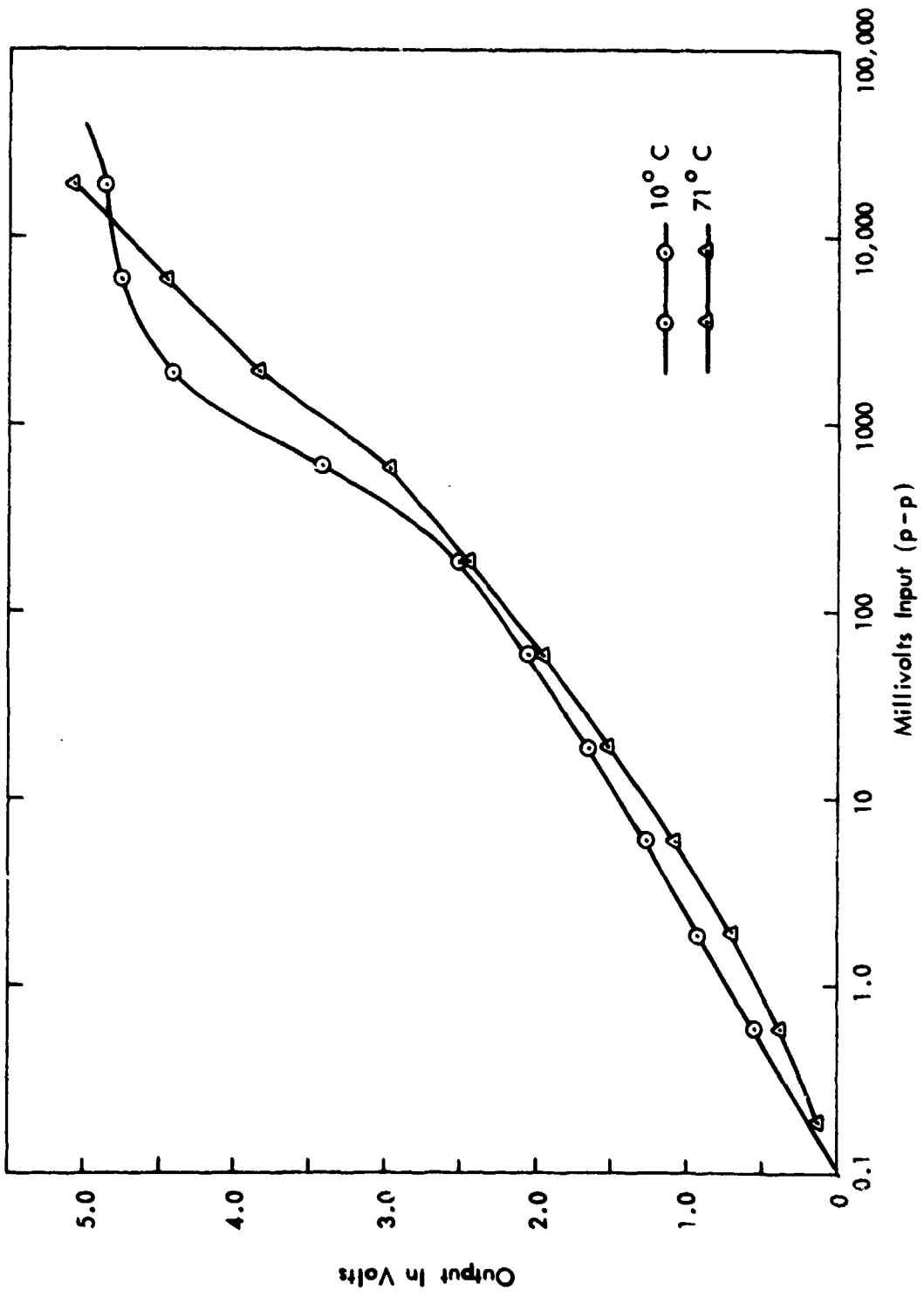
AM-2, SERIAL NUMBER 9

FIGURE 40   PVM BLAM CALIBRATION
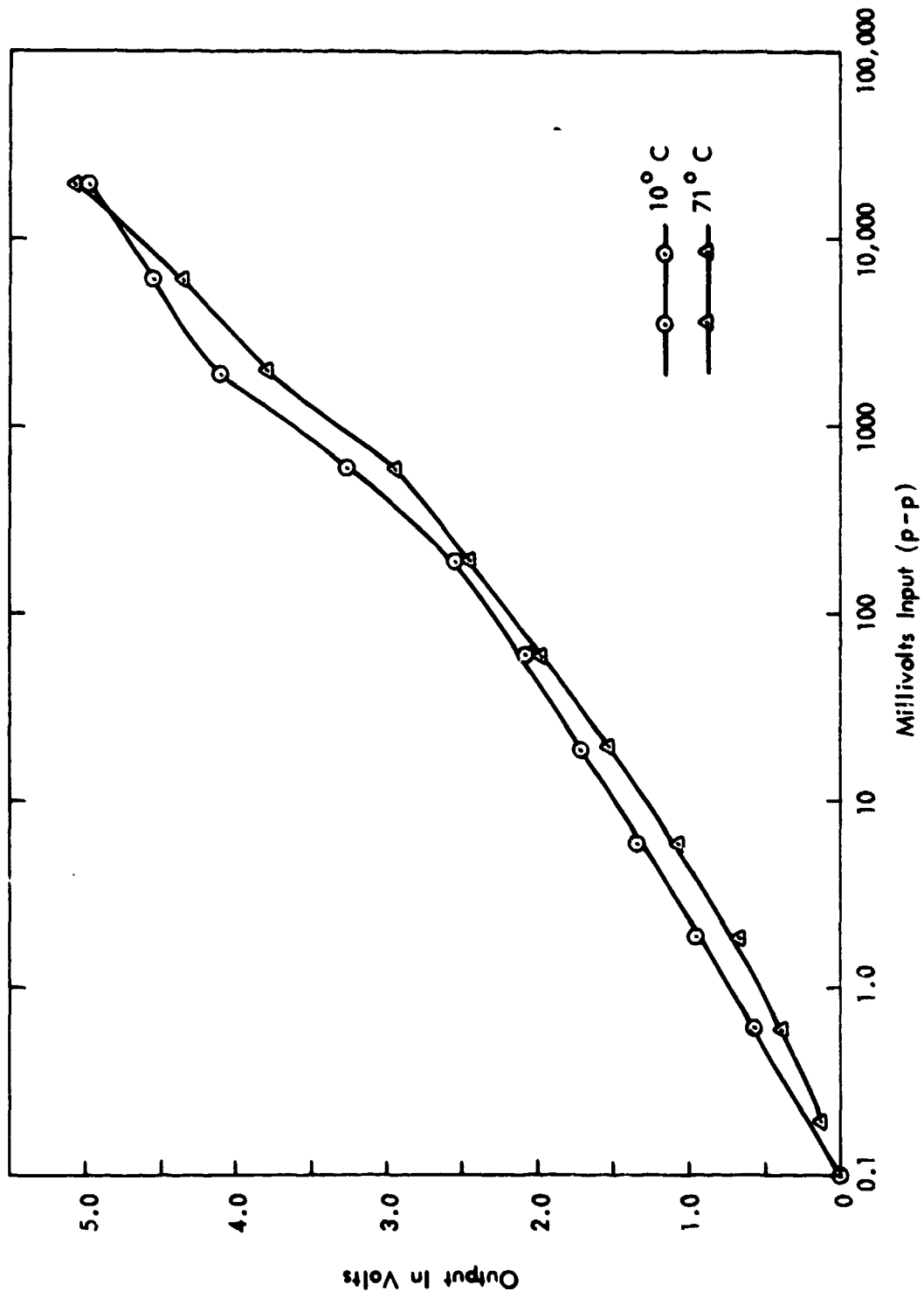
AM-2, SERIAL NUMBER 10

FIGURE 41   PVM BLAM CALIBRATION
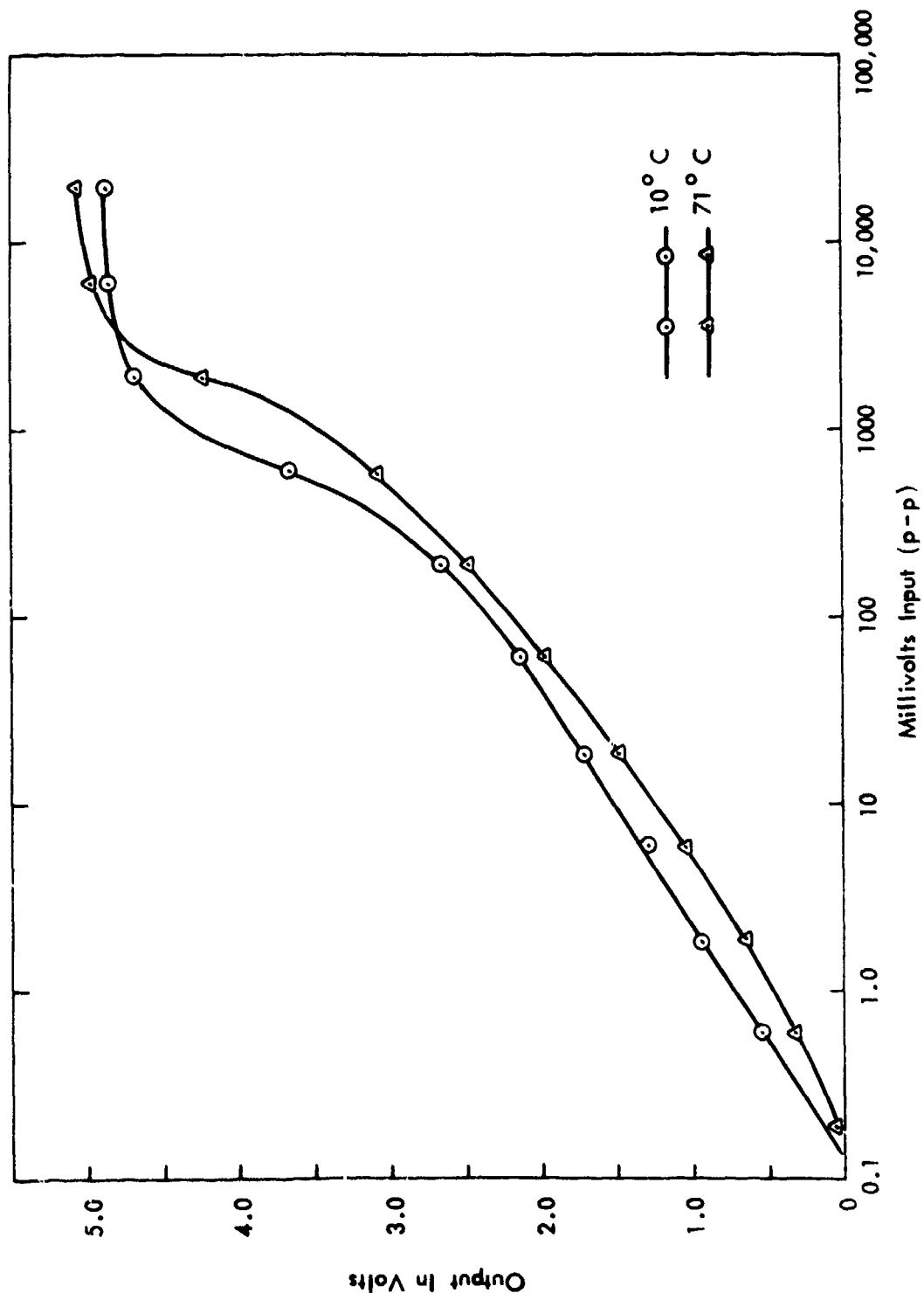
AM-2, SERIAL NUMBER 11

FIGURE 42   PV/M BLAM CALIBRATION
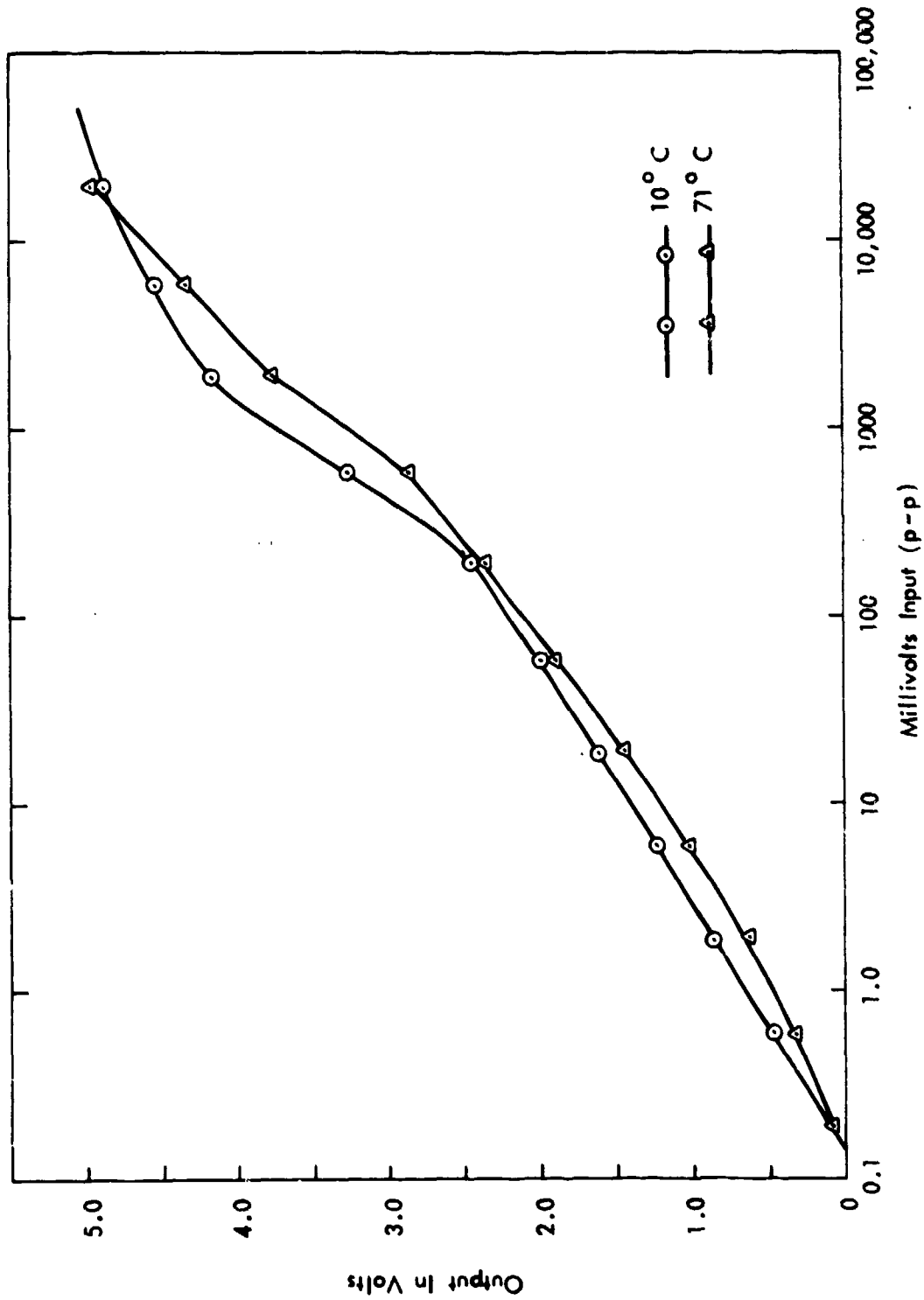
AM-2, SERIAL NUMBER 12

FIGURE 43   PV/M BLAM CALIBRATION
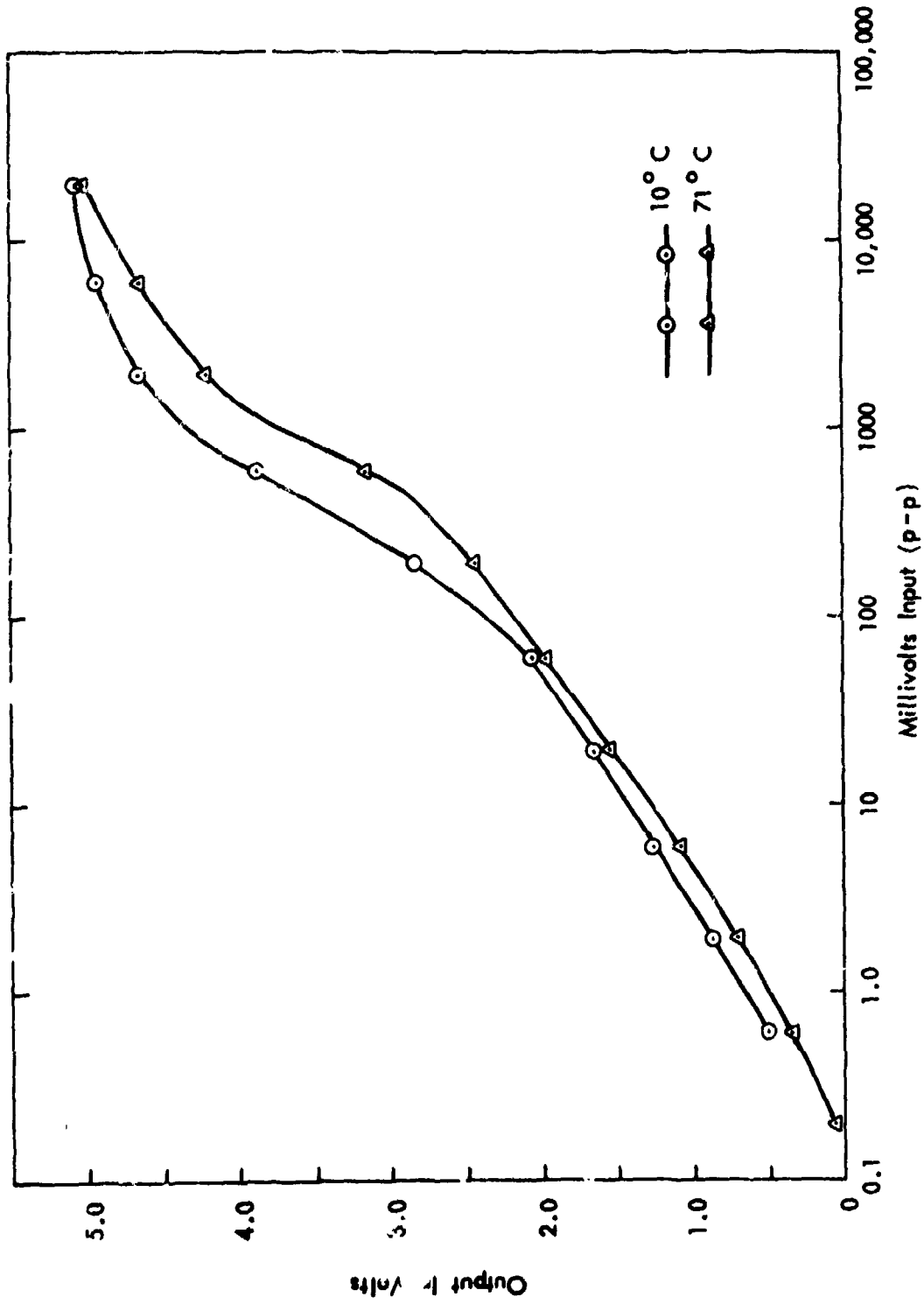
AM-2, SERIAL NUMBER 13

FIGURE 44   PVM BLAM CALIBRATION
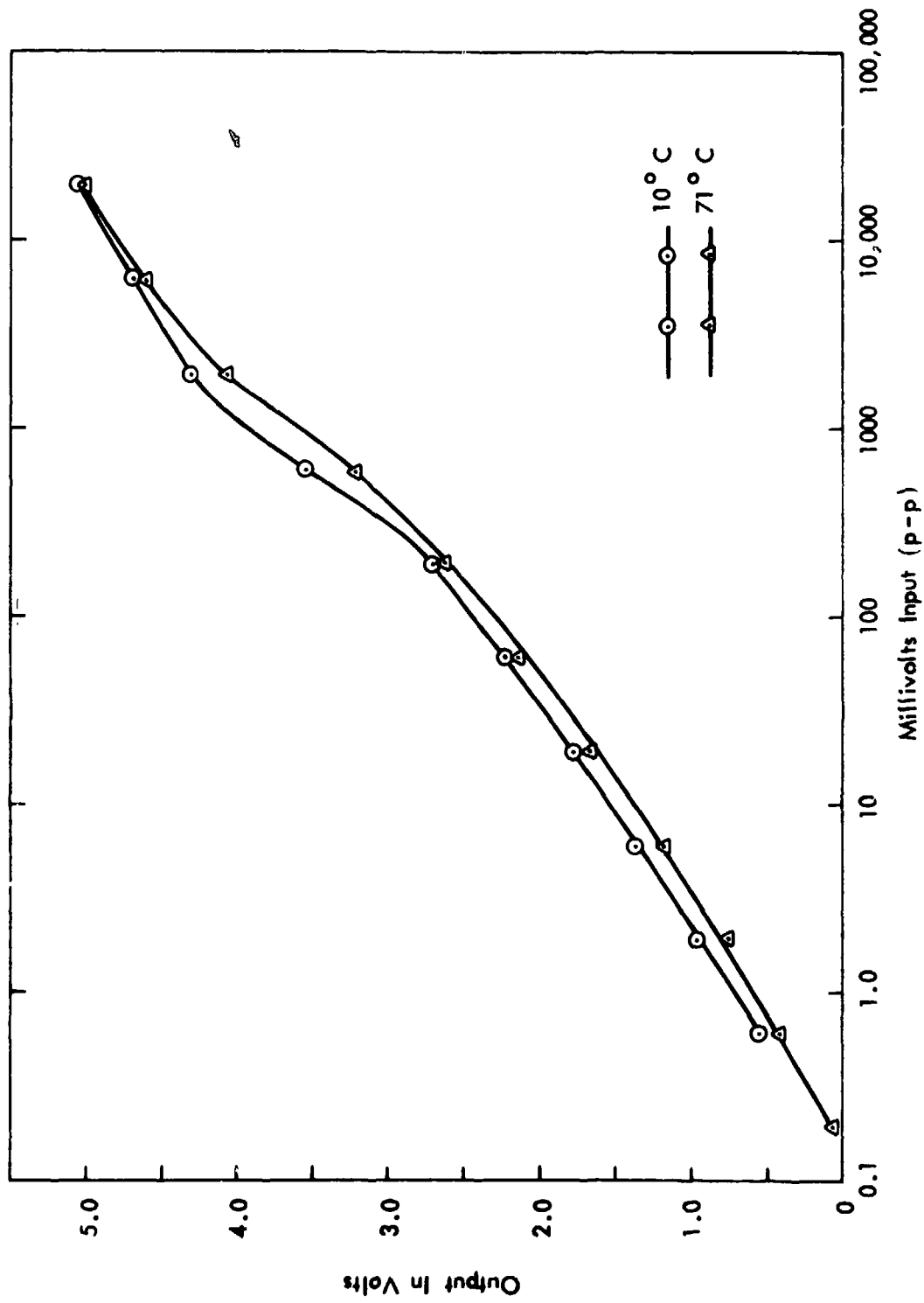
AM-2, SERIAL NUMBER 14

FIGURE 45   PV/M BLAM CALIBRATION
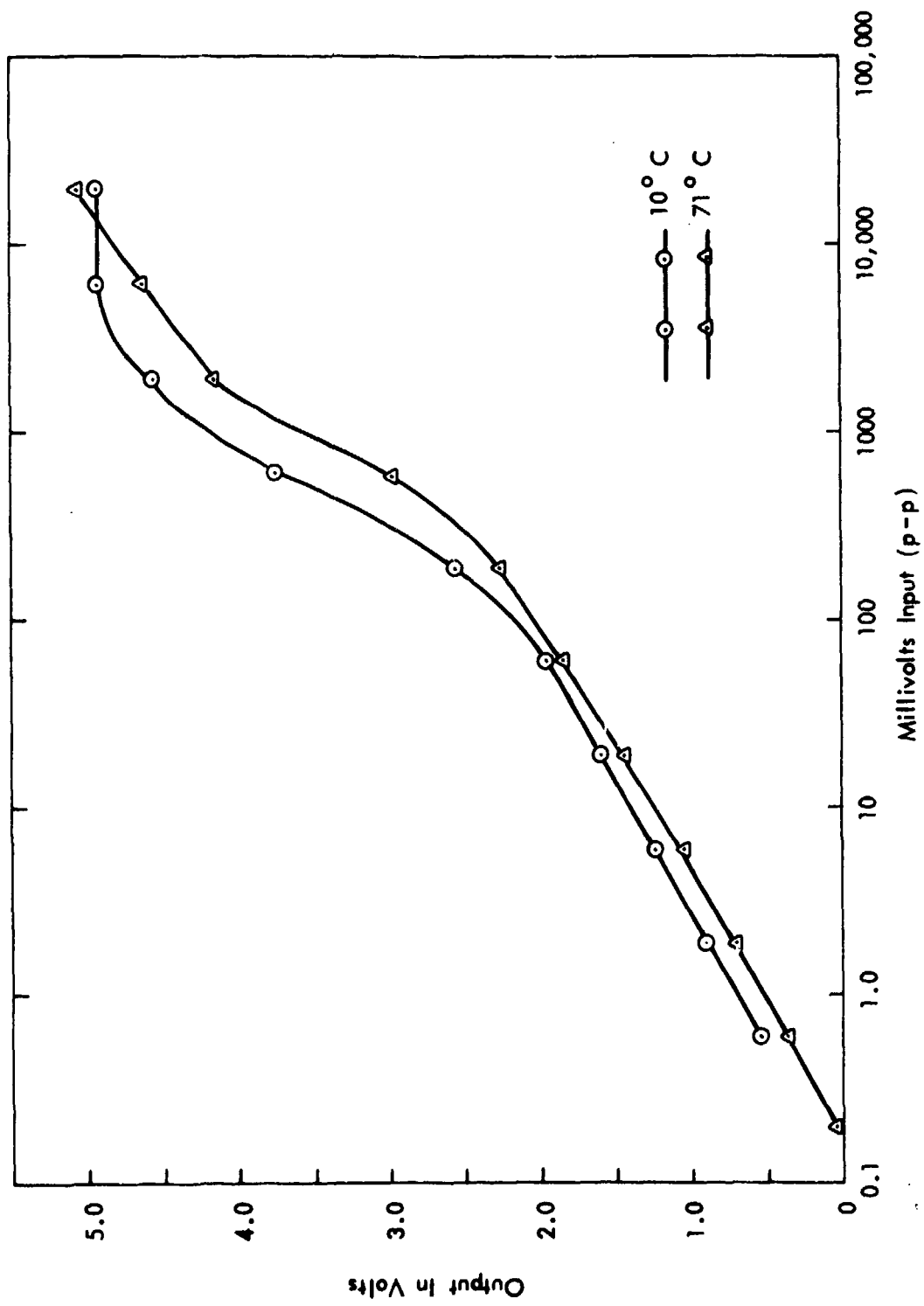
AM-2, SERIAL NUMBER 15

FIGURE 46   PVM BLAM CALIBRATION
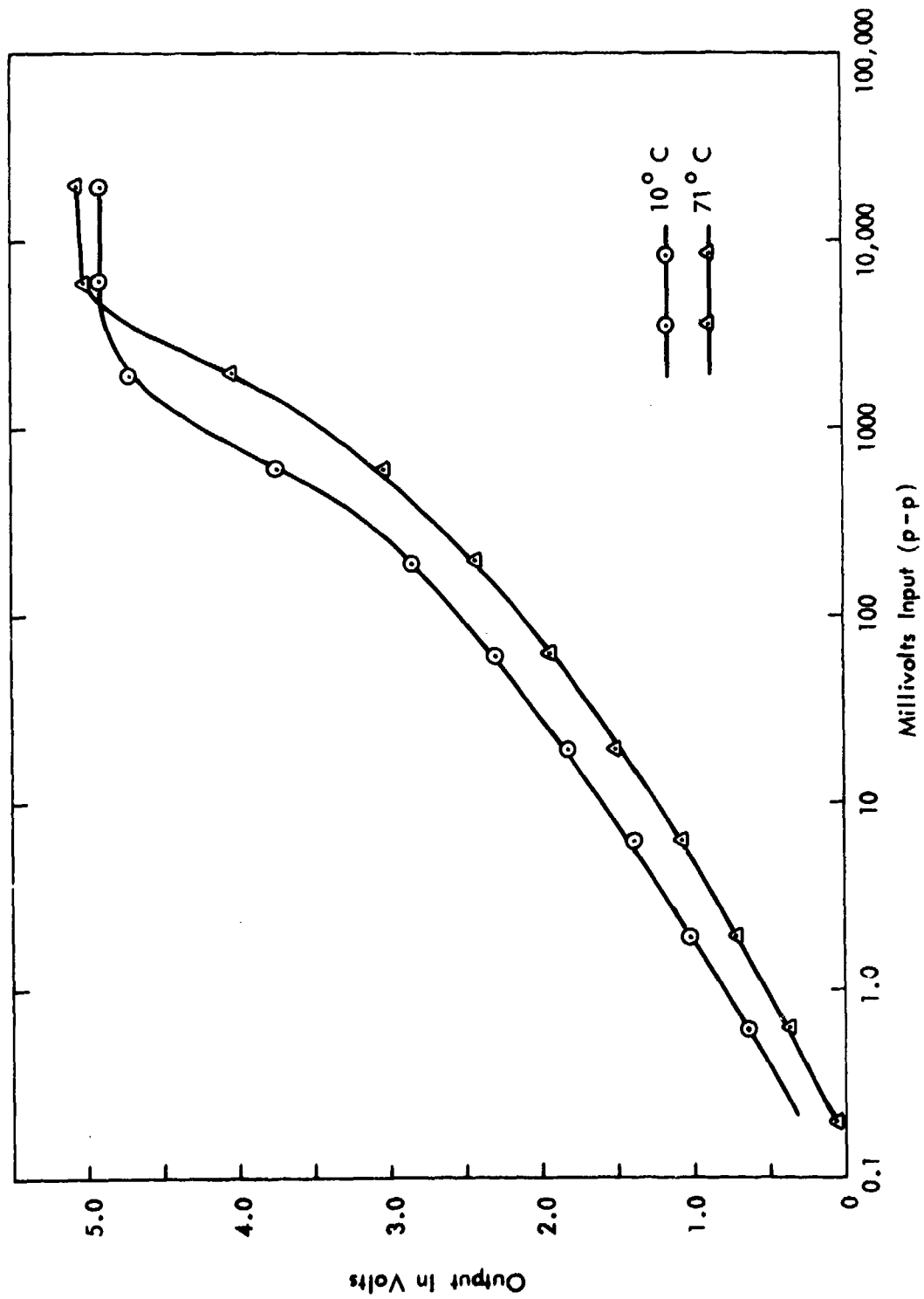
AM-2, SERIAL NUMBER 16

FIGURE 47   PVM BLAM CALIBRATION

85
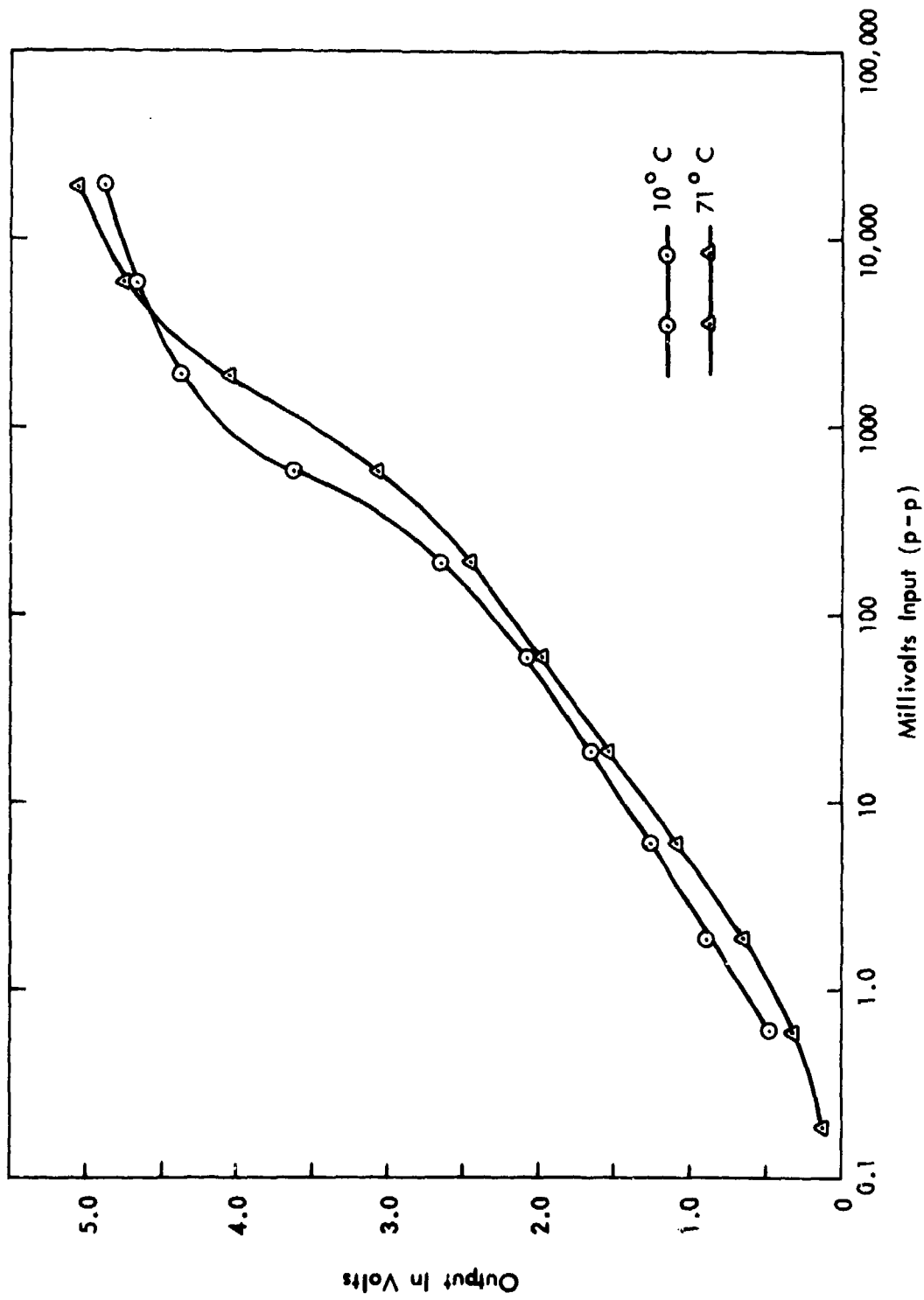
AM-2, SERIAL NUMBER 17

FIGURE 48   PVM BLAM CALIBRATION
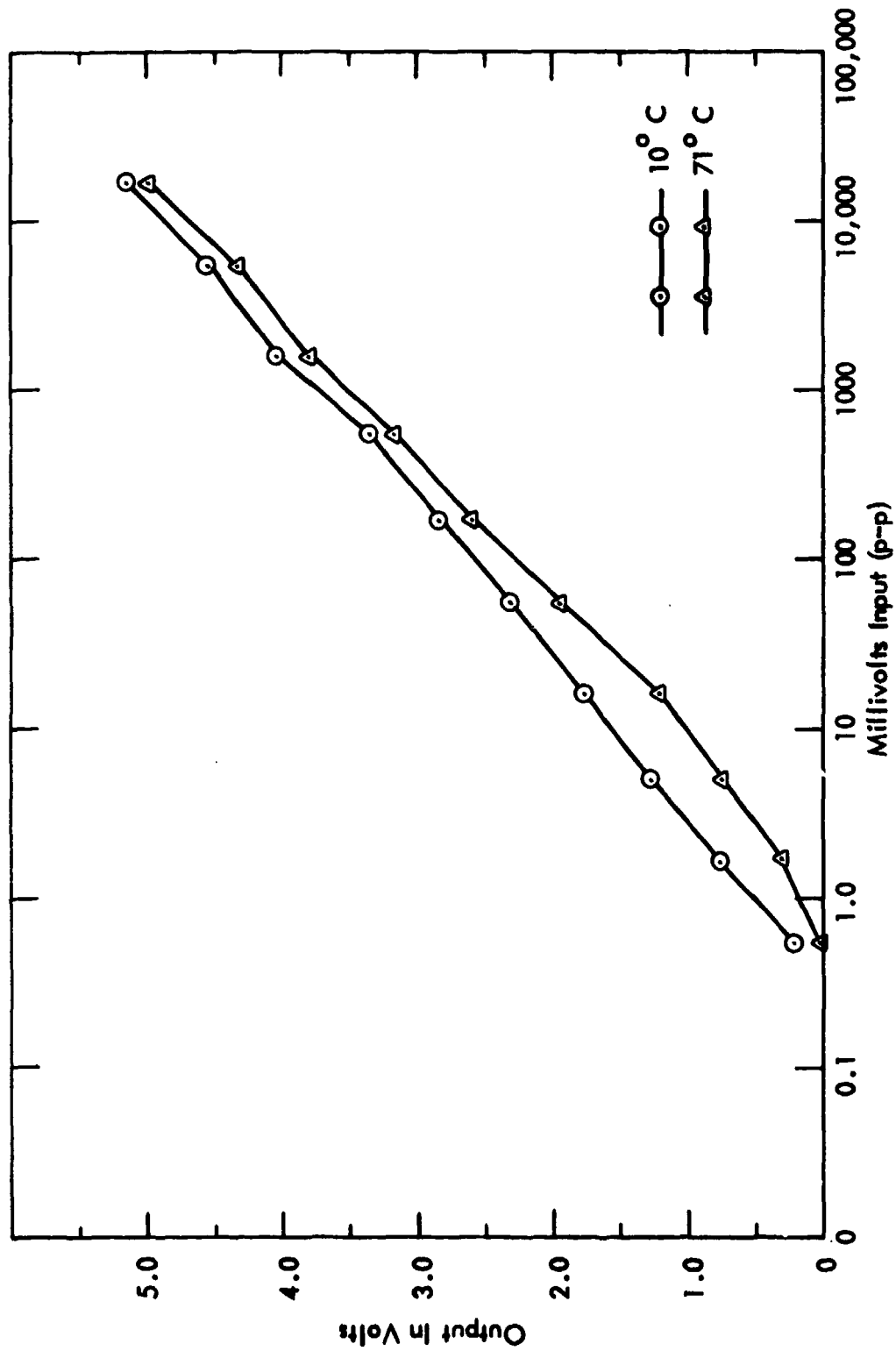
AM-2, SERIAL NUMBER 18

FIGURE 49   STM 12 BLAM CALIBRATION
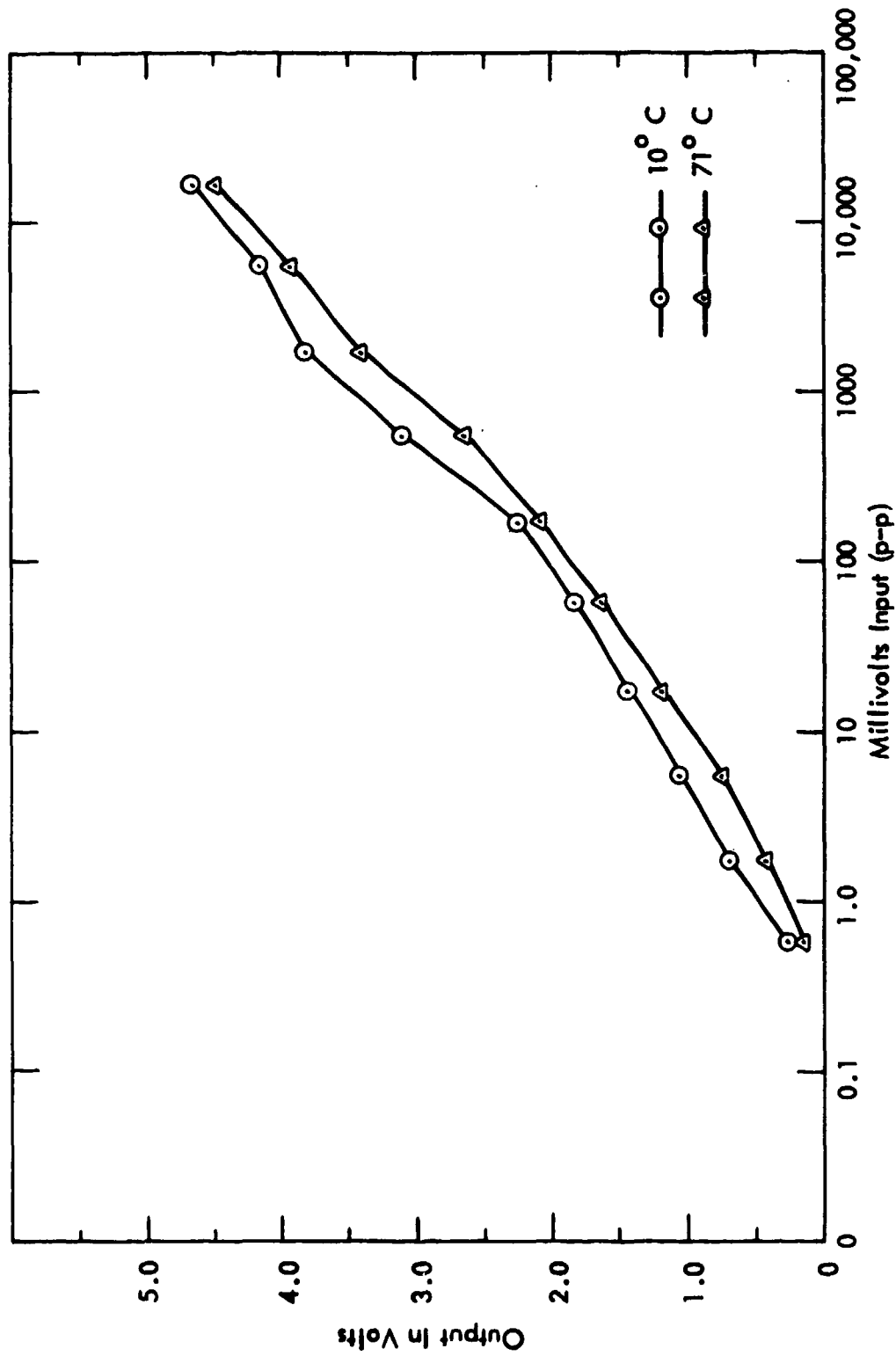
AM-2, SERIAL NUMBER 19

FIGURE 50   STM 12 BLAM CALIBRATION
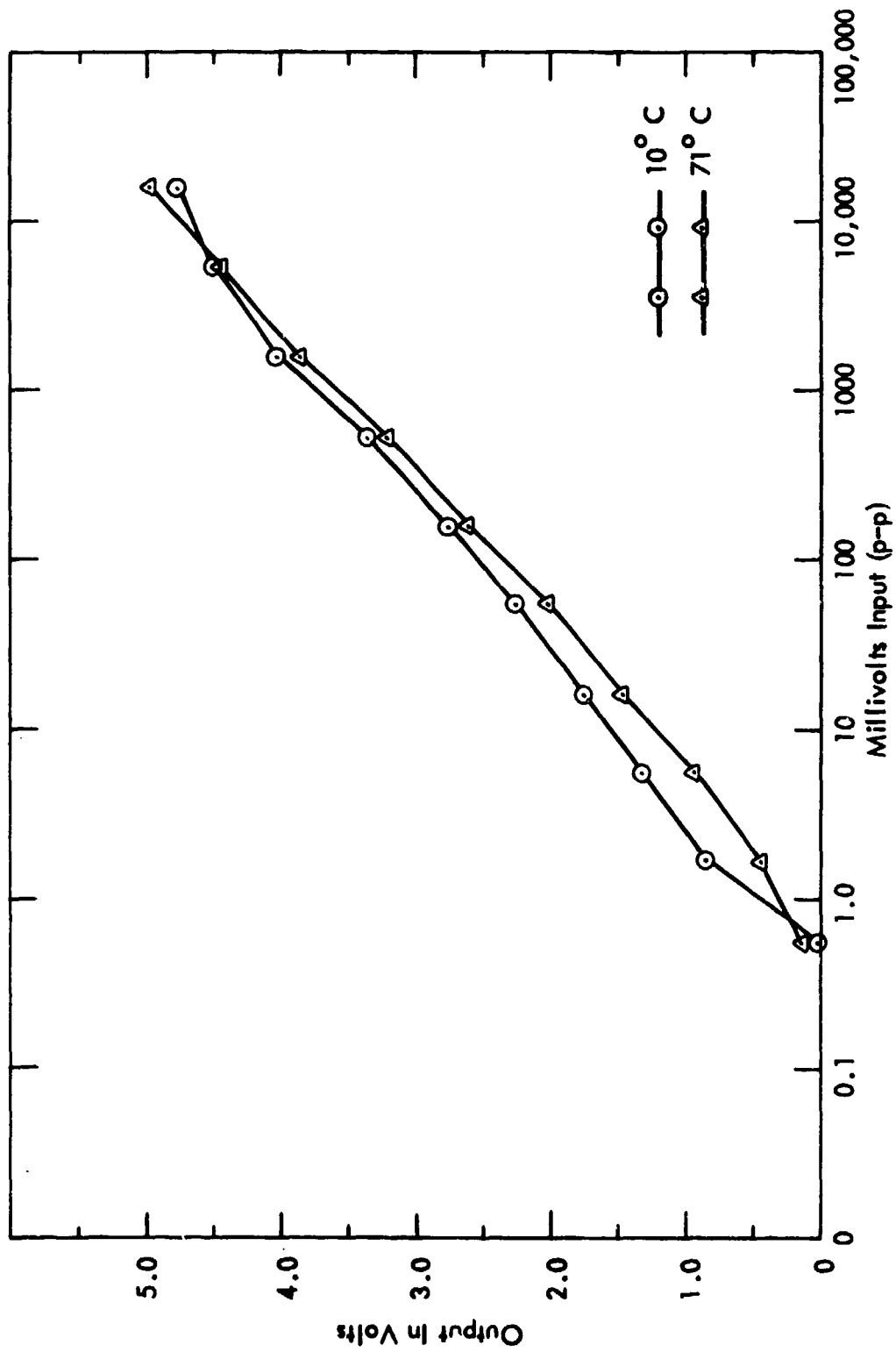
FIGURE 51   STM 12 BLAM CALIBRATION
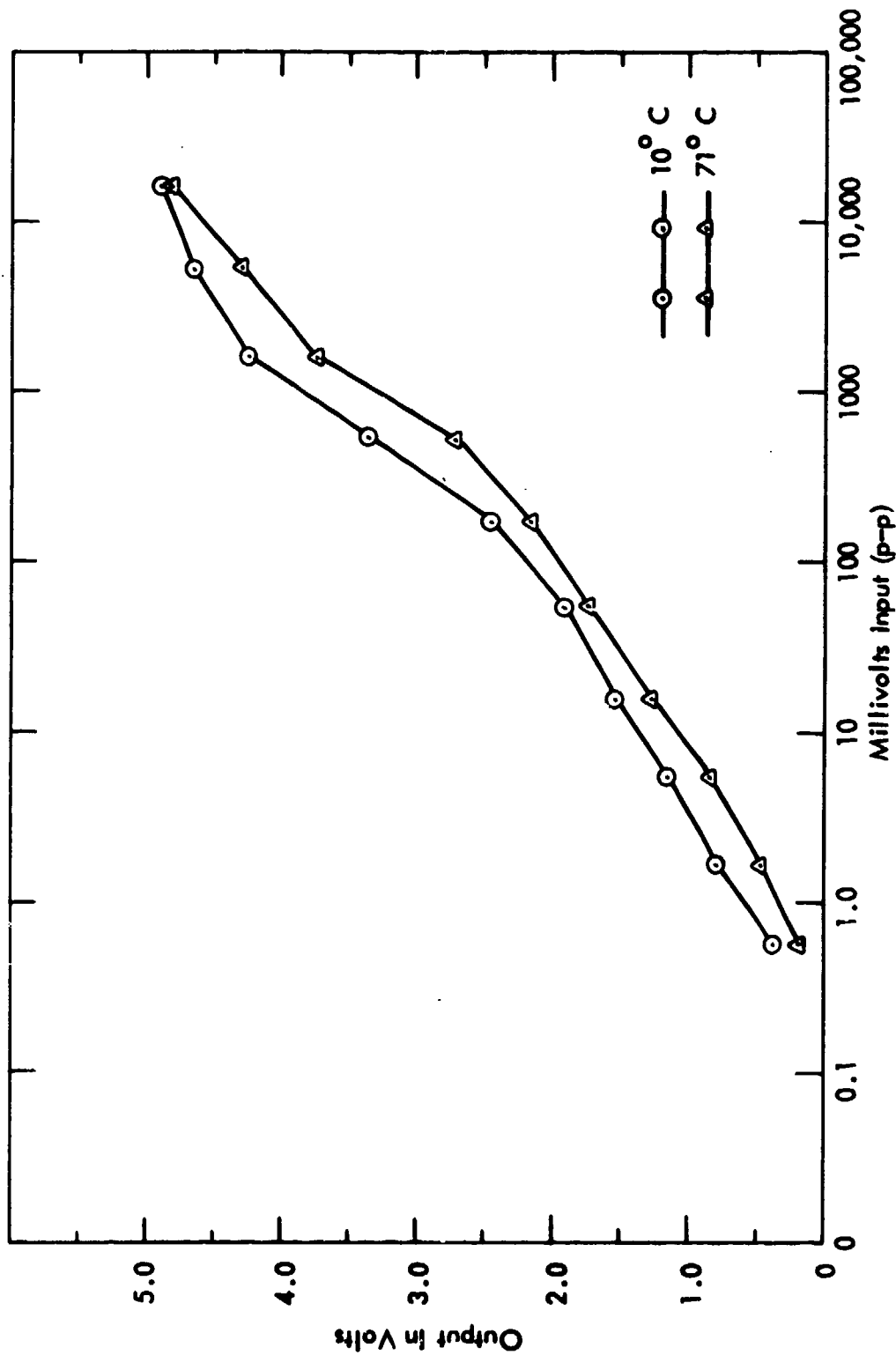
FIGURE 52   STM 12 BLAM CALIBRATION
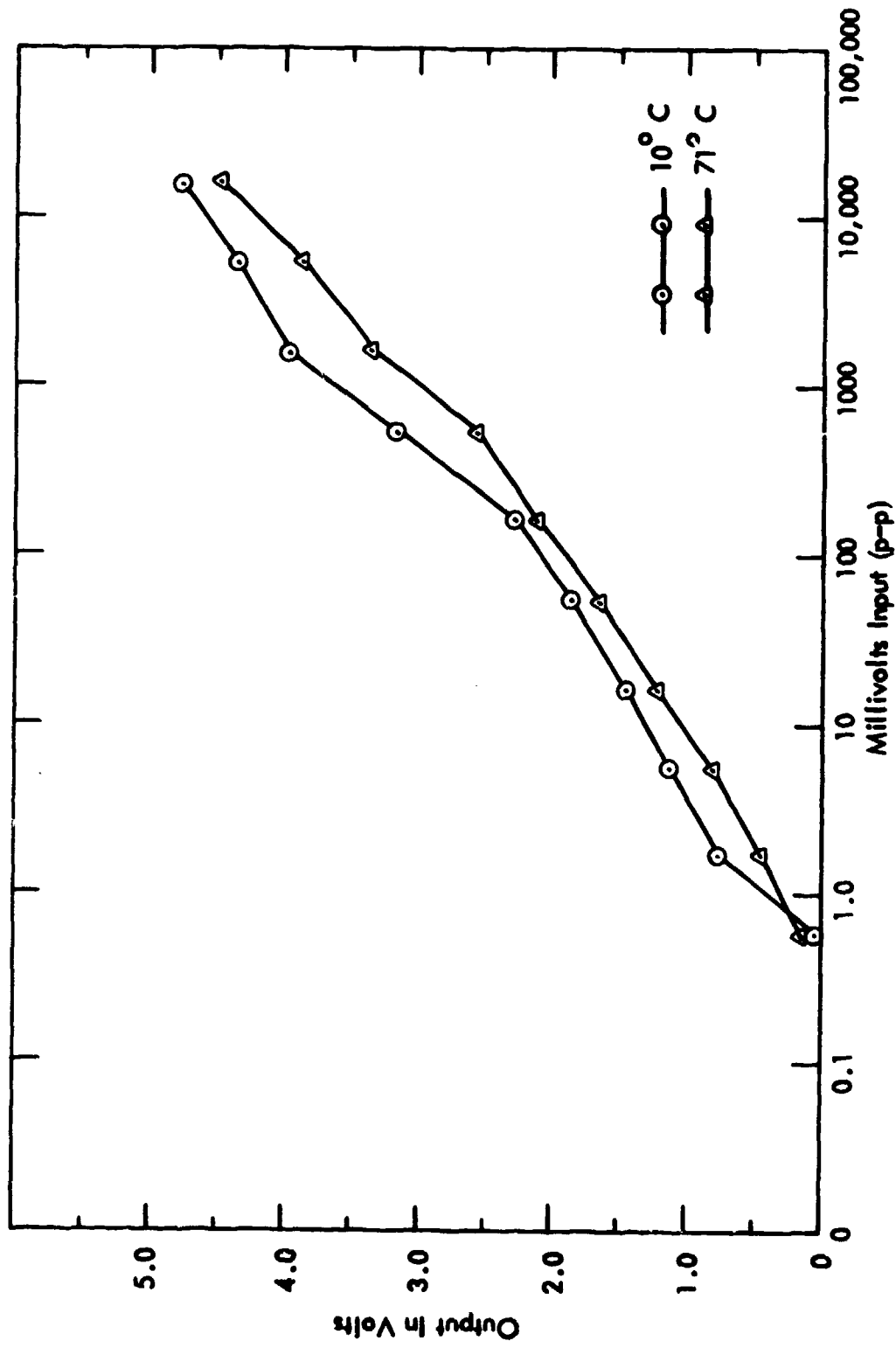
FIGURE 53   STM 12 BLAM CALIBRATION

AM-2, SERIAL NUMBER 23

APPENDIX B

RUN 3 SCHLEIREN PHOTOS
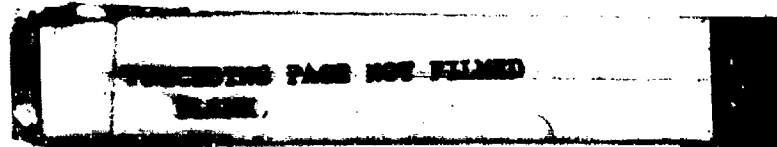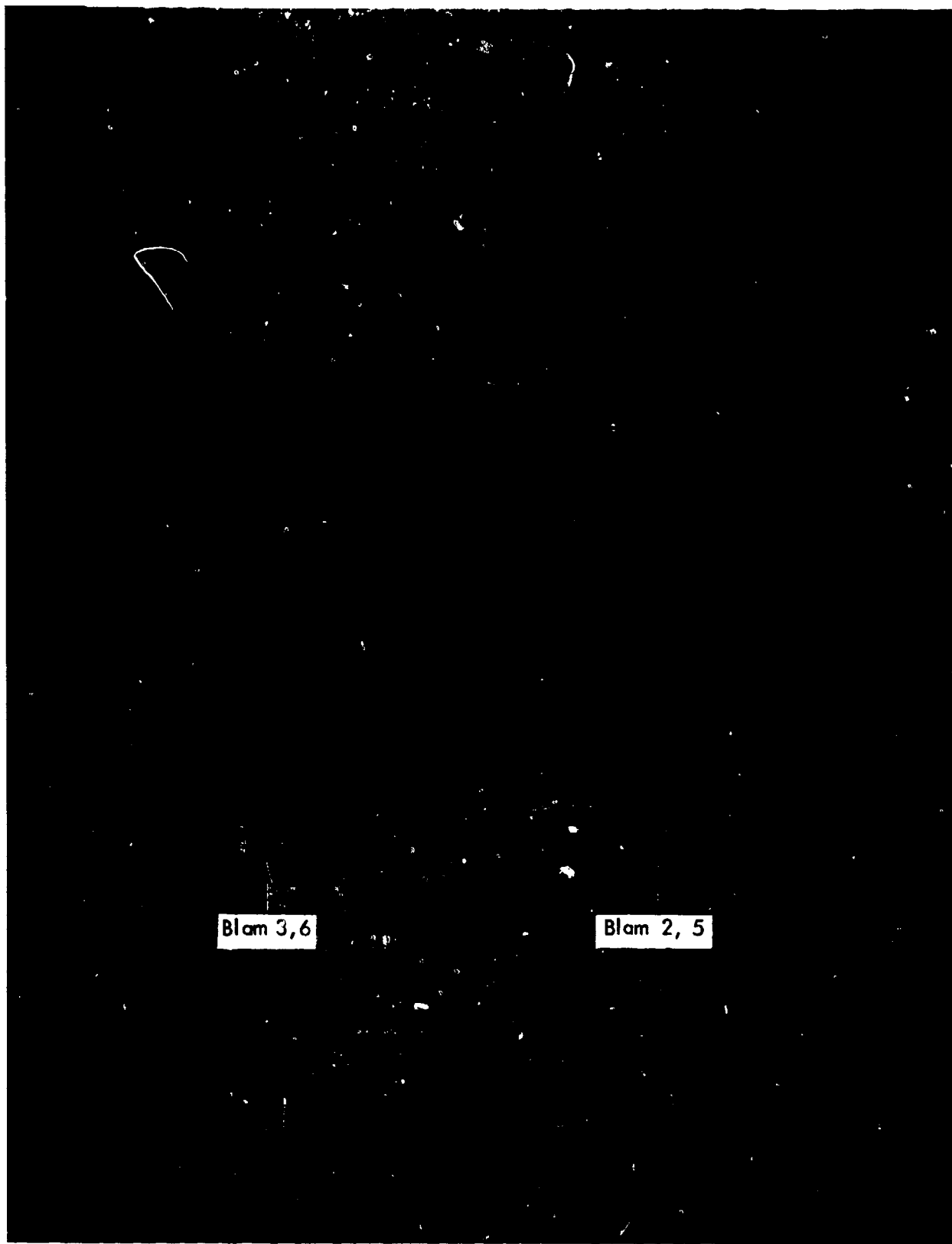
FIGURE 54 RUN 3 SCHLEIREN PHOTO
$R_\infty = 3 \times 10^6 / meter$
Run Time = 5.7 sec.
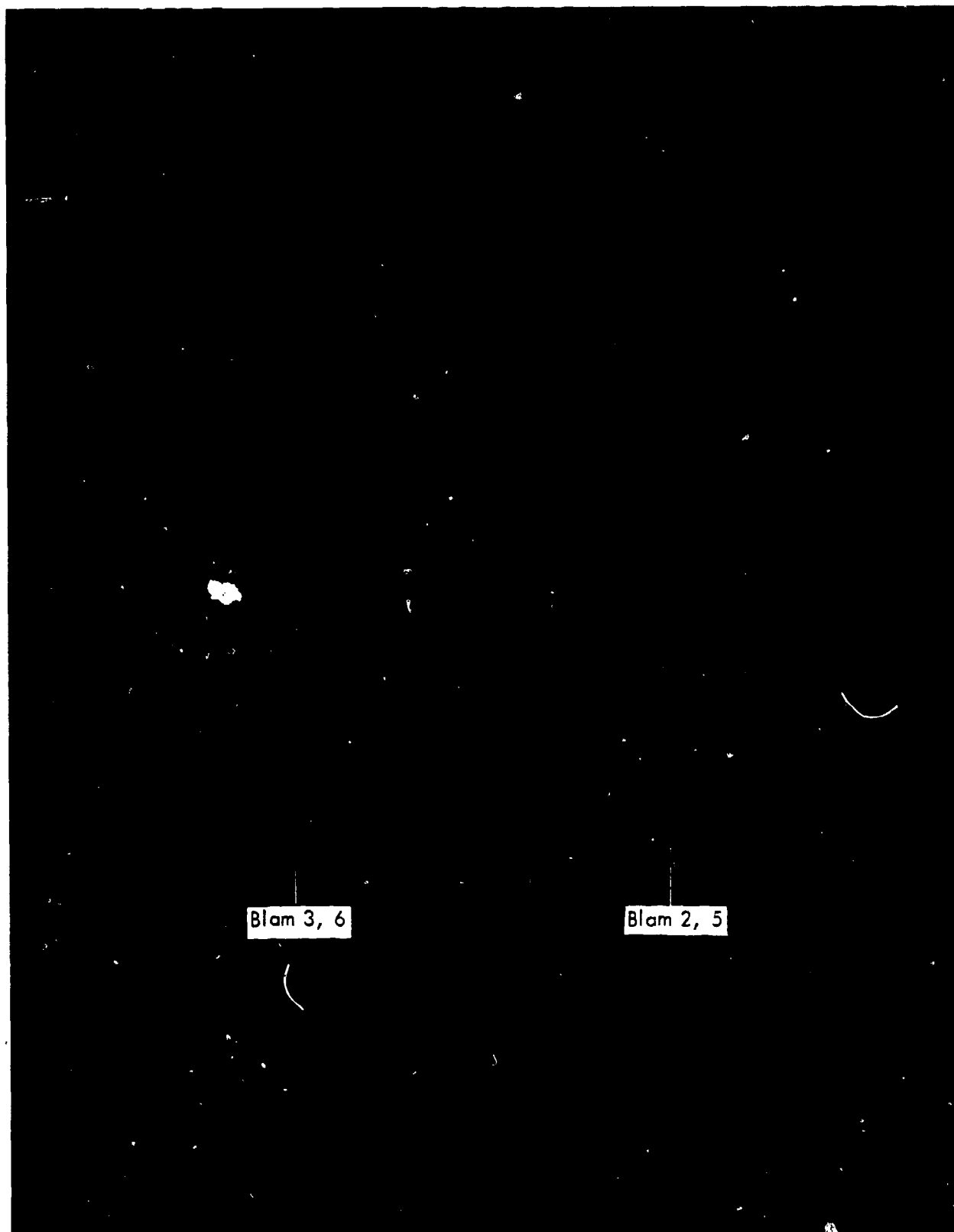
FIGURE 55   RUN 3 SCHLEIREN PHOTO

$R_{\infty} = 4 \times 10^6/\text{meter}$

Run Time = 7.6 sec.
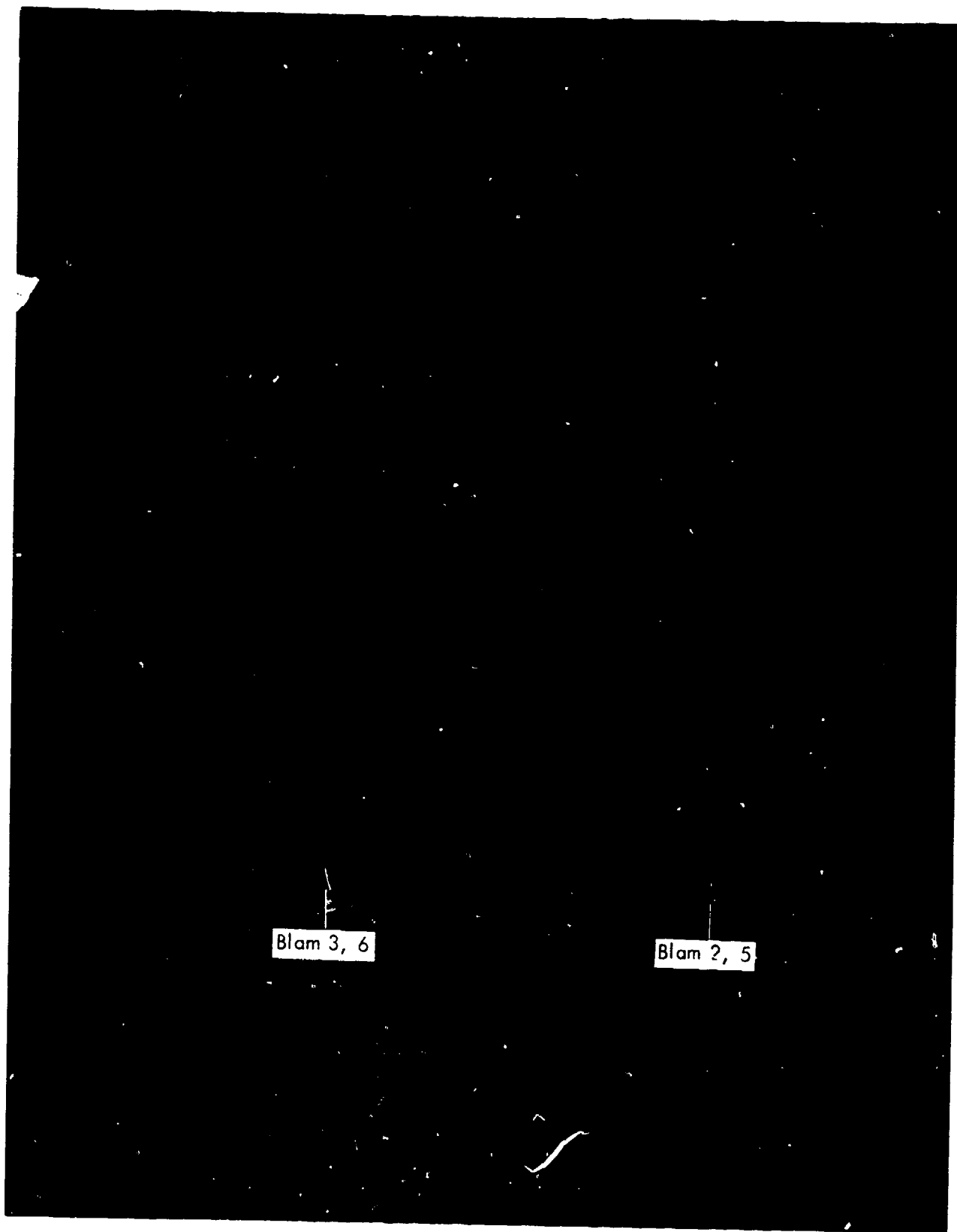
FIGURE 56   RUN 3 SCHLEIREN PHOTO
$R_\infty = 5.6 \times 10^6/$meter
Run Time = 10 sec.
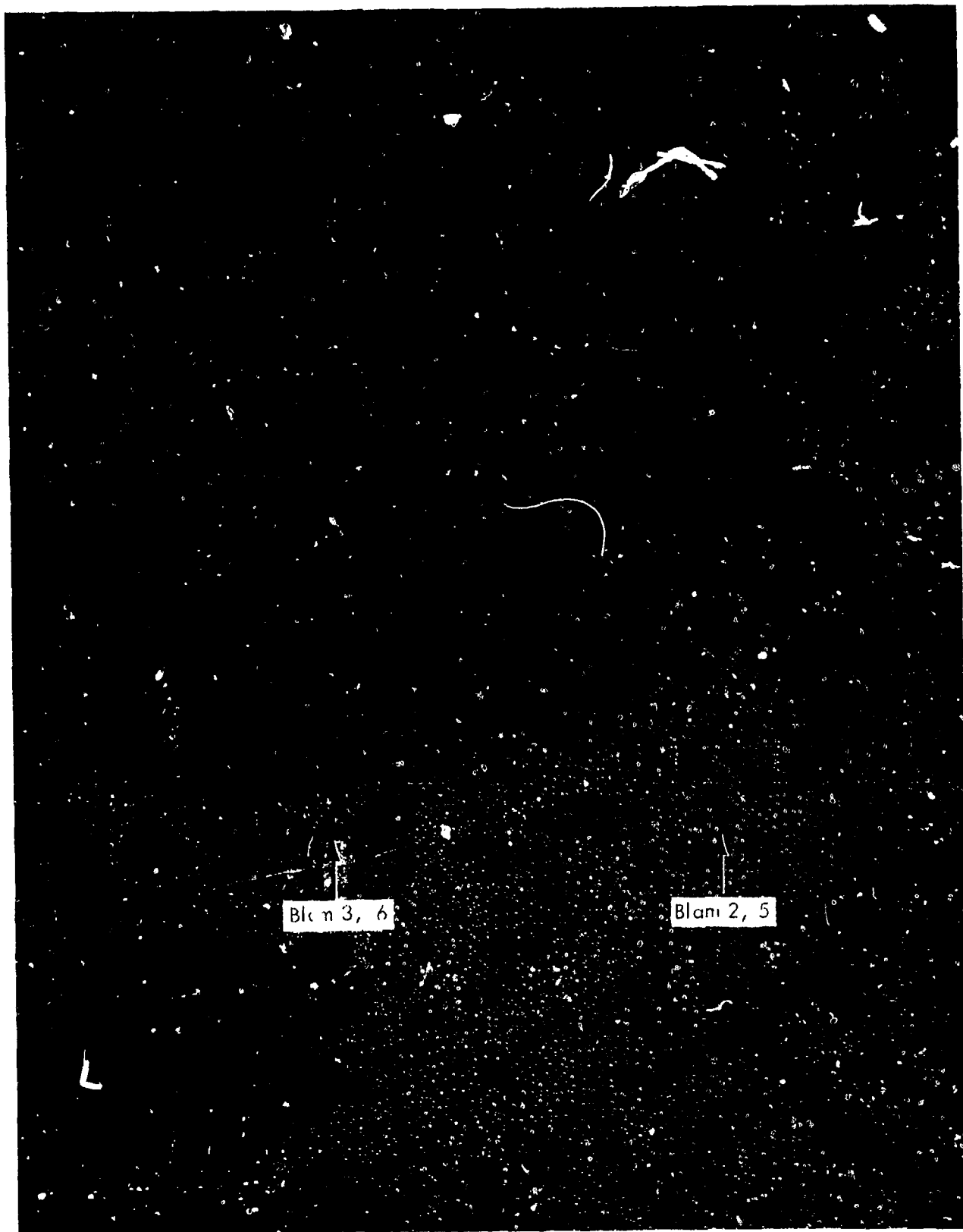
FIGURE 57 RUN 3 SCHLEIREN PHOTO
$R_\infty = 7.2 \times 10^6/\text{meter}$
Run Time = 12 sec.
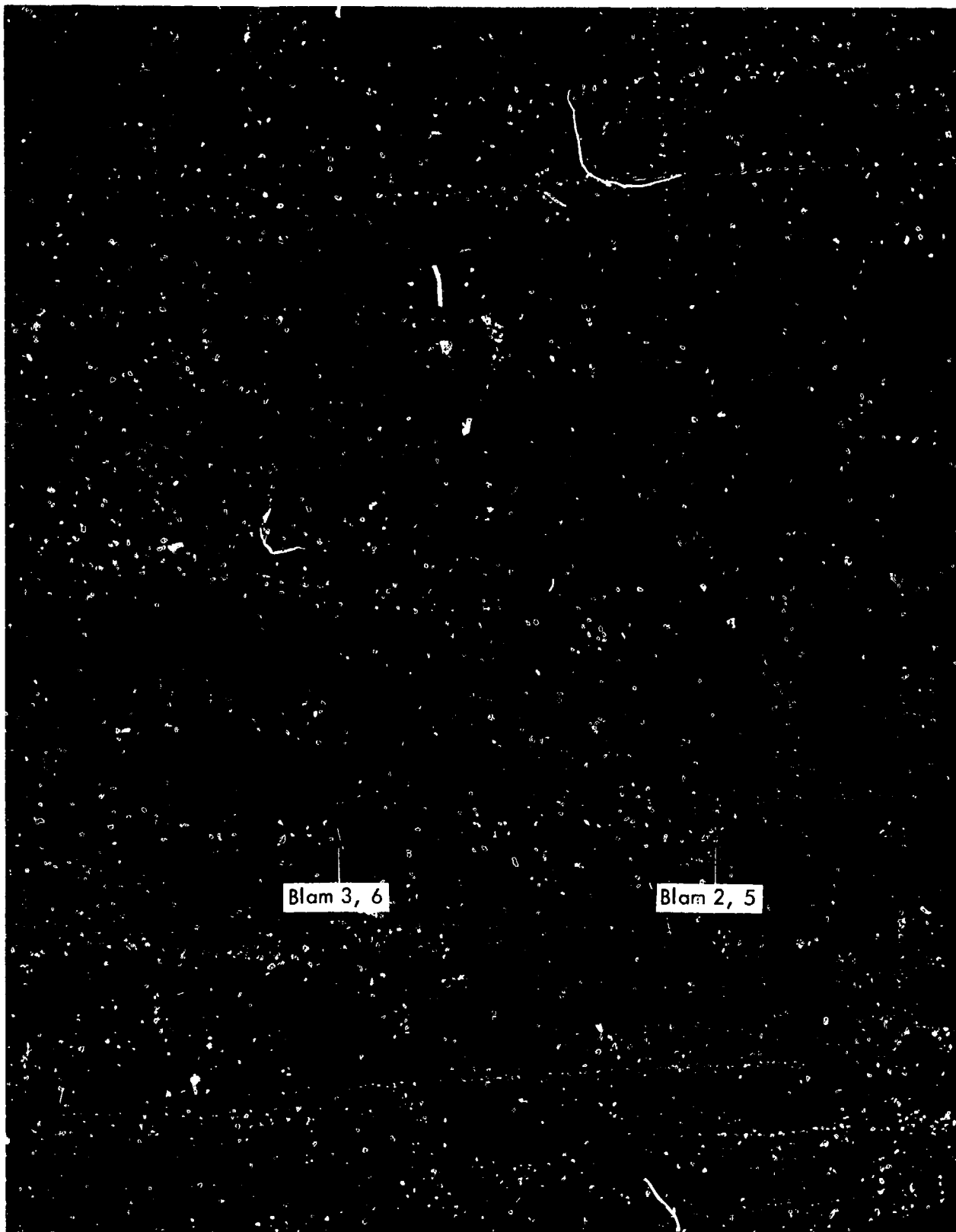
FIGURE 58 RUN 3 SCHLEIREN PHOTO

$K_\omega = 12.5 \times 10^6$ /meter

Run Time = 19 sec.
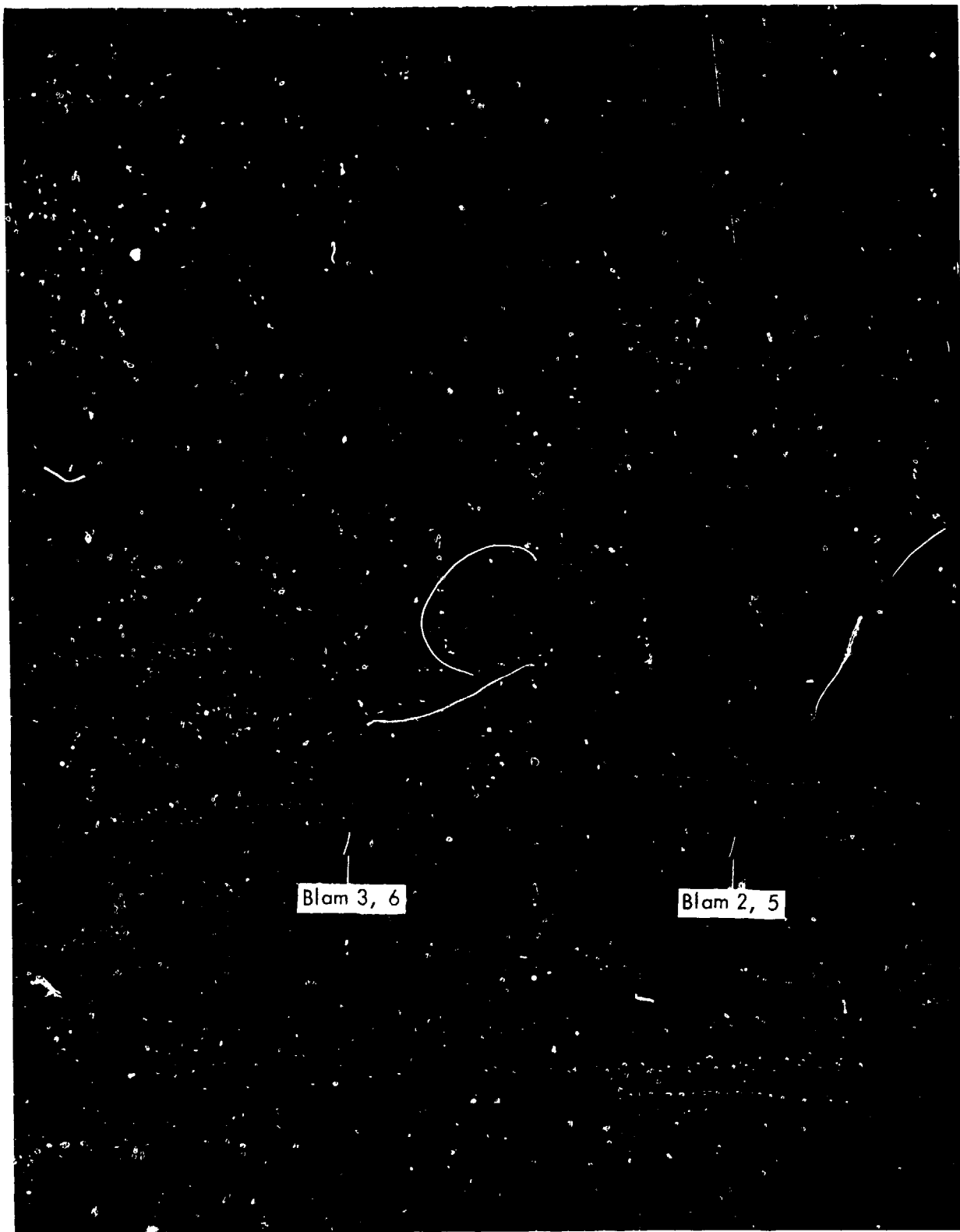
FIGURE 59   RUN 3 SCHLEIREN PHOTO

$R_\infty = 14.5 \times 10^6 / \text{meter}$

Run Time = 26 sec.

DISTRIBUTION LIST

DEPARTMENT OF DEFENSE

Assistant to the Secretary of Defense
Atomic Energy
    ATTN: Executive Assistant

Defense Advanced Rsch. Proj. Agency
    ATTN: TIO

Defense Documentation Center
12 cy ATTN: DD

Defense Intelligence Agency
    ATTN: DT-1B
    ATTN: DT-2

Defense Nuclear Agency
    ATTN: DDST
    ATTN: SPAS
    ATTN: STSP
4 cy ATTN: TITL

Field Command
Defense Nuclear Agency
    ATTN: FCPR

Field Command
Defense Nuclear Agency
Livermore Division
    ATTN: FCPRL

Joint Chiefs of Staff
    ATTN: J-5, Nuclear Division

Joint Strat. Tgt. Planning Staff
    ATTN: JPTM
    ATTN: JLTW-2

NATO School (SHAPE)
    ATTN: U.S. Documents Officer

Undersecretary of Defense for Rsch. & Engrg.
    ATTN: Strategic & Space Systems (OS)

DEPARTMENT OF THE ARMY

BMD Advanced Technology Center
Department of the Army
    ATTN: ATC-M

Deputy Chief of Staff for Ops. & Plans
Department of the Army
    ATTN: DAMO-NCZ

Deputy Chief of Staff for Rsch., Dev., & Acq.
Department of the Army
    ATTN: DAMA-CSS-N

Harry Diamond Laboratories
Department of the Army
    ATTN: DELHD-N-RBH
    ATTN: DELHD-RC

BMD Program Office
Department of the Army
    ATTN: Technology Division

DEPARTMENT OF THE ARMY (Continued)

U.S. Army Ballistic Research Labs
    ATTN: DRDAR-BL, R. Eichelberger

U.S. Army Material & Mechanics Rsch. Ctr.
    ATTN: DRXMR-HH

U.S. Army Materiel Dev. & Readiness Cmd.
    ATTN: DRCDE-D

U.S. Army Missile R&D Command
    ATTN: DRDMI-XS

DEPARTMENT OF THE NAVY

Naval Research Laboratory
    ATTN: Code 2627

Naval Sea Systems Command
    ATTN: SEA-0351

Naval Surface Weapons Center
    ATTN: Code K06
2 cy ATTN: Code K82

Office of the Chief of Naval Operations
    ATTN: OP 604C

Strategic Systems Project Office
Department of the Navy
    ATTN: NSP-272

DEPARTMENT OF THE AIR FORCE

Air Force Flight Dynamics Laboratory
    ATTN: FBC
    ATTN: FXG

Air Force Geophysics Laboratory
    ATTN: LY, C. Touart

Air Force Materials Laboratory
    ATTN: MBE
    ATTN: LTM
    ATTN: MXE
    ATTN: MBC
    ATTN: MXS

Air Force Rocket Propulsion Laboratory
    ATTN: LKCP

Air Force Systems Command
    ATTN: DLW

Air Force Weapons Laboratory
Air Force Systems Command
    ATTN: SUL
    ATTN: DYV

Arnold Engineering Development Center
Air Force Systems Command
    ATTN: Library Documents

Foreign Technology Division
Air Force Systems Command
    ATTN: SDBG

DEPARTMENT OF THE AIR FORCE (Continued)

Research, Development, & Acq.
Department of the Air Force
  ATTN: AFRDQSM
  ATTN: AFRDQ

Space & Missile Systems Organization
Air Force Systems Command
  ATTN: DYS
  ATTN: DYSE
  ATTN: DYTE
  ATTN: DYSR

Space & Missile Systems Organization
Air Force Systems Command
  ATTN: MNNR
  ATTN: MNNH

Strategic Air Command
Department of the Air Force
  ATTN: XPFS
  ATTN: XOBM

DEPARTMENT OF ENERGY CONTRACTORS

Lawrence Livermore Laboratory
  ATTN: Document Control for L-10, H. Kruger
  ATTN: Document Control for L-92, C. Taylor

Los Alamos Scientific Laboratory
  ATTN: Document Control for J. Taylor

Sandia Laboratories
  ATTN: Document Control for R. Clem
  ATTN: Document Control for A. Chabai
  ATTN: Document Control for D. Rigali

Sandia Laboratories
Livermore Laboratory
  ATTN: Document Control for T. Gold

DEPARTMENT OF DEFENSE CONTRACTORS

Acurex Corp.
  ATTN: J. Sapenstein
  ATTN: J. Huntington
  ATTN: C. Powars
  ATTN: C. Nardo
  ATTN: J. Crenshaw

Aerojet Liquid Rocket Co.
  ATTN: R. Jenkins

Aeronautical Rsch. Assoc. of Princeton, Inc.
  ATTN: C. Donaldson

Aerospace Corp.
  ATTN: P. Legendre
  ATTN: R. Palmer
  ATTN: W. Portenier
  ATTN: M. Gyetvay
  ATTN: H. Dyner
  ATTN: D. Platus
  ATTN: W. Grabowsky
  ATTN: R. Mortensen
  ATTN: D. Nowlan

ARO, Inc.
  ATTN: G. Norfleet
  ATTN: J. Adams

DEPARTMENT OF DEFENSE CONTRACTORS (Continued)

AVCO Research & Systems Group
  ATTN: W. Broding

Boeing Co.
  ATTN: B. Lempriere

Calspan Corp.
  ATTN: M. Holden

Effects Technology, Inc.
  ATTN: R. Wengler

Fiber Materials, Inc.
  ATTN: M. Subilia

Ford Aerospace & Communications Corp.
  ATTN: A. Demetriades

General Electric Co.
Re-Entry & Environmental Systems Div.
  ATTN: P. Cline

General Electric Company—TEMPO
  ATTN: DASIAC

General Research Corp.
  ATTN: R. Rosenthal

Institute for Defense Analyses
  ATTN: J. Bengston
  ATTN: Classified Library

ION Physics Corp.
  ATTN: R. Evans

Kaman Sciences Corp.
  ATTN: F. Shelton
  ATTN: J. Nickell
  ATTN: V. Peckham

Lockheed Missiles & Space Co., Inc.
  ATTN: C. Lee
  ATTN: D. Price
  ATTN: R. Au
  ATTN: P. Schneider
  ATTN: G. Chrusciel

Lockheed Missiles and Space Co., Inc.
  2 cy ATTN: T. Fortune

Martin Marietta Corp.
  ATTN: R. Cramer

McDonnell Douglas Corp.
  ATTN: G. Fitzgerald

National Academy of Sciences
National Materials Advisory Board
  ATTN: D. Groves

Pacific-Sierra Research Corp.
  ATTN: G. Lang

Physical Sciences, Inc.
  ATTN: M. Finson

Prototype Development Associates, Inc.
  ATTN: J. Dunn
  3 cy ATTN: C. Thacker

DEPARTMENT OF DEFENSE CONTRACTORS (Continued)

R&D Associates
    ATTN: F. Field
    ATTN: R. Ross
    ATTN: P. Rausch
    ATTN: C. MacDonald

Science Applications, Inc.
    ATTN: J. Warner

Science Applications, Inc.
    ATTN: K. Kratsch
    ATTN: L. Dunbar

Science Applications, Inc.
    ATTN: A. Martellucci

Southern Research Institute
    ATTN: C. Pears

DEPARTMENT OF DEFENSE CONTRACTORS (Continued)

Spectron Development Labs, Inc.
    ATTN: T. Lee

SRI International
    ATTN: D. Curran
    ATTN: G. Abrahamson

TRW Defense & Space Sys. Group
    ATTN: R. Myer
    ATTN: D. Baer
    ATTN: I. Alber
    ATTN: T. Williams
    ATTN: W. Wood

TRW Defense & Space Sys. Group
    ATTN: E. Allen
    ATTN: W. Polich
    ATTN: E. Wong
    ATTN: L. Berger
    ATTN: V. Blankenship